Chapter 12
Orbit Perturbations

12.1 Problem Setting

12.1.1 Origins of Perturbations

So far, we have studied the two-body problem, in which one body moves under a central Newtonian force, as given by a gravitational field of a second body, a point mass. This led to Keplerian orbits as the solutions of the respective equations of motion. However, in reality there are many external forces acting on the body, which are neither point symmetric nor Newtonian. For instance, a massive central body usually is not quite homogeneous and isotropic, which in general gives rise to non-central and non-Newtonian forces. In addition, the gravitational forces of other celestial bodies, in particular neighboring planets, or interactions with the space environment will perturb the Keplerian orbit around the central body. In total there exist the following major disturbing forces:

- gravitational forces resulting from the non-spherical geometry and mass distribution of the central body
- gravitational forces of other celestial bodies (such as the Sun, Moon, planets)
- acceleration force resulting from the solar radiation pressure
- acceleration force resulting from the drag of the remaining atmosphere

Figure 12.1 provides a graphical representation of all relevant perturbations acting on an Earth-orbiting S/C as a function of altitude. Obviously Earth's anisotropy generates various perturbation terms J_{nm} of different strength, and atmospheric drag decreases rapidly with increasing altitude. In addition, Table 12.1 gives an overview of the essential external perturbations giving rise to accelerations of the S/C in a LEO at 500 km altitude and in GEO for comparison.

Judged from their magnitudes the first four disturbing forces (except drag for GEO) have to be taken into account for real missions. The perturbations cause the

U. Walter, *Astronautics*, https://doi.org/10.1007/978-3-319-74373-8_12

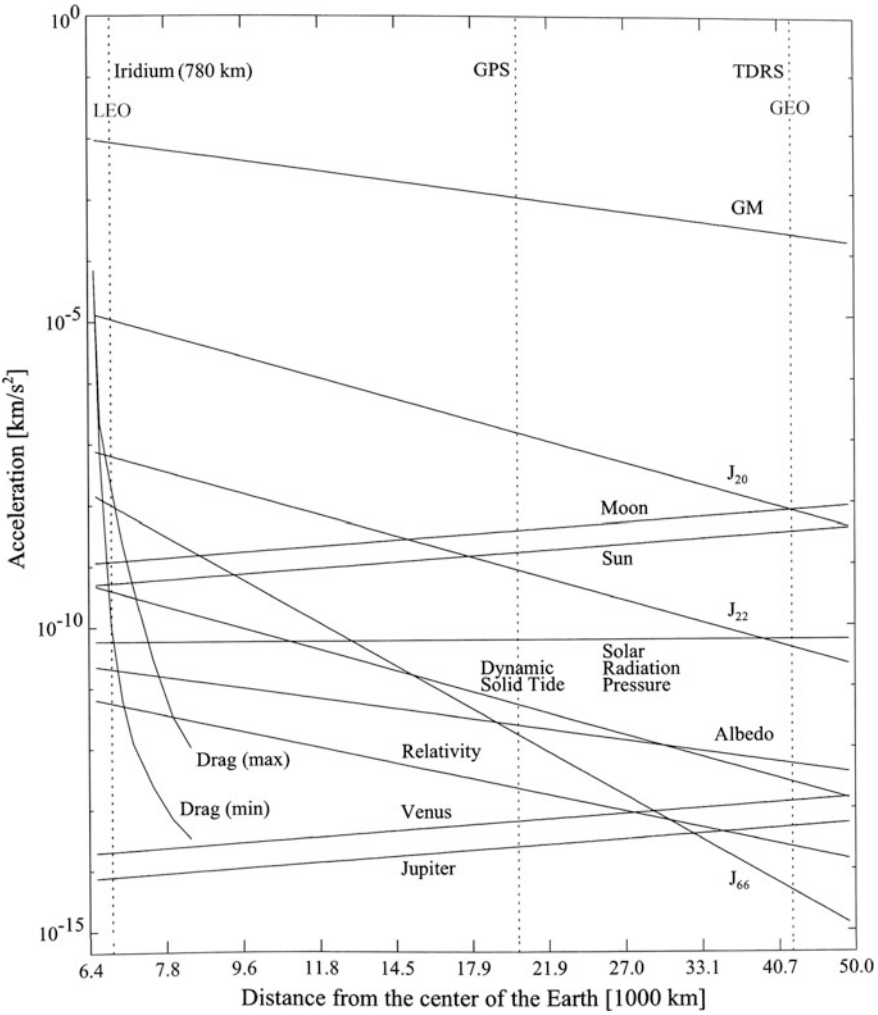

Fig. 12.1 Magnitudes of different perturbations of a satellite orbit: GM = regular gravitational force of the Earth; J_{nm} = gravitational multipoles; relativity = relativistic deviations; and the satellites Iridium, Lageos, GPS, TDRS at altitudes between LEO and GEO. *Credit* Montenbruck (2000)

orbits to be no longer Keplerian, but as long as the perturbations are small, which we can safely assume in the following, an orbit can be linearly approximated by a sequence of confocal Keplerian orbits, implying that the set of orbital elements

$$\vartheta_i \in (a, e, i, \Omega, \omega, M - n \cdot t)$$

Table 12.1 External perturbational accelerations on a S/C with a given $A_\perp/m$, where $A_\perp$ is the effective surface area perpendicular to the impinging force and m the mass of the S/C

Source of perturbation	Acceleration [m s^{-2}] in 500 km altitude	Acceleration [m s^{-2}] in GEO
Drag (mean)	$6 \times 10^{-5}\ A_\perp/m$	$1.8 \times 10^{-13}\ A_\perp/m$
Solar pressure	$4.67 \times 10^{-5}\ A_\perp/m$	$4.67 \times 10^{-5}\ A_\perp/m$
Sun (mean)	5.6×10^{-7}	3.5×10^{-6}
Moon (mean)	1.2×10^{-6}	7.3×10^{-6}
Jupiter (maximum)	8.5×10^{-12}	5.2×10^{-11}

changes with time from one Keplerian orbit to the adjacent one according to

$$\vartheta_i(t) \approx \vartheta_{i,0} + \dot{\vartheta}_i \cdot t \tag{12.1.1}$$

12.1.2 Osculating Orbits

Let us consider a concrete example. As we will see at the end of Sect. 12.3.3 the line of apsides rotates under the influence of Earth's equatorial bulge. By adopting a *PQW* coordinate system (see Fig. 13.3), where we orient the *P*-axis along the line of nodes, the orbit Eq. 7.3.5 then reads for a prograding apsidal line

$$r = \frac{p}{1 + e \cdot \cos[\theta - \omega(\theta)]} \tag{12.1.2}$$

So, at a given orbit angle θ_0, as measured against the line of nodes, the trajectory of this example can be approximated by the instantaneous Keplerian orbit

$$r = \frac{p}{1 + e \cdot \cos[\theta - \omega(\theta_0)]} \quad \textbf{osculating orbit} \tag{12.1.3}$$

which is called an *osculating orbit* (Latin "osculare" means "to kiss", see Fig. 12.2). Thus, any disturbed orbit is a continuous sequence of confocal osculating orbits. This osculation analysis reduces the perturbation problem to determining at a given point in time t_0 the elements $\vartheta_{i,0} \in (a_0, e_0, i_0, \Omega_0, \omega_0, M_0)$ of the osculating orbit (a.k.a. **osculating elements**), as we did in the above example, and finding the time derivatives $\dot{\vartheta}_i \in \left(\dot{a}, \dot{e}, \dot{i}, \dot{\Omega}, \dot{\omega}, \dot{M} - n\right)$ from theory.

Deriving the time derivatives for all major external perturbations in LEO and GEO as given in Table 12.1 is the objective of this chapter. To do so we need a general rule for how to calculate the derivatives from the perturbing forces. This is provided in the following section.

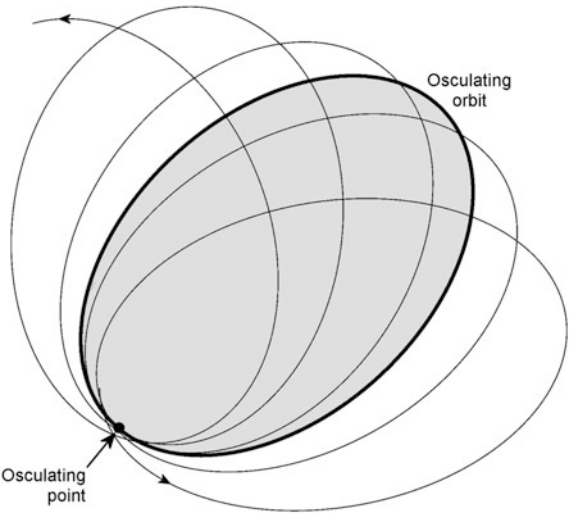

Fig. 12.2 An osculating ellipse (bold line) attached to an intermediate periapsis of a disturbed elliptic orbit (thin line, given by Eq. (12.1.2)) showing a progression of the apsidal line

12.1.3 Gaussian Variational Equations

Any perturbing force $\boldsymbol{F}_{perturb}$, or alternatively the corresponding acceleration $\boldsymbol{a}_{perturb} = \boldsymbol{F}_{perturb}/m$, acting on an orbiting body can be decomposed in the *RSW* coordinate system (see Fig. 13.4 in Sect. 13.1.4) into a radial component a_r, a cross-radial component a_θ, and into a component a_h perpendicular to the orbital plane, i.e., along the angular momentum $\boldsymbol{h}$, which perturbs the equation of motion according to

$$\ddot{\boldsymbol{r}} + \frac{\mu}{r^3}\boldsymbol{r} = \boldsymbol{a}_{perturb} = (a_r, a_\theta, a_h)_{RSW}$$

Most generally $\dot{\boldsymbol{\vartheta}}$ is derived by starting out from the general solution of the above differential equation having the functional form $\boldsymbol{r} = \boldsymbol{r}[\vartheta_i(t), t]$. Differentiation leads to $\dot{\boldsymbol{r}} = \boldsymbol{v} + \boldsymbol{\Phi}$, with $\boldsymbol{v} = \partial \boldsymbol{r}/\partial t$ the velocity of the perturbed orbit and $\boldsymbol{\Phi} = \sum_i \frac{\partial \boldsymbol{r}}{\partial \vartheta_i}\dot{\vartheta}_i$. It can be shown (see, e.g., Gurfil (2007) or Efroimsky (2006)) that by differentiating again and substituting the result into the above perturbed equation of motion one can derive $\dot{\boldsymbol{\vartheta}}$. Because this way of derivation is tedious and mathematically quite demanding (see, e.g., Vallado (2001), Schaub and Junkins (2003) or Danby (2003)) we will not attempt it here but defer to an exercise (Problem 12.1) for an ab initio approach. From any of these approaches one finds the so-called **Gaussian variational equations (GVEs)**

$$
\begin{aligned}
\dot{a} &= \frac{2a^2}{h}\left[e\,\sin\theta\,\cdot\,a_r + (1+e\,\cos\theta)a_\theta\right] \\
\dot{e} &= \frac{h}{\mu}\left[\sin\theta\,\cdot\,a_r + \left(\frac{e+\cos\theta}{1+e\,\cos\theta} + \cos\theta\right)a_\theta\right] \\
\dot{i} &= \frac{r\,\cos(\theta+\omega)}{h}a_h \\
\dot{\omega} &= \frac{h}{e\mu}\left[-\cos\theta\,\cdot\,a_r + \frac{2+e\,\cos\theta}{1+e\,\cos\theta}\sin\theta\,\cdot\,a_\theta\right] - \frac{r\,\sin(\theta+\omega)\cos i}{h\,\sin i}\,\cdot\,a_h \\
\dot{\Omega} &= \frac{r\,\sin(\theta+\omega)}{h\,\sin i}a_h \\
\dot{M} - n &= -\frac{h\sqrt{1-e^2}}{\mu}\left[\left(\frac{2}{1+e\,\cos\theta} - \frac{\cos\theta}{e}\right)a_r + \frac{\sin\theta}{e}\left(\frac{2+e\,\cos\theta}{1+e\,\cos\theta}\right)a_\theta\right] \\
&= -\sqrt{1-e^2}\left(\frac{2r}{h}a_r + \dot{\omega} + \dot{\Omega}\,\cos i\right)
\end{aligned}
\tag{12.1.4}
$$

Note *The elements $\dot{\vartheta}_i$ of the Gaussian variational equations become infinite or zero if accelerations act on orbits with $h \to 0$, i.e., on radial orbits or orbits close to those. In addition $\dot{\omega}$ and $\dot{M}$ become infinite if a_r or a_θ accelerations act on a circular orbit, $e \to 0$, and $\dot{\omega}$ and $\dot{\Omega}$ become infinite if an a_h acceleration acts on an orbit with $i \to 0$.*

Remark *The vector function $\mathbf{\Phi}$ is called* gauge function*, because it constitutes a gauge freedom, which means it can be chosen freely without having an impact on the result $\dot{\vartheta}_i$. As Lagrange already did, the so-called* Lagrange constraints *or* osculation constraints, $\mathbf{\Phi} = 0$*, are usually chosen, implying that the velocity vector of the perturbed orbit equals the one of the generating Keplerian orbit. This assumption, however, is fully arbitrary. Removing these constraints leads to the so-called* gauge-generalized equations*. Their evaluation is a very new and ongoing research and out of the scope of this book (see e.g. Efroimsky (2006)).*

In the following sections, we want to determine the perturbation accelerations listed above and calculate the corresponding variations of the orbital elements according to the Gaussian variational equations.

12.2 Gravitational Perturbations

12.2.1 Geoid

The gravitational field of the Earth is not absolutely isotropic, but has slightly different values in different directions. The reason is its non-spherical shape and its density variations within. The geometric body representing the corresponding asymmetrical gravitational field in the different directions is called *geoid* as depicted in Fig. 12.3. Strictly speaking, the geoid is the body representing the equipotential surface of the gravity potential at sea level, i.e., the surface to which the gravity vector g is always perpendicular. Graphically, the geoid is the equilibrium shape of the Earth, if its surface were fully covered with stationary water. In zero-order approximation Earth's masses are distributed evenly and the geoid is a sphere. The largest deviation from the sphere is caused by the rotation of the Earth, which displaces the masses to the equator due to the centrifugal forces. Earth's radius at the equator is 6378.14 km and hence is some 21.4 km longer than through the poles. Deducting a sphere from the geoid therefore results in a bumpy oblate spheroid, which never deviates more than 25 m from the true oblate spheroid (see Fig. 12.4, left).

Deducting the sphere and the oblate spheroid from the geoid results in a potato shaped figure (see Fig. 12.4, right, and color plates at the end of Sect. 12.2.2). Observe that its heights and downs do not follow the contours of the continents. Rather the Earth's interior is viscous with a high proportion of iron, magnesium, nickel, silicon, and oxygen. Temperature gradients between the hot interior of about

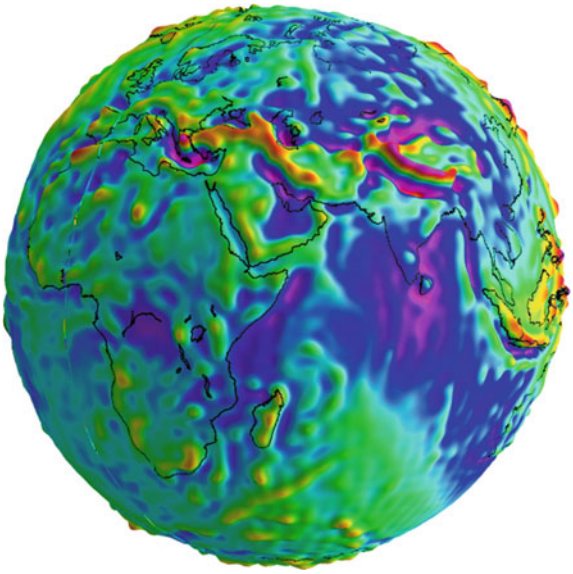

Fig. 12.3 Geoid of the Earth. *Credit* GFZ Potsdam

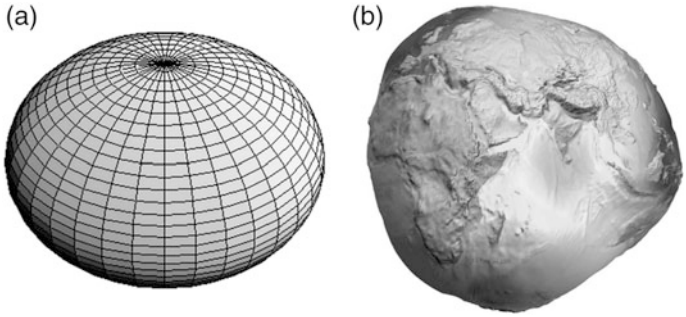

Fig. 12.4 (**a**, left) Earth has a bulge of 21.4 km height around the equator deforming the geoid to an oblate spheroid (excessively represented). (**b**, right) There are only small deviations from this spheroid (+20 m to −25 m), which make up a shape like a potato (= geoid – spheroid). For the entire shape of the "potato" see color plates at the end of Sect. 12.2.2. *Credit* GFZ Potsdam

4500 °C and the surface of the Earth cause vertical convection flows on the one hand, and slightly asymmetrical density distributions on the other, which is reflected in the potato shape of the geoid. Note that Fig. 12.3 depicts the real geoid, whereas Fig. 12.4 only shows the anisotropies, if the sphere and the spheroid are successively deducted. The deviations from the spheroid caused by the Earth's mass inhomogeneities are called *geoid undulations*.

As mountains embody a large amount of mass, the fine-structured geoid undulations clearly reflect the mountain ranges, which mainly account for the more complicated structure beyond the potato shape of the geoid. Because the finest details of the geoid reflect the mass proportions below the Earth's surface, one is able to determine from these structures for instance oil fields.

12.2.2 Gravitational Potential

The orbit of a spacecraft circling the Earth is influenced by these gravitational anisotropies, leading to slightly deformed Keplerian orbits. According to Eq. (7.7.1) the gravitational potential of an arbitrary mass distribution $\rho(\boldsymbol{r})$ is given by

$$U(\boldsymbol{r}) = -G \iiint_V \frac{\rho(\boldsymbol{r}')}{|\boldsymbol{r} - \boldsymbol{r}'|} d^3\boldsymbol{r}' \tag{12.2.1}$$

Let us assume we know Earth's mass distribution and we want to evaluate the above integral. To do so it can be shown that the expression $1/|\boldsymbol{r} - \boldsymbol{r}'|$ can be approximated by a series of spherical orthogonal functions, the so-called Legendre polynomials $P_n(x)$ of degree n,

$$\frac{1}{|\boldsymbol{r}-\boldsymbol{r}'|}=\frac{1}{r}\sum_{n=0}^{\infty}\left(\frac{r'}{r}\right)^n P_n(\cos\gamma)\quad @\ r'<r$$

where $\gamma=\angle(\boldsymbol{r},\boldsymbol{r}')$. We apply this result to the International Terrestrial Reference Frame (ITRF) (see Sect. 13.1.3), which is an Earth-centered Earth-fixed reference frame. Locations on Earth's surface are familiarly referenced by the geocentric latitude β (the spherical arc—i.e., without taking into account Earth's flattening—measured from the equator to the positive end of the z-axis) and geographic longitude λ (the arc from Greenwich meridian measured eastward, that is counterclockwise looking toward the origin from the positive end of the z-axis), i.e.,

$$\begin{aligned}\boldsymbol{r}&=r\begin{pmatrix}\cos\beta\,\cos\lambda\\ \cos\beta\,\sin\lambda\\ \sin\beta\end{pmatrix}_{ITRF}\\ &=r\begin{pmatrix}\cos(\Omega-\theta_{GMST})\cos u-\sin(\Omega-\theta_{GMST})\sin u\,\cos i\\ \sin(\Omega-\theta_{GMST})\cos u+\cos(\Omega-\theta_{GMST})\sin u\,\cos i\\ \sin u\,\sin i\end{pmatrix}_{ITRF}\end{aligned}$$

where the latter follows from Eq. (13.1.8b), θ_{GMST} is the *Greenwich Mean Sidereal Time*, which in the equatorial plane is the hour angle from the vernal point (First Point of Aries) to the Greenwich Meridian, and $u=\omega+\theta$ is the argument of latitude.

With these definitions the *spherical harmonic addition theorem* can be applied in the form

$$P_n(\cos\gamma)=P_n(\sin\beta)P_n(\sin\beta')+2\sum_{m=1}^{n}\frac{(n-m)!}{(n+m)!}P_n^m(\sin\beta)P_n^m(\sin\beta')\cos m(\lambda-\lambda')$$

where $P_n^m(x)$ are the so-called *(unnormalized) associated Legendre polynomials* of degree n and order m and $P_n^0\equiv P_n$. If the volume integral with the dashed coordinates is carried out over these functions weighted with the density $\rho(\boldsymbol{r}')$, we obtain (see, e.g., Kaplan (1976, p. 273)) expressions of the form $C_n^m P_n^m(\sin\beta)\cos m\lambda$ and $S_n^m P_n^m(\sin\beta)\sin m\lambda$, where the multipole coefficients C_n^m und S_n^m represent the performed integrals. By this procedure Eq. (12.2.1) can be written in the standard form, adopted by the International Astronomical Union (IAU) in 1961, as

$$U(r,\beta,\lambda)=-\frac{\mu_\oplus}{r}\left\{1+\sum_{n=1}^{\infty}\left(\frac{R_\oplus}{r}\right)^n\sum_{m=0}^{n}P_n^m(\sin\beta)\left[C_n^m\cos m\lambda+S_n^m\sin m\lambda\right]\right\}\tag{12.2.2}$$

with Earth's standard gravitational parameter $\mu_\oplus=3.9860044105\times10^5\ \mathrm{km^3\,s^{-2}}$ and Earth's mean equatorial radius $R_\oplus=6378.1363$ km (both values as from the Earth gravitational model EGM96). Note, from the condition in Sect. 7.1.1 that $r\geq$ maximal radial mass extension = mean equatorial radius $R_\oplus$ follows that the expansion Eq. (12.2.2) must be terms of $R_\oplus/r$. Because the anisotropic terms of the

gravitational potential are small, it is convenient to separate them from the spherical potential $-\mu_\oplus/r$ and lump them into the residual perturbational potential R

$$U(r,\beta,\lambda) = -\frac{\mu_\oplus}{r} - R(r,\beta,\lambda) \quad @\ r > R_\oplus \tag{12.2.3}$$

with

$$R(r,\beta,\lambda) = \frac{\mu_\oplus}{r}\sum_{n=2}^{\infty}\left(\frac{R_\oplus}{r}\right)^n\left[-J_n P_n(\sin\beta) + \sum_{m=1}^{n} J_{nm} P_n^m(\sin\beta)\cos m(\lambda-\lambda_{nm})\right]$$

Here the conventional definitions and substitutions for studying planetary perturbations

$$J_n := J_{n0} := -C_n^0 \quad m = 0 \tag{12.2.4}$$

$$\left.\begin{aligned} J_{nm}\cos m\lambda_{nm} &:= C_n^m \\ J_{nm}\sin m\lambda_{nm} &:= S_n^m \end{aligned}\right\} \quad m \geq 1$$

were applied resulting for $m \geq 1$ in

$$J_{nm} = \sqrt{\left(C_n^m\right)^2 + \left(S_n^m\right)^2} > 0 \quad \textbf{harmonic coefficients} \tag{12.2.5a}$$

$$\begin{aligned} m\lambda_{nm} &= \arctan\frac{S_n^m}{C_n^m} + \frac{\pi}{2}\left[1 - \operatorname{sgn}\left(C_n^m\right)\right]\cdot\operatorname{sgn}\left(S_n^m\right) \\ &= 2\arctan\frac{S_n^m}{C_n^m + J_{nm}} \end{aligned} \quad \textbf{equilibrium longitudes} \tag{12.2.5b}$$

with J_{nm} the so-called *harmonic coefficients* and λ_{nm} the *equilibrium longitudes*. The term with $\pi/2$ in Eq. (12.2.5a) and the alternative expression thereafter, derived from half the equilibrium longitude angle, ensures that, as required by Eq. (12.2.4), $\operatorname{sgn}(\cos m\lambda_{nm}) = \operatorname{sgn}\left(C_n^m\right)$ and $\operatorname{sgn}(\sin m\lambda_{nm}) = \operatorname{sgn}\left(S_n^m\right)$ and therefore $-180^\circ \leq m\lambda_{nm} \leq +180^\circ$.

Note *For the sake of clarity we recall that in this textbook a potential designated by the letter U is the classical physical potential, which satisfies the equation of motion* $\ddot{\boldsymbol{r}} = -\nabla U = \nabla(\mu/r) + \nabla R$. *In the literature, U is often defined with inverse sign, while the residual potential R is usually defined uniquely as in* Eq. (12.2.3). *The terms with* J_n *have opposite signs to the terms with* J_{nm} *that has historical reasons and is done throughout the literature and here.*

Legendre Polynomials

The Legendre polynomials $P_n(x) \equiv P_n^0(x)$ and associated Legendre polynomials $P_n^m(x)$ can be derived analytically and numerically via the recurrence relations

Recurrence iteration to derive $P_n(x)$ and $P_n^m(x)$

$s := \sin\beta = x$

$c := \cos\beta = \sqrt{1-x^2}$

$P_0 \equiv P_0^0 = 1$

Do $n = 1,\ \infty$

$nP_n = (2n-1)sP_{n-1} - (n-1)P_{n-2}$

$P_n^n = -(2n-1)cP_{n-1}^{n-1} = (-c)^n(2n-1)!!$

Do $m = n-1,\ 0,\ -1$

$(n-m)sP_n^m = cP_n^{m+1} + (n+m)P_{n-1}^m$

End Do

End Do

With this iteration we derive in the following the relevant associated Legendre polynomials $P_n^m(x)$ up to $n = 5$

$$P_2 \equiv P_2^0 = \frac{1}{2}\left(3s^2-1\right),\ P_2^1 = -3sc,\ P_2^2 = 3c^2$$

$$P_3 \equiv P_3^0 = \frac{1}{2}s\left(5s^2-3\right),\ P_3^1 = -\frac{3}{2}c\left(5s^2-1\right),\ P_3^2 = 15sc^2,\ P_3^3 = -15c^3$$

$$P_4 \equiv P_4^0 = \frac{1}{8}\left(35s^4-30s^2+3\right),\ P_4^1 = -\frac{5}{2}sc\left(7s^2-3\right),\ P_4^2 = \frac{15}{2}c^2\left(7s^2-1\right),$$

$$P_4^3 = -105sc^3,\ P_4^4 = 105c^4$$

$$P_5 \equiv P_5^0 = \frac{1}{8}s\left(63s^4-70s^2+15\right),\ P_5^1 = -\frac{15}{8}c\left(21s^4-14s^2+1\right),$$

$$P_5^2 = \frac{105}{2}sc^2\left(3s^2-1\right),\ P_5^3 = -\frac{105}{2}c^3\left(9s^2-1\right),\ P_5^4 = 945sc^4,\ P_5^5 = -945c^5 \tag{12.2.6}$$

Earth's Gravitational Multipoles

Because the detailed density distribution of the Earth is beyond our knowledge, the multipole coefficients C_n^m and S_n^m are available only by measuring them with particular satellites. The most famous and most precise of them is the GRACE satellite mission, which operated from 2002 to 2017. The values thereby obtained are given in Table 12.2. In this representation the origin of the polar reference frame is at the center of Earth's mass and the polar axis is Earth's axis of rotation.

Table 12.2 Multipole coefficients of Earth's gravitational potential

C_n^m	$m = 0$	1	2	3	4	5
$n = 0$	+1.000000					
1	0.00	0.00				
2	−1.082627 × 10−3	0.00	1.5745×10^{-6}			
3	2.5326×10^{-6}	-2.1926×10^{-6}	3.0899×10^{-7}	-1.0055×10^{-7}		
4	1.6196×10^{-6}	5.0880×10^{-7}	7.8418×10^{-8}	-5.9210×10^{-8}	-3.9841×10^{-9}	
5	-2.2730×10^{-7}	5.3180×10^{-8}	1.0559×10^{-7}	1.4930×10^{-8}	-2.2993×10^{-9}	-4.3082×10^{-10}
S_n^m	$m = 0$	1	2	3	4	5
$n = 0$	0.00					
1	0.00	0.00				
2	0.00	0.00	-9.0380×10^{-7}			
3	0.00	-2.6843×10^{-7}	-2.1144×10^{-7}	-1.9722×10^{-7}		
4	0.00	4.4914×10^{-7}	1.4818×10^{-7}	1.2008×10^{-8}	6.5257×10^{-9}	
5	0.00	8.0859×10^{-8}	-5.2329×10^{-8}	7.0973×10^{-9}	3.8671×10^{-10}	1.6482×10^{-9}

J_{nm}/λ_{nm}	$m = 0$	1	2	3	4	5
$n = 2$	**1.082627×10^{-3}**	0.0	1.8155×10^{-6}			
		–	−14.928°			
3	-2.5326×10^{-6}	2.2090×10^{-6}	3.7441×10^{-7}	2.2137×10^{-7}		
		−173.01°	−17.192°	−39.005°		
4	-1.6196×10^{-6}	6.7868×10^{-7}	1.6765×10^{-7}	6.0415×10^{-8}	7.6458×10^{-9}	
		41.436°	31.056°	56.180°	30.351°	
5	-2.2730×10^{-7}	9.6780×10^{-8}	1.1784×10^{-7}	1.6531×10^{-8}	2.3316×10^{-9}	1.7036×10^{-9}
		56.667°	−13.182°	8.4751°	42.613°	20.930°

$J_2 = 1.0826266 \times 10^{-3}$	$J_3 = -2.5326 \times 10^{-6}$	$J_4 = -1.6196 \times 10^{-6}$	$J_5 = -2.2730 \times 10^{-7}$
$J_6 = 5.4068 \times 10^{-7}$	$J_7 = -3.5236 \times 10^{-7}$	$J_8 = -2.0480 \times 10^{-7}$	$J_9 = -1.2062 \times 10^{-7}$

Note *The multipole coefficients* $\overline{C}_{nm}$, $\overline{C}_{nm}$ *as used in geodesy (see e.g., Earth Gravitational Model 1996 (EGM96),* http://cddis.gsfc.nasa.gov/926/egm96/getit.html*) are related to the more common coefficients* C_n^m, S_n^m *adopted also here through*

$$\begin{Bmatrix} C_n^m \\ S_n^m \end{Bmatrix} = (-1)^m \sqrt{\frac{(2-\delta_{0m})(2n+1)(n-m)!}{(n+m)!}} \begin{Bmatrix} \overline{C}_{nm} \\ \overline{S}_{nm} \end{Bmatrix}$$

with Kronecker delta

$$\delta_{0m} = \begin{cases} 1 & @\ m = 0 \\ 0 & @\ m > 0 \end{cases}$$

Table 12.2 is incomplete. In fact, multipole coefficients are known today of order up to $n = 2159$. Some of them vanish for the following reasons:

- $S_n^0 = 0$, because for $m = 0$ $S_n^0 \sin(0 \cdot \lambda) = 0$. Therefore the coefficients S_n^0 are undetermined and can be set to zero;
- $C_1^0 = C_1^1 = S_1^1 = 0$, because the center of mass is chosen to be at the origin of the reference frame, which is why the sum in Eq. (12.2.3) starts with $n = 2$;
- $C_2^1 = S_2^1 = 0$, because the z-axis points along Earth's principal moment of inertia;
- S_2^2 would vanish if the coordinate axes would coincide with the principal axes of inertia (see Sect. 15.1.1). But traditionally the x-axis is chosen to lie in the Greenwich meridian.

Physically speaking, the successive terms of the sums in Eq. (12.2.2) correspond to a stepwise spherical approximation (multipole approximation) of the anisotropic gravitational potential, i.e., of the geoid. The terms $P_n^m(\sin\beta)\cos(m\lambda)$ and $P_n^m(\sin\beta)\sin(m\lambda)$ are so-called *spherical harmonics* (see Figs. 12.5 and 12.6). They are the spherical distribution functions (multipoles) of order (n, m), and are

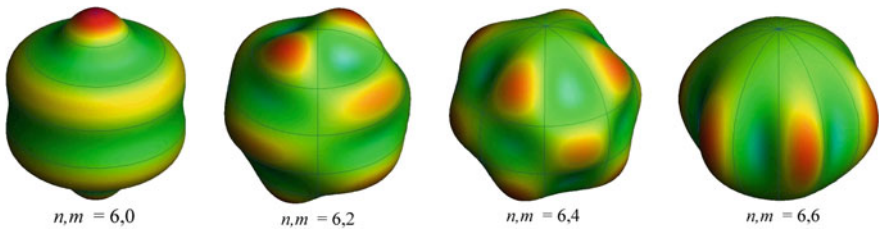

Fig. 12.5 The spherical harmonics of degree 6 and even order. *Credit* GFZ Potsdam

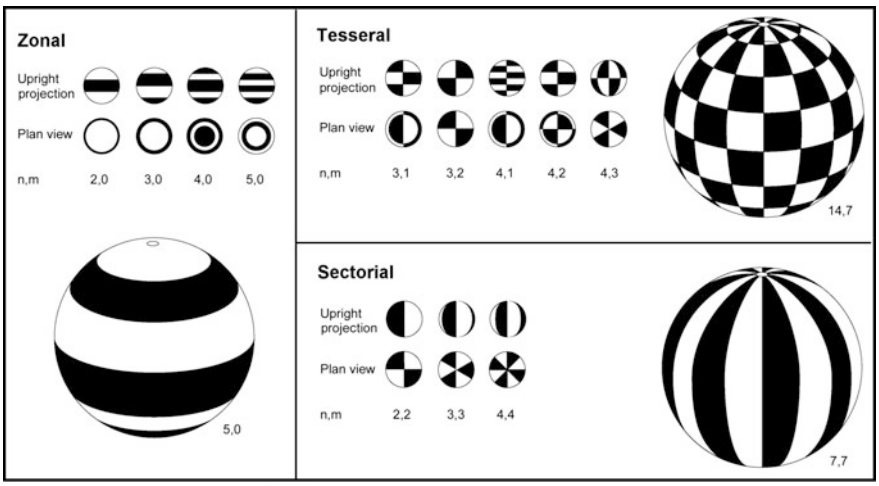

Fig. 12.6 The nodal surfaces of spherical harmonics of degree n and order m: zonal harmonics, tesseral harmonics, and sectorial harmonics

called *zonal harmonics* for $(n, 0)$ because they describe just latitudinal variations, *sectorial harmonics* for (n, n) describing only longitudinal variations, and *tesseral harmonics* for $(n,\ 0 < m < n)$ describing mixed variations. The multipole coefficients J_{nm} as given in Table 12.2 determine the strength of these multipoles: $J_0 = -C_0^0 = 1$ causes the predominant geoid sphere, $J_2 = -1.082627 \times 10^{-3}$ the **oblate spheroid**, and the J_{nm} of order 10^{-6} the general shape of the potato (see figures of the potato on color plates on page 568 and 569).

Note *In earlier literature one may find the statement that Earth is pear shaped (symmetry axis = polar axis, pear stalk at south pole) beyond the spheroid. This discovery dates back to a publication of J. A. O'Keefe, A. Eckles, and R. Squires from 1959. They derived a pear shape from the analysis of long-periodic effects of orbital eccentricities of the first US satellite Vanguard I. Because such effects stem only from zonal multipoles (see below), from this method only the C_n^0 coefficients (in particular the pear shaped C_3^0,) are derivable and not the C_2^2 and C_3^1 coefficients, which extend the pear to a potato.*

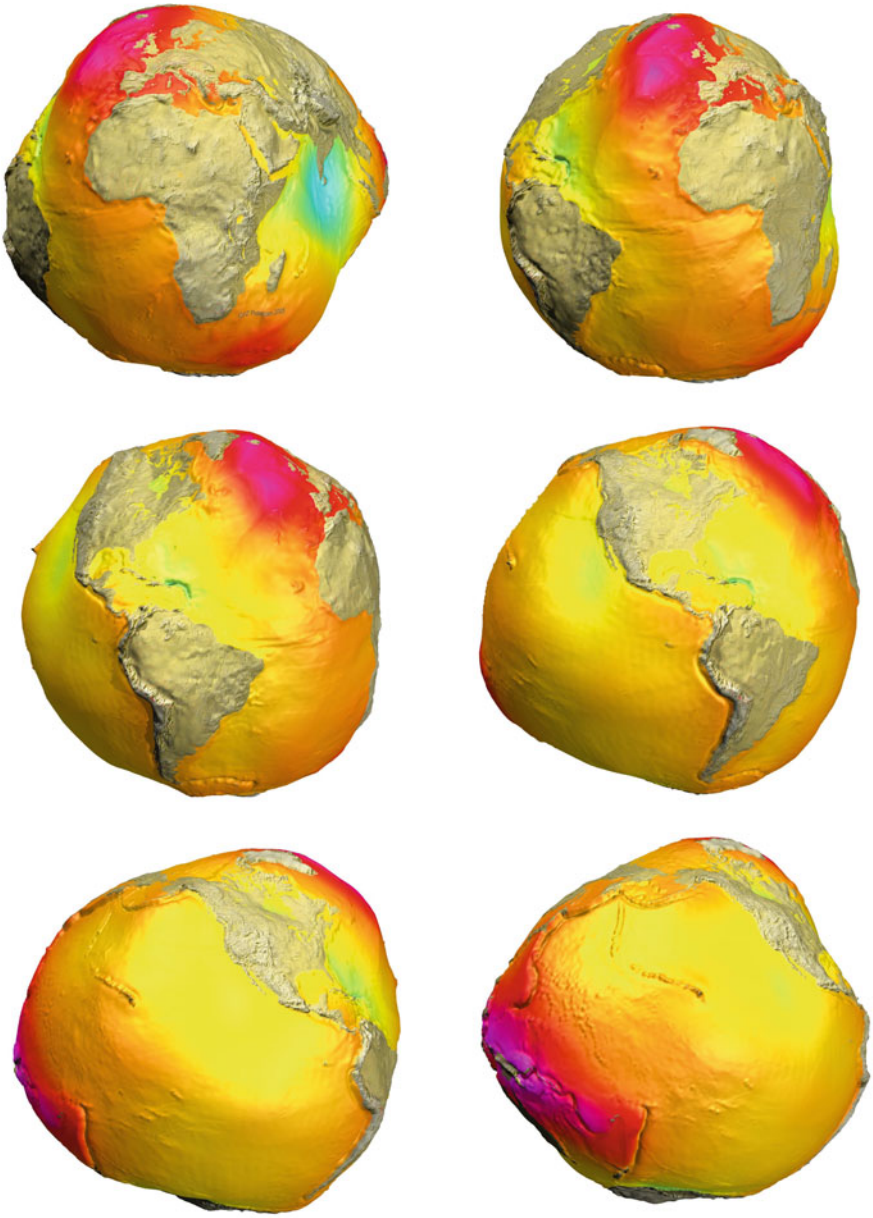

The potato residual of the geoid at different view angles in the equatorial plane

Credit GFZ Potsdam

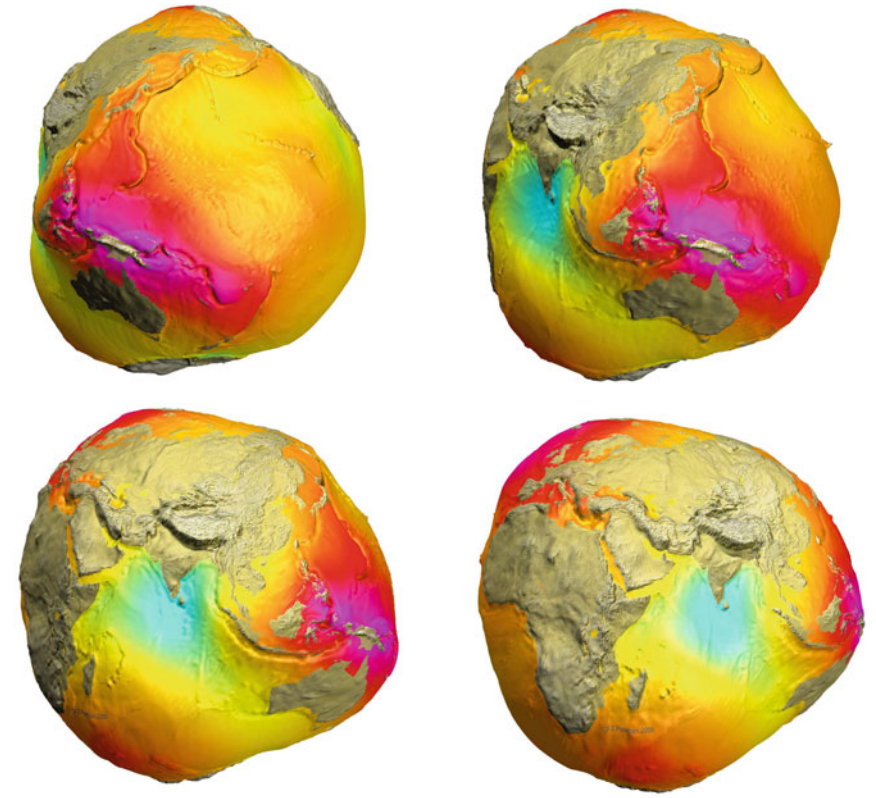

The potato residual of the geoid at different view angles in the equatorial plane (continued)

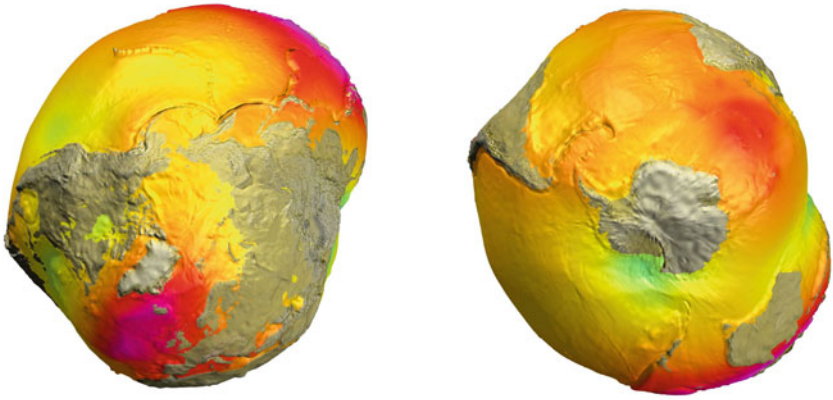

The potato residual of the geoid as viewed from the North Pole (left) and the South Pole (right)

Credit GFZ Potsdam

12.2.3 Lagrange's Planetary Equations

In order to understand the key effects of the gravitational anisotropy on orbital elements, we shall now look for analytic perturbation solutions. This is facilitated by the special property that the gravitational perturbation can be expressed in terms of a potential R, and hence the perturbational force and the perturbational acceleration $\boldsymbol{a}_p = (a_r, a_\theta, a_h)_{RSW}$ (see Sect. 12.1.2) is just the gradient of it (see Eq. 7.1.5)

$$\boldsymbol{a}_p = \frac{1}{m}\boldsymbol{F}_p = -\frac{dR}{d\boldsymbol{r}}$$

If this gradient is inserted into the Gaussian variational Eq. (12.1.4), then the time-derivatives of the orbital elements can simply be expressed by partial derivatives of the perturbation function R. Linear perturbation theory thus delivers the so-called *Lagrange's planetary equations* (see, e.g., Schaub and Junkins 2003, p. 508f)

$$\begin{aligned}
\dot{a} &= \frac{2a}{h}\sqrt{1-e^2}\,\frac{\partial R}{\partial M} \\
\dot{e} &= \frac{1-e^2}{he}\left[\sqrt{1-e^2}\,\frac{\partial R}{\partial M} - \frac{\partial R}{\partial \omega}\right] \\
\dot{i} &= \frac{1}{h\,\sin i}\left[\cos i\,\frac{\partial R}{\partial \omega} - \frac{\partial R}{\partial \Omega}\right] \\
\dot{\omega} &= \frac{1}{h}\left[\frac{1-e^2}{e}\frac{\partial R}{\partial e} - \cot i\,\frac{\partial R}{\partial i}\right] \\
\dot{\Omega} &= \frac{1}{h\,\sin i}\frac{\partial R}{\partial i} \\
\dot{M} - n &= -\frac{\sqrt{1-e^2}}{h}\left[\frac{1-e^2}{e}\frac{\partial R}{\partial e} + 2a\frac{\partial R}{\partial a}\right]
\end{aligned}$$

Lagrange's planetary equations (LPEs) (12.2.7)

These are the basic equations by which we will qualitatively study the perturbational effects in Sect. 12.3.

12.2.4 Numerical Perturbation Methods

In this section we consider the different numerical methods to determine a perturbed orbit.

Cowell's Method by Recurrence Iteration
According to Eq. (7.7.2) the equation of motion for a general gravitational potential U reads

$$\ddot{\boldsymbol{r}} = -\frac{dU}{d\boldsymbol{r}} \tag{12.2.8}$$

Employing Eq. (12.2.2) for U and choosing an Earth-fixed Cartesian reference system, in which the trajectory vector is $\boldsymbol{r} = (x, y, z)$, this equation can be solved numerically to determine the perturbed orbit. This is known as **Cowell's method**. Owing to its high accuracy it is widely used today although at the cost of high computing time.

For practical purposes it can be shown (see Montenbruck and Gill (2000)) that the terms $V_{n,m}(\boldsymbol{r})$, $W_{n,m}(\boldsymbol{r})$; $n = 0, \ldots, n_{\max}+1$; $m = 0, \ldots, n$ can be calculated recursively by the following iteration:

Recurrence Iteration

$$\alpha_x := \frac{xR_\oplus}{r^2}, \alpha_y := \frac{yR_\oplus}{r^2}, \alpha_z := \frac{zR_\oplus}{r^2}, \alpha_R := \frac{R_\oplus^2}{r^2}$$

$$V_{0,0} = \frac{R_\oplus}{r}, \quad W_{0,0} = 0$$

Do $m = 0, n_{\max}$

$$V_{m-1,m} = W_{m-1,m} = 0$$

Do $n = m, n_{\max}$

$$V_{n+1,m} = \alpha_z \frac{2n+1}{n-m+1} \cdot V_{n,m} - \alpha_R \frac{n+m}{n-m+1} \cdot V_{n-1,m}$$

$$W_{n+1,m} = \alpha_z \frac{2n+1}{n-m+1} \cdot W_{n,m} - \alpha_R \frac{n+m}{n-m+1} \cdot W_{n-1,m}$$

End Do

$$V_{m+1,m+1} = (2m+1)\left(\alpha_x V_{m,m} - \alpha_y W_{m,m}\right)$$

$$W_{m+1,m+1} = (2m+1)\left(\alpha_x W_{m,m} + \alpha_y V_{m,m}\right)$$

End Do

Remark: *Observe that the recurrence iteration implies* $W_{n,0} = 0$

With these quantities Eq. (12.2.8) can be rewritten as follows:

$$\begin{aligned}
\ddot{x} &= -\frac{\mu_\oplus}{R_\oplus^2}\sum_{n=0}^{n_{\max}}\left[C_{n0}V_{n+1,1} + \frac{1}{2}\sum_{m=1}^{n}\left\{C_{nm}V_{n+1,m+1} + S_{nm}W_{n+1,m+1}\right.\right. \\
&\quad \left.\left. -\frac{(n-m+2)!}{(n-m)!}\left(C_{nm}V_{n+1,m-1} + S_{nm}W_{n+1,m-1}\right)\right\}\right] \\
\ddot{y} &= -\frac{\mu_\oplus}{R_\oplus^2}\sum_{n=0}^{n_{\max}}\left[C_{n0}W_{n+1,1} + \frac{1}{2}\sum_{m=1}^{n}\left\{C_{nm}W_{n+1,m+1} - S_{nm}V_{n+1,m+1}\right.\right. \\
&\quad \left.\left. +\frac{(n-m+2)!}{(n-m)!}\left(C_{nm}W_{n+1,m-1} - S_{nm}V_{n+1,m-1}\right)\right\}\right] \\
\ddot{z} &= -\frac{\mu_\oplus}{R_\oplus^2}\sum_{n=0}^{n_{\max}}\sum_{m=1}^{n}(n-m+1)\left(C_{nm}V_{n+1,m} + S_{nm}W_{n+1,m}\right)
\end{aligned} \tag{12.2.9}$$

with

$$\left\{\begin{matrix} C_{nm} \\ S_{nm} \end{matrix}\right\} = \sqrt{\frac{(2-\delta_{0m})(2n+1)(n-m)!}{(n+m)!}}\left\{\begin{matrix} \overline{C}_{nm} \\ \overline{S}_{nm} \end{matrix}\right\} = (-1)^m\left\{\begin{matrix} C_n^m \\ S_n^m \end{matrix}\right\}$$

and

$$\delta_{0m} = \begin{cases} 1 & @\ m = 0 \\ 0 & @\ m > 0 \end{cases}$$

and $\overline{C}_{nm}, \overline{S}_{nm}$ given at ftp://cddis.gsfc.nasa.gov/pub/egm96/general_info/egm96_to360.ascii plus ftp://cddis.gsfc.nasa.gov/pub/egm96/general_info/readme.egm96, and

$$\begin{aligned}
\mu_\oplus &= 3.986004415 \times 10^5\ \text{km}^3\,\text{s}^{-2} \\
R_\oplus &= 6378.1363\ \text{km}
\end{aligned}$$

If one takes into account only the biggest perturbation, the spheroid, $n_{\max} = 2$ and $m = 0$, the explicit equations read:

$$\begin{aligned}
\ddot{x} &= -\frac{x\mu_\oplus}{r^3}\left[1 + C_2^0\frac{3}{2}\frac{R_\oplus^2}{r^2}\left(5\frac{z^2}{r^2} - 1\right)\right] \\
\ddot{y} &= -\frac{y\mu_\oplus}{r^3}\left[1 + C_2^0\frac{3}{2}\frac{R_\oplus^2}{r^2}\left(5\frac{z^2}{r^2} - 1\right)\right] = \frac{y}{x}\ddot{x} \\
\ddot{z} &= -\frac{z\mu_\oplus}{r^3}\left[1 + C_2^0\frac{3}{2}\frac{R_\oplus^2}{r^2}\left(5\frac{z^2}{r^2} - 3\right)\right]
\end{aligned} \tag{12.2.10}$$

So, for calculating a trajectory, first the maximum order $n_{\max}$ of the perturbation is chosen depending on the accuracy of the initial data and of the orbit needed. Then the coupled differential Eqs. (12.2.9) or (12.2.10) are solved, whereby one of the currently best solvers is the Runge–Kutta–Nyström algorithm RKN12(10)17M (see Brankin et al. 1989), which can be found in the NAG Library under the name of D02LAF. The initial step size should be $h = 0.1$ for all Keplerian problems. Note that also other perturbations like neighboring planets can easily be taken into account by Eq. (12.2.9) by just adding the perturbational terms in the Cartesian coordinate form. Observe that the solution is given in an Earth-fixed reference system. In order to find the result in an inertial (sidereal) system an appropriate coordinate transformation has to be applied to the solution $\boldsymbol{r} = (x, y, z)$.

Encke's Method

If the perturbational acceleration $\boldsymbol{a}_p$ is very small, as in our case of gravitational perturbation, it can be separated and calculated as such. The undisturbed Keplerian orbit $\boldsymbol{r}_0(t)$ then is called *osculating orbit*, and the residual $\boldsymbol{\delta}(t) := \boldsymbol{r} - \boldsymbol{r}_0$. Figure 12.7 illustrates the defined values. It can be shown that for this residual the following equation of motion holds (see, e.g., Schaub and Junkins 2003)

$$\ddot{\boldsymbol{\delta}} = -\frac{\mu}{r_0^3}\left(3q\frac{1+q+q^2/3}{1+(1+q)^{3/2}}\boldsymbol{r}+\boldsymbol{\delta}\right)+\boldsymbol{a}_p \approx \frac{\mu}{r_0^3}\left(6\frac{\boldsymbol{\delta}\cdot\boldsymbol{r}}{r^2}\boldsymbol{r}-\boldsymbol{\delta}\right)+\boldsymbol{a}_p \qquad (12.2.11)$$

with

$$q = \frac{\boldsymbol{\delta}\cdot\boldsymbol{\delta} - 2\boldsymbol{\delta}\cdot\boldsymbol{r}}{r^2}$$

This differential equation is also solved with a high-quality Runge–Kutta algorithm. This approach of separating the perturbation from the osculating orbit is called **Encke's method**. It is a very accurate method, as the numerical integration only treats the perturbation in question, and does not have to "drag along" the full Keplerian orbit. However, because it is not well documented and tested in literature

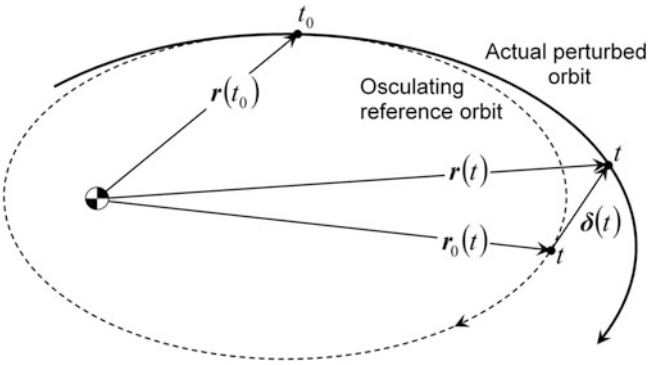

Fig. 12.7 Illustration of Encke's method

and due to the increased numerical precision of today's CPUs it is more convenient to apply the above recurrence type of Cowell's method.

Solving the LPEs
Another method is to directly integrate the LPEs (12.2.7) by applying the residual gravitational term R of Eq. (12.2.3). Although this method is fast and yields a good accuracy it is not widely used in the space community because it is not well documented (see Herrick (1972) for method details) and the dominance of Cowell's method.

12.3 Gravitational Perturbation Effects

12.3.1 Classification of Effects

General Considerations
The gravitational potential U as given by Eq. (12.2.3) and depicted by the geoid in Fig. 12.3 is solely position-dependent. Therefore (see insert Box *Conservative Force* in Sect. 7.1.2 and Fig. 7.3) Earth's gravitational force can still be derived as a gradient of U, $\boldsymbol{F} = -m \cdot dU/d\boldsymbol{r}$, and hence is a conservative field, implying that the work done by Earth's gravitational field on a closed orbit is zero. So, in any gravitational potential the orbital energy over one closed orbital revolution, which essentially is one orbital period (strictly speaking: one period of long-periodic variations; see Eq. (12.3.6)), remains unchanged and according to Eq. (7.3.19) the mean semi-major axis therefore must remain constant

$$\bar{a} \equiv \langle a \rangle_P = const \quad @ \text{ geoid} \tag{12.3.1}$$

However, the gravitational force derived from the geoid is no longer simply radial

$$\boldsymbol{F}(\boldsymbol{r}) = -m\frac{dU}{d\boldsymbol{r}} \neq -mg(r)\hat{\boldsymbol{r}} \quad @ \text{ geoid}$$

and therefore is no longer a central force field, though still being conservative. This is because the gravitational potential residual $R(r, \beta, \lambda)$ as given in Eq. (12.2.3), and hence $\boldsymbol{F}$, does not depend solely on r, as did the mass point potential $-\mu/r$, but also on β, λ. We saw from Sect. 7.2.2 that a non-central force field quite generally exerts a torque on the orbit and thus changes its angular momentum both in orientation and absolute value. In particular, the orbital plane will tilt. We therefore expect that

> The small non-spherical fraction of Earth's gravitational field slightly varies all orbital elements over time. This holds even if the elements are averaged over one orbital period, except for the semi-major axis.

This general behavior can be seen also from Lagrange's planetary equations (12.2.7).

Mean Orbital Elements and Short-Periodic Variations

Generally, a gravitational perturbation affects the trajectory momentarily at any point along its path. Therefore, the orbital elements $\vartheta_i \in (a, e, i, \Omega, \omega, M - n \cdot t)$ vary periodically and significantly over each orbit, which is on the order of an hour (LEO) to a day (GEO). Usually, we are not interested in such recurring periodic effects in the course of an orbit. Therefore we average the effects over one orbital period T and define the mean orbital elements as

$$\bar{\vartheta}_i(t) := \langle \vartheta_i \rangle_P = \frac{1}{T} \cdot \int_0^T \vartheta_i \cdot dt = \frac{1}{2\pi} \int_0^{2\pi} \vartheta_i \cdot dM \quad \textbf{mean orbital elements} \tag{12.3.2}$$

The latter holds because $M = n(t - t_0)$ and hence $dt = dM/n = T/2\pi \cdot dM$. Given the mean orbital elements we define the short-periodic deviations and *short-periodic variations* in the course of an orbit as

$$\vartheta_{i,short}(M) := \vartheta_i - \bar{\vartheta}_i \quad \textbf{short-periodic deviations} \tag{12.3.3}$$

$$\dot{\vartheta}_{i,short}(M) := \dot{\vartheta}_i - \dot{\bar{\vartheta}}_i \quad \textbf{short-periodic variations} \tag{12.3.4}$$

which vary with the **fast variable** true anomaly θ or mean anomaly M, equivalently (see for instance Eq. (12.3.22)).

Secular Elements and Long-Periodic Variations

Though short-periodic effects are significant, they often are opposite on the two halves of an orbit, such that overall they fully cancel out over one orbital period. However, as we will see in Sect. 12.3.3, oblateness perturbations constantly vary the argument of periapsis ω such that the line of apsides constantly rotates. A slowly rotating apsidal line implies that over one orbit the perturbational effects at any θ are little different from those at $-\theta$. This imperfect cancellation of opposite contributions accumulates and leads to slow variations of the mean orbital elements. Therefore, $\bar{\omega}$ is a **slow variable**, which may modulate the mean orbital elements in pace with the rotation of the line of apsides, the period being typically a couple of months for Earth. By the same token $\bar{\Omega}$ in general is also a slow variable, and hence $\dot{\bar{\vartheta}}_i(\bar{\omega}, \bar{\Omega})$. We can also remove these long-period variations by integration over both one revolution of the line of apsides and the line of nodes, which results in the so-called secular variations

$$\dot{\vartheta}_{i,\mathrm{sec}}(t) := \frac{1}{4\pi^2} \int_0^{2\pi} \int_0^{2\pi} \dot{\bar{\vartheta}}_i \cdot d\bar{\omega} \cdot d\bar{\Omega} \quad \textbf{secular variations} \tag{12.3.5}$$

Secular variations of orbital elements usually vary steadily and monotonically (usually linearly) with time so that secular orbital elements $\vartheta_i = \vartheta_{i,0} + \dot{\vartheta}_i \cdot t$ grow progressively and unbounded.

Variations owing to slow variables, so-called **long-periodic** variations, can thus be separated by

$$\dot{\vartheta}_{i,long}(\bar{\omega}, \bar{\Omega}) \equiv \dot{\bar{\vartheta}}_i - \dot{\vartheta}_{i,\text{sec}} \quad \textbf{long-periodic variations} \tag{12.3.6}$$

In summary we have

$$\dot{\vartheta}_i = \dot{\bar{\vartheta}}_i + \dot{\vartheta}_{i,short} = \dot{\vartheta}_{i,\text{sec}} + \dot{\vartheta}_{i,long}(\bar{\Omega}, \bar{\omega}) + \dot{\vartheta}_{i,short}(M) \tag{12.3.7}$$

Note that according to Eq. (7.3.11) $M = n(t - t_p) = \langle \omega \rangle_P (t - t_p)$ and hence is already a quantity averaged over one orbital period.

12.3.2 Removing Short-Periodic Effects

In the following we are not interested in the recurring short-periodic effects in the course of one orbit, but only in the variations of the mean orbital elements. From the LPEs (12.2.7) we see that $\dot{\vartheta}_i \propto \partial R / \partial \vartheta_i$. Hence the variation of the mean orbital elements are determined as

$$\dot{\bar{\vartheta}}_i = \frac{1}{2\pi} \int_0^{2\pi} \dot{\vartheta}_i \cdot dM \propto \frac{1}{2\pi} \int_0^{2\pi} \frac{\partial R}{\partial \vartheta_j} \cdot dM = \frac{\partial \bar{R}}{\partial \vartheta_j} \tag{12.3.8}$$

with

$$\bar{R} := \frac{1}{T} \int_0^T R \cdot dt = \frac{1}{2\pi} \int_0^{2\pi} R \cdot dM =: \langle R \rangle_{P,M}$$

From Eq. (12.2.3) we obtain the mean residual perturbational potential

$$\begin{aligned} \bar{R}(r, \beta) &= -\left\langle \frac{\mu_\oplus}{r} \sum_{n=2}^{\infty} \left(\frac{R_\oplus}{r} \right)^n \sum_{m=0}^{n} J_{nm} P_n^m (\sin \beta) \cos m(\lambda - \lambda_{nm}) \right\rangle_{P,M} \\ &= -\frac{\mu_\oplus}{a} \left(\frac{R_\oplus}{a} \right)^n \sum_{n=2}^{\infty} \sum_{m=0}^{n} J_{nm} \left\langle \left(\frac{a}{r} \right)^{n+1} P_n^m (\sin \beta) \cos m(\lambda - \lambda_{nm}) \right\rangle_{P,M} \end{aligned}$$

In order to carry out the averaging integration, we recall from Napier's rules of spherical trigonometry that $\sin \beta = \sin i \cdot \sin(\theta + \omega)$ holds between inclination i, argument of periapsis ω, and true anomaly θ. Owing to this and because the orbit

equation (7.3.5) also relates r and θ we switch the variables $dM \to d\theta$ to carry out the integral. We have from Eq. (7.3.12)

$$dM = \left(\frac{r}{a}\right)^2 \frac{1}{\sqrt{1-e^2}} d\theta$$

With this we get for the average residual perturbational potential

$$\bar{R}(r,\beta) = -\frac{\mu_\oplus}{a\sqrt{1-e^2}} \left(\frac{R_\oplus}{a}\right)^n \sum_{n=2}^{\infty} \sum_{m=0}^{n} J_{nm} \left\langle \left(\frac{a}{r}\right)^{n-1} P_n^m(\sin\beta) \cos m(\lambda - \lambda_{nm}) \right\rangle_{P,\theta} \tag{12.3.9}$$

Note that in this notation actually $a \equiv \bar{a}$, $e \equiv \bar{e}$ for convenience, which holds for the rest of this chapter. Substituting the orbit Eq. (7.3.5)

$$\frac{a}{r} = \frac{1 + e\,\cos\theta}{1-e^2}$$

delivers

$$\begin{aligned} \bar{R}(r,\beta) = &-\frac{\mu_\oplus}{a}\sqrt{1-e^2}\left[\frac{R_\oplus}{a(1-e^2)}\right]^n \\ &\times \sum_{n=2}^{\infty}\sum_{m=0}^{n} J_{nm} \left\langle (1+e\cos\theta)^{n-1} P_n^m(\sin\beta)\cos m(\lambda-\lambda_{nm}) \right\rangle_{P,\theta} \end{aligned}$$

For further convenience (see Eqs. (12.3.15) and (12.3.20)) we now define the *reduced harmonic coefficients*

$$j_{nm} := \frac{3}{2} J_{nm} \left[\frac{R_\oplus}{a(1-e^2)}\right]^n \quad \textbf{reduced harmonic coefficients} \tag{12.3.10}$$

The common factor $3/2$ is a remnant of orbit averaging. Observe that for the derivatives $\partial R/\partial e$ in the LPEs, Eq. (12.2.7), it needs to be considered that the reduced harmonic coefficients are a function of eccentricity, i.e. $j_{nm}(e)$. With this we finally obtain the mean residual perturbational potential

$$\begin{aligned} \bar{R} &= \sum_{n=2}^{\infty}\sum_{m=0}^{n} \bar{R}_{nm} \\ \bar{R}_{nm} &:= -\frac{2}{3}\frac{\mu_\oplus}{a}\sqrt{1-e^2}\, j_{nm}(e) \cdot \bar{P}_n^m \\ \bar{P}_n^m &:= \left\langle (1+e\,\cos\theta)^{n-1} P_n^m(\sin\beta)\cos m(\lambda-\lambda_{nm}) \right\rangle_{P,\theta} \end{aligned} \tag{12.3.11}$$

12.3.3 Oblateness Perturbation

Table 12.2 shows that Earth's oblateness, given by $(n,m)=(2,0)$, $C_2^0=-J_2=1.0826266\times 10^{-3}$ and depicted in Fig. 12.3a, constitutes by far the strongest perturbation of the gravitational potential. We therefore want study the effects of this perturbation in detail.

Relation to Earth's Polar Flattening
It can be shown (exercise, Problem 12.2) that

$$J:=\frac{3}{2}J_2\approx f\left(1-\frac{1}{2}f\right)-\frac{\omega^2R_\oplus^3}{2\mu_\oplus}\left(1-\frac{3\omega^2R_\oplus^3}{2\mu_\oplus}-\frac{2}{7}f\right)\approx f-\frac{\omega^2R_\oplus^3}{2\mu_\oplus} \tag{12.3.12}$$

where the defined quantity J is frequently used in literature and has the indicated relation to Earth's polar flattening $f:=\left(R_\oplus-R_{polar}\right)/R_\oplus\approx 1/298.264$ with $R_\oplus\equiv R_{equatorial}$.

Average Oblateness Potential
The oblateness perturbation is a enlightening case to see how the removal of the short-periodic effects works. With $P_2\equiv P_2^0=\frac{1}{2}\left(3\sin^2\beta-1\right)$ from Eq. (12.2.6) we have from Eq. (12.3.11)

$$\begin{aligned}\bar{P}_2&=-\frac{1}{2}\left\langle(1+e\,\cos\theta)\left(1-3\sin^2\beta\right)\right\rangle_{P,\theta}\\&=-\frac{1}{2}\left[\left\langle(1+e\,\cos\theta)\right\rangle_{P,\theta}-3\left\langle(1+e\,\cos\theta)\sin^2\beta\right\rangle_{P,\theta}\right]\end{aligned}$$

In order to perform the averaging over one period, we need to express β in terms of θ. This is given by Napier's rule $\sin\beta=\sin i\cdot\sin(\theta+\omega)$, from which follows

$$\sin^2\beta=\sin^2 i\cdot\sin^2(\theta+\omega)=\frac{1}{2}\sin^2 i[1-\cos 2(\theta+\omega)]$$

Because $\cos\theta$ and $\cos 2(\theta+\omega)$ are periodic functions of θ, integrals comprising these two terms vanish over one period. Thus we have

$$\begin{aligned}\left\langle(1+e\,\cos\theta)\right\rangle_{P,\theta}&=\left\langle 1\right\rangle_{P,\theta}+e\left\langle\cos\theta\right\rangle_{P,\theta}=1+0=1\\\left\langle(1+e\,\cos\theta)\sin^2\beta\right\rangle_{P,\theta}&=\left\langle\sin^2\beta\right\rangle_{P,\theta}=\frac{1}{2}\sin^2 i\left\langle 1-\cos 2(\theta+\omega)\right\rangle_{P,\theta}=\frac{1}{2}\sin^2 i\end{aligned}$$

hence

$$\bar{P}_2=-\frac{1}{2}\left(1-\frac{3}{2}\sin^2 i\right) \tag{12.3.13}$$

We finally get for the average oblateness potential

$$\bar{R}_2 = \frac{\mu_\oplus j_2(e)}{3a}\sqrt{1-e^2}\left(1-\frac{3}{2}\sin^2 i\right) \tag{12.3.14}$$

Variation of Orbital Elements

We now carry out the partial derivatives according to Eq. (12.3.8), which can be done straightforwardly, and get from Eq. (12.2.7) the variations of the orbital elements averaged over one period, i.e., $\dot{\vartheta} \equiv \bar{\dot{\vartheta}} := \langle \dot{\vartheta} \rangle_P$, $\dot{\vartheta} = \dot{a}, \dot{e}, \dot{i}, \dot{\omega}, \dot{\Omega}, \dot{M}$

$$\begin{aligned}
&\dot{\Omega}_{\text{sec}} = -nj_2 \cos i && \textbf{regression of nodes}\\
&\dot{\omega}_{\text{sec}} = 2nj_2\left(1-\frac{5}{4}\sin^2 i\right) && \textbf{progression of line of apsides}\\
&\dot{M}_{\text{sec}} - n = nj_2\sqrt{1-e^2}\left(1-\frac{3}{2}\sin^2 i\right) && \textbf{progression of epoch}\\
&\dot{a}_{\text{sec}} = \dot{e}_{\text{sec}} = \dot{i}_{\text{sec}} = 0
\end{aligned} \tag{12.3.15}$$

with

$$n = \sqrt{\frac{\mu_\oplus}{a^3}},\ j_2 = \frac{3}{2}J_2\left[\frac{R_\oplus}{a(1-e^2)}\right]^2 > 0,$$
$$J_2 = -C_2^0 = 0.0010826266$$

First we note that all these variations of the mean orbital elements are not periodic but **secular variations**, i.e., they constantly increase with time. Thus, after one orbital period T the node has shifted by $\Delta\Omega = \dot{\Omega}_{\text{sec}}\, T$, the periapsis by $\Delta\omega = \dot{\omega}_{\text{sec}}\, T$ (see Figs. 12.9 and 12.2), and the orbital phase by $\Delta M = \left(\dot{M}_{\text{sec}} - n\right) T$. The progression or regression of the line of apsides due to $\Delta\omega$ is called *orbital* or *apsidal precession*.

Second, the averaged variations vanish at critical inclinations, namely

$$\begin{aligned}
\dot{\Omega}_{\text{sec}} &= 0 \quad @\ i_{crit} = 90^\circ\\
\dot{\omega}_{\text{sec}} &= 0 \quad @\ i_{crit} = \arcsin\frac{2}{\sqrt{5}} = 63.43^\circ\\
\dot{M}_{\text{sec}} &= n \quad @\ i_{crit} = \arcsin\sqrt{\frac{2}{3}} = 54.74^\circ
\end{aligned}$$

Expanding the term n by $R_\oplus^{3/2}$ and with $\sqrt{\mu_\oplus/R_\oplus^3} = 1.23945 \times 10^{-3}\text{s}^{-1}$ the term nj_2 can be expressed for Earth in the convenient form

$$nj_2 = 9.96404 \cdot \frac{(R_\oplus/a)^{7/2}}{(1-e^2)^2}\ \left[^\circ\ \text{day}^{-1}\right] \quad @\ \text{Earth} \tag{12.3.16}$$

So, for low Earth orbits $nj_2 \approx 7^\circ\ \text{day}^{-1}$. Therefore in LEO $\Delta\Omega$ and $\Delta\omega$ are typically of order 0.5° per revolution or a couple of degrees per day and are therefore of high significance for orbit determination.

The shift of nodes caused by the oblateness of the Earth can be explained as follows: the oblateness can be considered a bulge around the equator of a spherical Earth (see Fig. 12.8), which attracts the body on its orbit. This causes a torque triggering the rotation of the orbital plane (see Fig. 12.9), just as with a spinning top.

The total effect of the equatorial bulge on the orbit can be understood as follows: if its gravitational pull is considered as continuous kick-burns of type $\delta v_{\perp\perp} \propto \sin(\theta+\omega)$ and type $\delta v_{\perp\text{O}} \propto \cos(\theta+\omega)$. According to Eq. (8.1.1) this causes $\delta e(-\theta) = -\delta e(\theta)$ and $\delta i(-\theta) = -\delta i(\theta)$, i.e., the effects cancel out over one period, and therefore $\langle \delta a \rangle_P = \langle \delta e \rangle_P = \langle \delta i \rangle_P = 0$. On the other hand $\delta\omega(-\theta) = \delta\omega(\theta)$ and $\delta\Omega(-\theta) = \delta\Omega(\theta)$, i.e., they sum up and hence $\langle \delta\Omega \rangle_P \neq 0$, implying a shift of the node, and $\langle \delta\omega \rangle_P \neq 0$, a shift of the periapsis and thus also a shift of the epoch, δt_0. For inclinations $i < 63.4^\circ$ the periapsis shifts along the line of motion (progression of the line of apsides). Therefore the orbital period increases and accordingly the mean anomaly and the epoch. The two bordering inclinations, at which the shift of line of apsides and the shift of epoch change direction, do not coincide, as one would expect, is due to the minor contribution of the shift of nodes to the orbital period. In conclusion it can be said that

> The oblateness of the Earth—the by far biggest contribution to a variation of orbital elements—only changes the orientation of the elliptic orbit, but not its size and its shape.

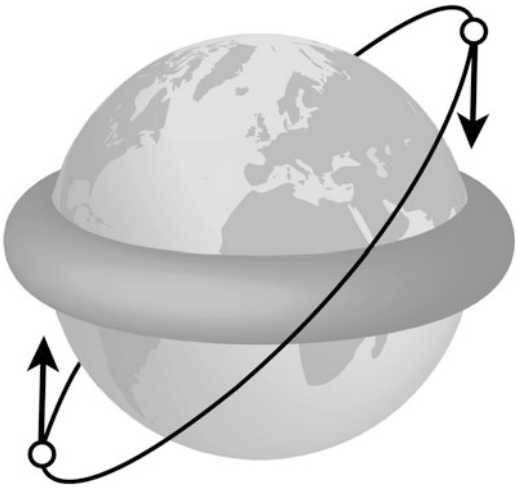

Fig. 12.8 Oblateness of the Earth interpreted as an equatorial bulge attracting the orbiting body

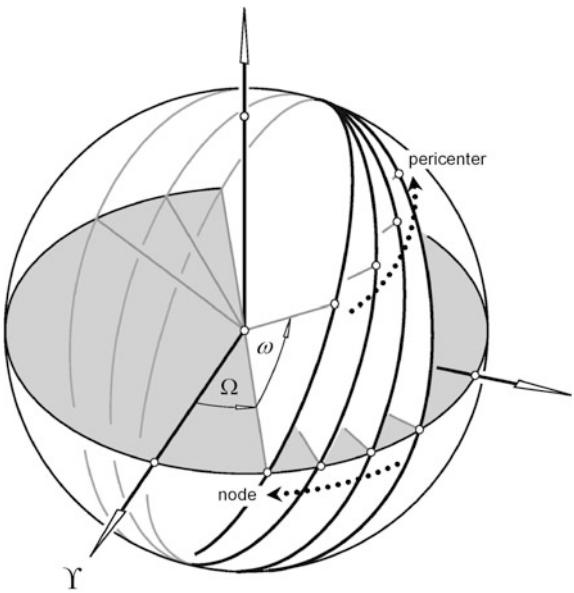

Fig. 12.9 The joint orbital regression of nodes and progression of the line of apsides

The Perturbed Elliptic Orbit

Having derived the variation of orbital elements under oblateness perturbation, we are now able to determine the trajectory in the orbital plane. To include oblateness perturbations in the orbit equation we have to reconsider the motion in the orbit. Under gravitational perturbations the body in the orbit suffers the positional shift $\left(\dot{M} - n\right)t$ and the rotation of the orbit's line of apsides is $\dot{\omega}\, t$. For the radial position only the position relative to the periapsis matters. By assuming for the sake of simplicity $t_0 = 0$ and $\omega(t = 0) = 0$, we have for the argument of periapsis $\omega(t) = \dot{\omega} \cdot t$ with $\dot{\omega} = const$. According to Sect. 12.1.2 the orbit equation 7.3.5 therefore reads

$$r = \frac{p}{1 + e \cdot \cos(\theta - \omega)} = \frac{p}{1 + e \cdot \cos(\theta - \dot{\omega} \cdot t)}$$

We now assume $e \ll 1$ and because $\dot{\omega}t = 2j_2\left(1 - \frac{5}{4}\sin^2 i\right)nt \ll 1$ we can safely approximate $nt = M \approx \theta$ and therefore

$$\frac{p}{r(\theta)} = 1 + e \cdot \cos\left\{\left[1 + 2j_2\left(1 - \frac{5}{4}\sin^2 i\right)\right] \cdot \theta\right\}$$

Such a rotating ellipse is depicted in Fig. 12.2. We recall that

$$j_2 = \frac{3}{2}J_2\left[\frac{R_\oplus}{a(1-e^2)}\right]^2 \approx \frac{3}{2}J_2\left[\frac{R_\oplus}{a}\right]^2 > 0$$

and because $\dot{\omega}t = 2j_2\left(1 - \frac{5}{4}\sin^2 i\right)nt \ll 1$, only an approximate value of a needs to be known.

For Kepler's equation (7.4.15) only positional shift matters and therefore $M(t) = \left[n + \left(\dot{M} - n\right)\right]\left(t - t_p\right)$. Hence from Eq. (12.3.15) follows

$$E(t) - e\ \sin E(t) = \left[1 + j_2\sqrt{1-e^2}\left(1 - \frac{3}{2}\sin^2 i\right)\right] \cdot n\left(t - t_p\right)$$

Note that E by definition measures the eccentric angle relative to the periapsis (see Fig. 7.13), which itself shifts owing to the apsidal precession $\dot{\omega}$. The combined shift is the draconitic motion as given in Eq. (12.4.1).

12.3.4 Higher-Order Perturbations

According to Lagrange's planetary equations (12.2.7) and (12.2.3) the variations of orbital elements caused by a perturbation R of degree n are of magnitude $R/h \propto 1/hr^{n+1} \approx 1/a^{n+3/2}$. Therefore the impact of higher-order perturbations on an orbit quickly diminishes with increasing orbital radii and increasing degree n as can be observed in Fig. 12.1. For instance, the radius of a geostationary orbit, $r = a \approx 42{,}000$ km, is larger by a factor 6.2 than those of LEO. Hence the secular variations of the orbital elements caused by the biggest perturbation, i.e., Earth's oblateness (see Fig. 12.4a), are smaller by a factor of $6.2^{-3.5} \approx 0.17\ \%$ and therefore negligible in the short-term. According to Table 12.2 this is even more so because the corresponding multipole coefficients also decline with increasing degree n and also with increasing order m. Thus the most considerable perturbation contribution stems from the first-order oblateness perturbations. Nonetheless, for high-precision long-term orbit propagation calculations sectorial perturbations of second order and the perturbations of at least third order have to be considered. In practice, this can be done numerically (see Sect. 12.2.4). In the following we want to explore the impact of higher-order perturbations at least qualitatively.

Higher-order perturbations can be distinguished into:

- **Higher-order multipole perturbations**
  They are due to higher-order multipoles of the gravity field with terms of $J_{22}, J_{3m}, J_{4m} \ldots$.

- **Higher-order oblateness perturbations**
  The LPEs (12.2.7) are the result of first-order perturbation theory. Applying second-order perturbation theory leads to non-linear LPEs (The non-linearity arises from short-period perturbations $\Delta i_{short}, \Delta e_{short}$ due to J_2 oblateness perturbations, which in turn cause both secular and long-periodic perturbations of order J_2^2 via the terms $\partial R/\partial i, \partial R/\partial e$ on the right-hand side of the LPEs (12.2.7)).

Because according to Table 12.2, second part

$$J_2 = O\left(10^{-3}\right)$$
$$J_{22}, J_3, J_{31}, J_4, J_2^2 = O\left(10^{-6}\right)$$

the oblateness perturbation is by far the leading effect, while all of the latter perturbations are equally relevant (gray shaded in Table 12.2, second part). In the following we will determine their corresponding average perturbation potentials. We conclude that the higher-order oblateness perturbations are of the same order of magnitude as the higher-order multipole perturbations, namely $O\left(10^{-6}\right)$, and hence have taken into account in general, which often is not done in the literature.

Average Zonal Harmonics
We first consider the average of the zonal harmonics over one orbit

$$\bar{P}_n \equiv \bar{P}_n^0 = \left\langle (1 + e\cos\theta)^{n-1} P_n(\sin\beta) \right\rangle_{P,\theta}$$

with $P_n(x)$ given in Eq. (12.2.6). In general, the averaging integrals can be treated by applying the power reduction formulas

$$\sin^n x = \frac{1}{2^n} \sum_{k=0}^{n} \binom{n}{k} \cos\left[(n-2k)\left(x - \frac{\pi}{2}\right)\right]$$

$$\cos^n x = \frac{1}{2^n} \sum_{k=0}^{n} \binom{n}{k} \cos[(n-2k)x]$$

$$x = \sin\beta = \sin i \cdot \sin(\theta + \omega)$$

to reduce the $P_n(x)$ to trigonometric expressions with terms $\sin m(\theta+\omega)$, $\cos m(\theta+\omega)$, $m \le n$. These in turn can be expressed through trigonometric angle sum identities by the terms $\sin m\theta$, $\cos m\theta$, $m \le n$. By expanding the integrands it is easily verified that quite generally

$$\left\langle (1+e\,\cos\theta)^{n-1}\sin m\theta\right\rangle_{P,\theta}=0 \quad @\ 0\le m\le n$$

$$\left\langle (1+e\,\cos\theta)^{n-1}\cos m\theta\right\rangle_{P,\theta}=0 \quad @\ m=n$$

while for $n=2-5$ the following relevant averaging integrals hold exactly:

$$\langle (1+e\,\cos\theta)\rangle_{P,\theta}=1, \qquad \langle (1+e\,\cos\theta)\cos\theta\rangle_{P,\theta}=\frac{1}{2}e$$

$$\left\langle (1+e\,\cos\theta)^2\right\rangle_{P,\theta}=1+\frac{1}{2}e^2, \qquad \left\langle (1+e\,\cos\theta)^2\cos\theta\right\rangle_{P,\theta}=e,$$
$$\left\langle (1+e\,\cos\theta)^2\cos 2\theta\right\rangle_{P,\theta}=\frac{1}{4}e^2$$

$$\left\langle (1+e\,\cos\theta)^3\right\rangle_{P,\theta}=1+\frac{3}{2}e^2, \qquad \left\langle (1+e\,\cos\theta)^3\cos\theta\right\rangle_{P,\theta}=\frac{3}{8}e\left(4+e^2\right),$$
$$\left\langle (1+e\,\cos\theta)^3\cos 2\theta\right\rangle_{P,\theta}=\frac{3}{4}e^2, \qquad \left\langle (1+e\,\cos\theta)^3\cos 3\theta\right\rangle_{P,\theta}=\frac{1}{8}e^3$$

$$\left\langle (1+e\,\cos\theta)^4\right\rangle_{P,\theta}=1+3e^2+\frac{3}{8}e^4, \qquad \left\langle (1+e\,\cos\theta)^4\cos\theta\right\rangle_{P,\theta}=\frac{1}{2}e\left(4+3e^2\right),$$
$$\left\langle (1+e\,\cos\theta)^4\cos 2\theta\right\rangle_{P,\theta}=\frac{1}{4}e^2\left(6+e^2\right), \quad \left\langle (1+e\,\cos\theta)^4\cos 3\theta\right\rangle_{P,\theta}=\frac{1}{2}e^3,$$
$$\left\langle (1+e\,\cos\theta)^4\cos 4\theta\right\rangle_{P,\theta}=\frac{1}{16}e^4$$

Note that

$$\left\langle (1+e\,\cos\theta)^{n-1}\begin{bmatrix}\sin m\theta\\ \cos m\theta\end{bmatrix}\right\rangle_{P,\theta}=\left(1-e^2\right)^{n-1}\left\langle \left(\frac{a}{r}\right)^{n-1}\begin{bmatrix}\sin m\theta\\ \cos m\theta\end{bmatrix}\right\rangle_{P,\theta}$$

The latter expressions are usually provided in literature. Explicitely we derive by the help of a symbolic integrator the following exact equations

$$\begin{aligned}
\bar{P}_2&=-\frac{1}{2}\left(1-\frac{3}{2}\sin^2 i\right)\\
\bar{P}_3&=-\frac{3}{2}e\,\sin i\,\sin\omega\left(1-\frac{5}{4}\sin^2 i\right)\\
\bar{P}_4&=\frac{3}{8}\left\{\begin{array}{l}\left[1-5\sin^2 i\left(1-\frac{7}{8}\sin^2 i\right)\right]\left(1+\frac{3}{2}e^2\right)\\ -\frac{15}{4}e^2\cos 2\omega\cdot\ \sin^2 i\left(1-\frac{7}{6}\sin^2 i\right)\end{array}\right\}\\
\bar{P}_5&=\frac{15}{4}e\,\sin i\left\{\begin{array}{l}\sin\omega\left[1-\frac{7}{2}\sin^2 i\left(1-\frac{3}{4}\sin^2 i\right)\right]\left(1+\frac{3}{4}e^2\right)\\ +\ \frac{7}{24}e^2\sin 3\omega\cdot\ \sin^2 i\left(1-\frac{9}{8}\sin^2 i\right)\end{array}\right\}
\end{aligned} \tag{12.3.17}$$

We recall that all orbital elements in these equations and from now on in Sect. 12.3 are meant to be mean orbital values, i.e., $a \equiv \bar{a}$, $e \equiv \bar{e}$, $i \equiv \bar{i}$, $\omega \equiv \bar{\omega}$, $\Omega \equiv \bar{\Omega}$, $M \equiv \bar{M}$.

Average Tesseral and Sectorial Harmonics

Although tesseral and sectorial harmonics do not contribute to secular perturbations, as we will see later, they have a significant effect on long-periodic dynamics. Rather than expounding the derivation of the mean perturbational potentials (see Zhong and Gurfil 2013) we just provide them here

$$\begin{aligned}
\bar{P}_2^2 &= -\frac{3}{2}\sin^2 i \cdot \cos 2(\Omega_{22} - \Omega) \\
\bar{P}_3^1 &= \frac{3}{2}e\left\{\sin(\Omega_{31} - \Omega)\sin\omega\cos i\left(1 - \frac{15}{4}\sin^2 i\right) + \cos(\Omega_{31} - \Omega)\cos\omega\left(1 - \frac{5}{4}\sin^2 i\right)\right\} \\
\bar{P}_3^2 &= -\frac{15}{2}e\sin^2 i\left\{\sin 2(\Omega_{32} - \Omega)\cos\omega\cos i - \cos 2(\Omega_{32} - \Omega)\sin\omega\left(1 - \frac{3}{2}\sin^2 i\right)\right\} \\
\bar{P}_3^3 &= -\frac{45}{2}e\left\{\sin 3(\Omega_{33} - \Omega)\sin\omega\left(1 - \frac{3}{2}\sin^2 i\right) + \cos 3(\Omega_{33} - \Omega)\cos\omega\cos i\right\}
\end{aligned} \tag{12.3.18}$$

with

$$\Omega_{nm} := \lambda_{nm} + \theta_{GMST}$$

where λ_{nm} are given in Table 12.2, second part, and θ_{GMST} is the *Greenwich Mean Sidereal Time*, which is the hour angle from the vernal point (First Point of Aries) to the Greenwich Meridian in the equatorial plane. We recall from Eq. (12.3.11) that the averaged perturbation potentials are derived from these as

$$\bar{R}_{nm} = -\frac{2}{3}\frac{\mu_\oplus}{a}\sqrt{1 - e^2}\, j_{nm}(e) \cdot \bar{P}_n^m$$

Second-Order Oblateness Perturbations

We finally consider the average potential of the second-order oblateness perturbation (indicated by a double dash). This is given by (see e.g. Zhong and Gurfil 2013) as

$$\begin{aligned}
\bar{P}_2'' &= -\frac{33}{16}\left(1 - \frac{21}{11}\sin^2 i + \frac{19}{22}\sin^4 i\right) + O(e^4) \\
&\quad - \frac{3}{32}e^2\left[5\left(1 - 2\sin^2 i + \frac{23}{20}\sin^4 i\right) + 7\sin^2 i\left(1 - \frac{15}{14}\sin^2 i\right)\cos 2\omega\right] \\
\bar{R}_2'' &= -\frac{4}{9}\frac{\mu_\oplus}{a}\sqrt{1 - e^2}\, j_2^2(e) \cdot \bar{P}_2''
\end{aligned} \tag{12.3.19}$$

Mean Variation of Orbital Elements

Inserting the above averaged perturbation potentials into the LPEs (12.2.7) would yield in extension to Eq. (12.3.15) the full-fledged set for the long-period variation of orbital elements (Zhong et Gurfil 2013; Chao 2005, p. 22; Liu 1980; Cook 1966; Shapiro 1995). This, however, not only is quite long-winded but also unreasonable because most satellites in Earth's orbits have small eccentricities. We therefore provide here the set of equations reduced to $e \ll 1$. They read (recall that here $a \equiv \bar{a},\ e \equiv \bar{e},\ i \equiv \bar{i},\ \omega \equiv \bar{\omega},\ \Omega \equiv \bar{\Omega},\ M \equiv \bar{M}$ and $J_{21} = 0$)

$$\dot{a} = 0 \tag{12.3.20}$$

$$\begin{aligned}\frac{1}{n}\dot{e} = &-\left[j_{n,odd}\right]\cos\omega + j_{31}\begin{bmatrix}\sin(\Omega_{31}-\Omega)\cos\omega\,\cos i\left(1-\frac{15}{4}\sin^2 i\right)\\ -\cos(\Omega_{31}-\Omega)\sin\omega\left(1-\frac{5}{4}\sin^2 i\right)\end{bmatrix}\\ &+O\left(j_2^2 e\,\sin 2\omega, j_4 e\,\sin 4\omega, j_{41} e\,\sin\Omega\,\cos\omega\right)\end{aligned}$$

$$\begin{aligned}\frac{1}{n}\dot{i} = &-2j_{22}\sin 2(\Omega_{22}-\Omega)\sin i\\ &+O(j_3 e\,\cos 3\omega, j_{31} e\,\cos\omega\,\sin\Omega, j_{41} e\,\cos\omega\,\sin\Omega)\end{aligned}$$

$$\begin{aligned}\frac{1}{n}\dot{\omega} = &\,2j_2\left(1-\frac{5}{4}\sin^2 i\right) - 2j_{22}\cos 2(\Omega_{22}-\Omega)\left(1-\frac{5}{2}\sin^2 i\right)\\ &+\frac{1}{e}\left\{\left[j_{n,odd}\right]\sin\omega - j_{31}\begin{bmatrix}\sin(\Omega_{31}-\Omega)\sin\omega\,\cos i\left(1-\frac{15}{4}\sin^2 i\right)\\ +\cos(\Omega_{31}-\Omega)\cos\omega\left(1-\frac{5}{4}\sin^2 i\right)\end{bmatrix}\right\}\\ &+j_2^2\left[6\left(1-\frac{79}{72}\sin^2 i\right)\left(1-\frac{5}{4}\sin^2 i\right) - \frac{7}{12}\sin^2 i\left(1-\frac{15}{14}\sin^2 i\right)\cos 2\omega\right]\\ &-5j_4\left[\left(1-\frac{31}{8}\sin^2 i+\frac{49}{16}\sin^4 i\right)+\frac{3}{8}\sin^2 i\left(1-\frac{7}{6}\sin^2 i\right)\cos 2\omega\right]\\ &+O(j_6, j_3 e\,\cos 3\omega, j_{31} e\,\cos\omega\,\sin\Omega, j_{41} e\,\cos\omega\,\sin\Omega)\end{aligned}$$

$$\begin{aligned}\frac{1}{n}\dot{\Omega} = &-\cos i\left[j_2+\frac{5}{2}j_2^2\left(1-\frac{19}{15}\sin^2 i\right)-\frac{5}{2}j_4\left(1-\frac{7}{4}\sin^2 i\right)\right]\\ &+2j_{22}\cos 2(\Omega_{22}-\Omega)\cos i\\ &+O(j_6, j_3 e\,\cos 3\omega, j_{31} e\,\cos\omega\,\sin\Omega, j_{41} e\,\cos\omega\,\sin\Omega)\end{aligned}$$

$$\begin{aligned}\frac{1}{n}(\dot{M}-n) &= j_2\left(1-\frac{3}{2}\sin^2 i\right)\sqrt{1-e^2}+3j_{22}\cos 2(\Omega_{22}-\Omega)\sin^2 i\\ &\quad -\frac{1}{e}\left\{\left[j_{n,odd}\right]\sin\omega - j_{31}\left[\begin{array}{l}\sin(\Omega_{31}-\Omega)\sin\omega\,\cos i\left(1-\frac{15}{4}\sin^2 i\right)\\ +\cos(\Omega_{31}-\Omega)\cos\omega\left(1-\frac{5}{4}\sin^2 i\right)\end{array}\right]\right\}\\ &\quad +\frac{3}{2}j_2^2\left[\left(1-\frac{49}{18}\sin^2 i+\frac{137}{72}\sin^4 i\right)+\frac{7}{18}\sin^2 i\left(1-\frac{15}{14}\sin^2 i\right)\cos 2\omega\right]\\ &\quad +\frac{15}{8}j_4\sin^2 i\left(1-\frac{7}{6}\sin^2 i\right)\cos 2\omega\\ &\quad -\frac{35}{24}j_6\left(1-\frac{21}{2}\sin^2 i+\frac{189}{8}\sin^4 i-\frac{231}{16}\sin^6 i+O(\cos 4\omega)\right)\\ &\quad +O(j_8, j_3 e\,\cos 3\omega, j_{31}e\,\cos\omega\,\sin\Omega, j_{41}e\,\cos\omega\,\sin\Omega)\end{aligned}$$

with

$$\Omega_{nm} := \lambda_{nm} + \theta_{GMST}$$

where λ_{nm} are given in Table 12.2, second part, and θ_{GMST} is the *Greenwich Mean Sidereal Time*, which is the hour angle from the vernal point (First Point of Aries) to the Greenwich Meridian in the equatorial plane, and the sum of odd zonals terms

$$\begin{aligned}\left[j_{n,odd}\right] &:= -\frac{2}{3}\sum_{n\ odd} j_n\frac{n-1}{n(n+1)}P_n^1(0)P_n^1(\cos i)+O\left(j_3 e^2\right)\\ &= \sin i\left[\begin{array}{l}j_3\left(1-\frac{5}{4}\sin^2 i\right)-\frac{5}{2}j_5\left(1-\frac{7}{2}\sin^2 i+\frac{21}{8}\sin^4 i\right)\\ +\frac{35}{8}j_7\left(1-\frac{27}{4}\sin^2 i+\frac{99}{8}\sin^4 i-\frac{429}{64}\sin^6 i\right)\\ -\frac{105}{16}j_9\left(1-11\sin^2 i+\frac{143}{4}\sin^4 i-\frac{715}{16}\sin^6 i+\frac{2431}{128}\sin^8 i\right)\\ +O(j_{11})+O(j_3 e^2)\end{array}\right]\end{aligned} \tag{12.3.21}$$

where

$$P_n^1(\cos i) = \frac{\sin i}{2^n}\sum_{k=0}^{(n-1)/2}(-1)^k\frac{(2n-2k)!}{(n-1-2k)!(n-k)!k!}(\cos i)^{n-1-2k}$$

The variations listed above include long-periodic variations (terms with ω, Ω) plus secular variations (see below). Observe that the higher-order oblateness perturbations j_2^2 contribute only to $\dot{\omega}, \dot{M}$.

Short-Periodic Deviations

We recall that in Eq. (12.3.20) all the orbital elements and their variations are meant to be values averaged over one orbital period. The osculating elements exhibit the following small short-periodic deviations (see Eq. (12.3.3)) from these averaged values in the course of one orbital period (Kozai 1959, see Zhong et Gurfil 2013)

$$\begin{aligned}
\frac{a_{short}}{a} &= j_2 \sin^2 i \cdot \cos 2(\omega+\theta) \\
e_{short} &= -\frac{1}{2} j_2 \sin^2 i \left[\begin{array}{l} \cos(2\omega+\theta) + \frac{1}{3}\cos(2\omega+3\theta) \\ -\,3\cos\theta \cdot \cos(2\omega+2\theta) \end{array} \right] \quad @\ e \ll 1 \qquad (12.3.22) \\
i_{short} &= \frac{1}{4} j_2 \sin 2i \cdot \cos 2(\omega+\theta)
\end{aligned}$$

and hence they all are of the order $j_2 \approx 10^{-3}$. Observe that although the gravitational potential is a conservative one and hence $\langle a \rangle_P = const$ (see Box *Conservative Force* in Sect. 7.1.2 and Eq. (12.3.1)) the osculating a varies slightly over one orbit.

Secular Variations

From Eq. (12.3.20) and with Eq. (12.3.2) we can directly read off the total secular variations

$$\begin{aligned}
\dot{a} \equiv \dot{a}_{\text{sec}} &= 0, \\
\dot{e}_{\text{sec}} &= 0, \\
\dot{i}_{\text{sec}} &= 0,
\end{aligned}$$

$$\begin{aligned}
\frac{1}{n}\dot{\omega}_{\text{sec}} &= 2j_2\left(1-\frac{5}{4}\sin^2 i\right) + 6j_2^2\left(1-\frac{79}{72}\sin^2 i\right)\left(1-\frac{5}{4}\sin^2 i\right) \\
&\quad - 5j_4\left(1-\frac{31}{8}\sin^2 i+\frac{49}{16}\sin^4 i\right) + O(j_6) \qquad (12.3.23) \\
&= 2j_2\left(1-\frac{5}{4}\sin^2 i\right)\left[1+O\left(10^{-3}\right)\right]
\end{aligned}$$

$$\begin{aligned}
\frac{1}{n}\dot{\Omega}_{\text{sec}} &= -\cos i\left[j_2+\frac{5}{2}j_2^2\left(1-\frac{19}{15}\sin^2 i\right)-\frac{5}{2}j_4\left(1-\frac{7}{4}\sin^2 i\right)+O(j_6)\right] \\
&= -j_2\cos i\left[1+O\left(10^{-3}\right)\right]
\end{aligned}$$

$$\begin{aligned}
\frac{1}{n}\left(\dot{M}-n\right) &= j_2\left(1-\frac{3}{2}\sin^2 i\right)\sqrt{1-e^2}+\frac{3}{2}j_2^2\left\{\left(1-\frac{49}{18}\sin^2 i+\frac{137}{72}\sin^4 i\right)\right\} \\
&\quad -\frac{35}{24}j_6\left(1-\frac{21}{2}\sin^2 i+\frac{189}{8}\sin^4 i-\frac{231}{16}\sin^6 i\right)+O(j_8) \\
&= j_2\left(1-\frac{3}{2}\sin^2 i\right)\sqrt{1-e^2}\left[1+O\left(10^{-3}\right)\right]
\end{aligned}$$

This means that the secular effects of the gravitational potential are essentially due to the oblateness perturbation. Observe that only even zonal harmonics contribute to secular effects, with the peculiarity that the fourth zonal harmonic does not contribute to $\dot{M}$ but only higher even orders of zonal harmonics. All other terms in Eq. (12.3.20) are long-periodic variations of the slow variables ω and Ω.

Near-Circular Orbits

According to Eq. (12.3.20) the variations of the orbital elements seem to be highly complicated. Though the upshot is quite easy: The variations are governed by the oblateness variations with factor $j_2 = O(10^{-3})$. All other effects owing to higher order harmonics are of order $j_{22}, j_2^2, j_3, j_{31}, j_4, j_6 = O\left(10^{-6}\right)$. They all contribute with either a small secular effect or a modulation of the oblateness effects. There exists, however, one exception from this rule, namely for near-circular orbits, when $e < 0.01$. Then the braces with the factor $1/e$ become significant, i.e., $O\left(\left[j_{n,odd}\right]/e, j_{31}/e\right) \approx O(10^{-3}) \approx O(j_2)$. Yet, the divergence of the $1/e$-term for $e \to 0$ is of no practical significance because in this limit there is no well-defined periapsis. Thus any tiny change of the orbital shape due to a gravitational anisotropy brings about an increasing variation in the position of the periapsis, which causes a diverging $\dot{\omega}$ and $\dot{M} - n$. This is a theoretical artifact that can also be seen from the fact that the orbital motion relative to Earth's surface, the so-called mean draconitic motion n_Ω (see Sect. 12.4.1), should be unaffected for $e \to 0$ and indeed in the expression $n_\Omega = n + \dot{\omega} + \left(\dot{M} - n\right)$ the j_3-terms cancel out each other. This holds for all higher perturbations that can be seen from the LPEs Eq. (12.2.7) where for $\dot{\omega} + \left(\dot{M} - n\right)$ the critical terms $e^{-1}\partial R/\partial e$ cancel out each other for $e \to 0$.

Nevertheless, we are interested how the odd harmonics affect the orbital elements $\dot{e}, \dot{\omega}$ for near-circular orbits. To study this we rewrite Eq. (12.3.20)

$$\begin{aligned}
\dot{e} &= -n\left[j_{n,odd}\right]\cos\omega \\
&\quad + nj_{31}\left[\begin{array}{l}\sin(\Omega_{31}-\Omega)\cos\omega\cos i\left(1-\frac{15}{4}\sin^2 i\right) \\ \qquad -\cos(\Omega_{31}-\Omega)\sin\omega\left(1-\frac{5}{4}\sin^2 i\right)\end{array}\right] \\
\dot{\omega} &= \dot{\omega}_{\text{sec}} + \underbrace{\dot{\omega}_{long}(\omega,\Omega)}_{negligible} \\
&\quad + \frac{n}{e}\left\{\left[j_{n,odd}\right]\sin\omega - j_{31}\left[\begin{array}{l}\sin(\Omega_{31}-\Omega)\sin\omega\cos i\left(1-\frac{15}{4}\sin^2 i\right) \\ \quad +\cos(\Omega_{31}-\Omega)\cos\omega\left(1-\frac{5}{4}\sin^2 i\right)\end{array}\right]\right\}
\end{aligned} \tag{12.3.24}$$

Since $\dot{\omega}_{long}(\omega,\Omega) = O\left(10^{-6}\right) \ll 1/e\left\{O\left(10^{-6}\right)\right\}$ we neglect this long-periodic term.

Effect of Odd Zonal Harmonics

For a preparatory treatment of these differential equations we also neglect the long-periodic j_{31}-terms for the time being arriving at

$$\begin{aligned}
\dot{e} &= -n\left[j_{n,odd}\right]\cos\omega \\
\dot{\omega} &= \dot{\omega}_{\text{sec}} + \frac{n}{e}\left[j_{n,odd}\right]\sin\omega
\end{aligned} \tag{12.3.25}$$

Observe that from Table 12.2, second part and Eq. (12.3.10) $O(j_3) = 10^{-6}$, but $O(j_5, j_7, j_9) = 10^{-7}$, and therefore

$$\dot{\omega}_{\text{sec}} \approx 2nj_2\left(1 - \frac{5}{4}\sin^2 i\right)$$
$$\left[j_{n,odd}\right] \approx j_3 \sin i\left(1 - \frac{5}{4}\sin^2 i\right)$$

We therefore define the more physical parameters

$$\begin{aligned} n_\omega &:= \dot{\omega}_{\text{sec}} = const \approx 2nj_2\left(1 - \frac{5}{4}\sin^2 i\right) \\ e_\omega &:= -\frac{n\left[j_{n,odd}\right]}{n_\omega} \approx -\frac{1}{2}\frac{j_3}{j_2}\sin i \\ &= 1.170 \times 10^{-3}\frac{R_\oplus}{a}\sin i \approx 10^{-3}\sin i < 0.001 \end{aligned} \tag{12.3.26}$$

With these we rewrite the differential equations

$$\begin{aligned} \dot{e} &= e_\omega n_\omega \cos\omega \\ \dot{\omega} &= n_\omega\left(1 - \frac{e_\omega}{e}\sin\omega\right) \end{aligned} \tag{12.3.27}$$

We treat these coupled differential equations by showing that from these follows

$$\frac{d}{dt}(e\,\sin\omega) = \dot{e}\,\sin\omega + e\,\dot{\omega}\,\cos\omega = n_\omega e\,\cos\omega$$

This gives rise to the substitution

$$x := e\,\sin\omega$$
$$y := e\,\cos\omega$$

With this we rewrite the above differential equations

$$\dot{x} = n_\omega y$$
$$\dot{y} = -n_\omega(x - e_\omega)$$

Thus we have transformed the problem into a set of coupled non-divergent linear differential equations. The solution is the well-known harmonic oscillator in 2 dimensions

$$x - e_\omega = r\,\sin(n_\omega t + \varphi)$$
$$y = r\,\cos(n_\omega t + \varphi)$$

where the parameters r, φ are given by the initial conditions. Since $(x - e_\omega)^2 + y^2 = r^2$, we recognize that the vector $(e \sin\omega,\ e \cos\omega)$ in the x, y reference frame is rooted at the point $(e_\omega,\ 0)$ with its tip rotating at orbital frequency n_ω on a circle with radius r. In the orbital plane $(e \sin\omega,\ e \cos\omega)$ is the eccentricity vector with component $e \sin\omega$ along the line of apsides. Due to the offset e_ω between both reference frames the angular velocity $\omega(t)$ and length $e(t)$ of the eccentricity vector varies in the course of its rotation. We recall that factually nothing rotates, but only the line of apsides of the virtual osculating orbit. To determine $e(t), \omega(t)$ we make use of $e = \sqrt{x^2 + y^2}$ and $\cos\omega(t) = y/e$. Hence we finally arrive at the solution of the differential equations (12.3.27)

$$\begin{aligned} e(t) &= \sqrt{e_\omega^2 + r^2 + 2e_\omega r \sin(n_\omega t + \varphi)} \\ \cos\omega(t) &= \frac{r}{e(t)} \cos(n_\omega t + \varphi) \end{aligned} \tag{12.3.28}$$

We define $e(0) =: e_0$ and $\omega(0) =: \omega_0$ as the initial conditions. This implies

$$\begin{aligned} r \sin\varphi &= e_0 \sin\omega_0 - e_\omega \\ r \cos\varphi &= e_0 \cos\omega_0 \end{aligned} \tag{12.3.29}$$

from which follows

$$\begin{aligned} r &= \sqrt{e_0^2 + e_\omega^2 - 2e_0 e_\omega \sin\omega_0} \\ \tan\varphi &= \tan\omega_0 - \frac{e_\omega}{e_0 \cos\omega_0} \end{aligned} \tag{12.3.30}$$

We now apply this general result to two significant and limiting cases.

In the first case, the initial eccentricity is $e_0 > e_\omega$, implying $e_0 \approx r > e_\omega$ and $\phi \approx \omega_0$. Then we derive from Eq. (12.3.28) and the general relation $\cos(\alpha + \varepsilon \cos\alpha) \approx \cos\alpha \cdot (1 - \varepsilon \sin\alpha)$ for $\varepsilon \ll 1$

$$\begin{aligned} e(t) &= e_0 + e_\omega \sin(n_\omega t + \omega_0) \\ \omega(t) &= \omega_0 + n_\omega t + \tfrac{e_\omega}{e_0}\left[\cos(n_\omega t + \omega_0) - \cos\omega_0\right] \end{aligned} \quad @ \begin{array}{l} e_0 > e_\omega \\ \approx 0.001 \end{array} \tag{12.3.31}$$

This result can be also found by directly integrating Eq. (12.3.27) assuming initially $\omega = \omega_0 + n_\omega t$. Hence the odd zonal harmonics, mainly the j_3-term, periodically modulate the eccentricity e_0 with modulation amplitude $10^{-3} \sin i$ and frequency n_ω (see Fig. 12.10, top). Note that very close to the critical inclination, $i = 63.435° \pm 0.06°$, where $1 - \frac{5}{4}\sin^2 i < 10^{-3}$, we have $n_\omega = \dot{\omega}_{\text{sec}} = n \cdot O\left(j_2^2, j_4\right) \approx n \cdot 10^{-6}$ and $\left[j_{n,odd}\right] \approx O(j_5) \approx 10^{-6}$, and hence the induced eccentricity becomes a maximum with $e_\omega = -n\left[j_{n,odd}\right]/n_\omega \approx 1$.

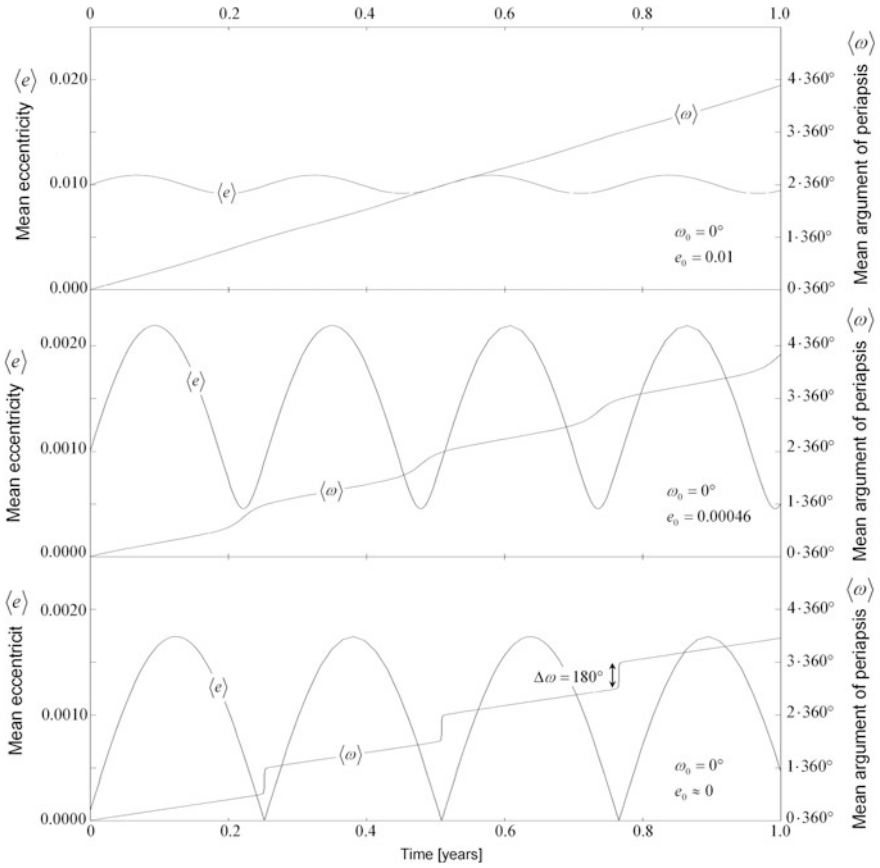

Fig. 12.10 Numerical computation of the evolution of the mean eccentricity and of the mean argument of periapsis of the ISS with $\iota = 51.6°$, $h = 350$ km for different e_0

The second significant case is when $e_0 < e_\omega$ and hence the second term in the brackets in Eq. (12.3.27) becomes significant. When $e \ll e_\omega$ the mean angular motion of the periapsis $\dot{\omega}$ becomes very big, i.e., the mean periapsis moves rapidly on the near-circular orbit. When the periapsis has turned by 180° the j_3-perturbational forces having decreased so far e will act inversely and now increase e. But once $e > e_\omega$ the excessive rotation stops and we are back to "normal". So, we recognize that the term $e_\omega / e \cdot \sin\omega$ ensures that the eccentricity is always positive. Mathematically speaking, if $e_0 = 0$, then we derive from Eq. (12.3.29) $\varphi = 270°$ and $r = e_\omega$ and we obtain from Eq. (12.3.28)

$$\begin{aligned} e(t) &= 2e_\omega \left|\sin\frac{n_\omega t}{2}\right| \\ \cos\omega(t) &= \frac{1}{2}\sin(n_\omega t)/\left|\sin\frac{n_\omega t}{2}\right| \end{aligned} \qquad @\ e_0 < e_\omega \tag{12.3.32}$$

The behavior of $e(t), \omega(t)$ in this case is depicted in Fig. 12.10 (bottom). Observe that when the eccentricity vanishes the periapsis jumps by 180° ensuring that $\sin\omega$ does not change sign when traversing null.

Example

The International Space Station at $h = 350$ km and $i = 51.6°$ and an assumed $e_0 = 0$ has $e_\omega = 8.66 \times 10^{-4}$ and $n_\omega = 7.68°\ \text{day}^{-1}$. Therefore the j_3-induced eccentricity is $e = 0.00173 \cdot \sin\omega$ and the cycle time is $T_c = 2\pi/n_\omega = 46.9$ days. The secular behavior of such e with the corresponding ω is depicted in Fig. 12.10 (bottom).

Effect of Odd Zonal Plus Tesseral Harmonics

We now consider also the contribution of the tesseral j_{31}-term in Eq. (12.3.24). It is an easy exercise to show that by the same line of treatment as above we get the following results

$$\begin{aligned}\dot{x} &= n_\omega y - n_{\cos\Omega}\cos(\Omega_{31} - \Omega)\\ \dot{y} &= -n_\omega(x - e_\omega) + n_{\sin\Omega}\sin(\Omega_{31} - \Omega)\end{aligned}$$

where

$$\begin{aligned}n_{\cos\Omega} &:= nj_{31}\left(1 - \frac{5}{4}\sin^2 i\right)\\ n_{\sin\Omega} &:= nj_{31}\cos i\left(1 - \frac{15}{4}\sin^2 i\right)\end{aligned} \tag{12.3.33}$$

We now make use of the fact that due to Earth's oblateness $\Omega(t)$ with high accuracy varies linearly, namely

$$\Omega(t) \approx \Omega_0 - n_\Omega \cdot t$$

$$n_\Omega := nj_2\cos i$$

The solution of the above set of differential equations then is

$$\begin{aligned}x - e_\omega &= r\ \sin(n_\omega t + \varphi) + r'\sin(n_\Omega t + \lambda)\\ y &= r\ \cos(n_\omega t + \varphi) + r''\cos(n_\Omega t + \lambda)\end{aligned}$$

with

$$\begin{aligned}&\lambda := \Omega_{31} - \Omega_0\\ &r' := \frac{n_\omega n_{\sin\Omega} + n_\Omega n_{\cos\Omega}}{n_\omega^2 - n_\Omega^2} = \frac{j_{31}\cos i\left(1 - \frac{5}{2}\sin^2 i\right)}{j_2\left(1 - 3\sin^2 i + \frac{25}{12}\sin^4 i\right)} = O\left(10^{-3}\right)\\ &r'' := \frac{n_\omega n_{\cos\Omega} + n_\Omega n_{\sin\Omega}}{n_\omega^2 - n_\Omega^2} = \frac{j_{31}\left(1 + \frac{13}{4}\sin^2 i + \frac{55}{24}\sin^4 i\right)}{j_2\left(1 - 3\sin^2 i + \frac{25}{12}\sin^4 i\right)} = O\left(10^{-3}\right)\end{aligned} \tag{12.3.34}$$

Since $O(e_\omega) = O(r') = O(r'') = 0.001$ while $O(r)$ depends on the initial orbit conditions we rewrite the solution

$$x = r\,\sin(n_\omega t + \varphi) + e_{\omega\Omega}$$
$$y = r\,\cos(n_\omega t + \varphi) + e_\Omega$$

as

$$\begin{aligned} e_{\omega\Omega}(t) &= r'\sin(n_\Omega t + \lambda) + e_\omega = O\left(10^{-3}\right) \\ e_\Omega(t) &= r''\cos(n_\Omega t + \lambda) = O\left(10^{-3}\right) \end{aligned} \tag{12.3.35}$$

and thus obtain

$$\begin{aligned} e(t) &= \sqrt{r^2 + 2r[e_{\omega\Omega}\sin(n_\omega t + \varphi) + e_\Omega\cos(n_\omega t + \varphi)] + e_\Omega^2 + e_{\omega\Omega}^2} \\ \cos\omega(t) &= \frac{r\cos(n_\omega t + \varphi) + e_\Omega}{e(t)} \end{aligned} \tag{12.3.36}$$

where r, φ are given by the initial conditions

$$\begin{aligned} r\,\sin\varphi &= e_0\sin\omega_0 - r'\sin\lambda - e_\omega \\ r\,\cos\varphi &= e_0\cos\omega_0 - r''\cos\lambda \end{aligned} \tag{12.3.37}$$

We now reconsider the above two limiting cases. For $e_0 > e_\omega$, implying $e_0 \approx r > e_{\omega\Omega}, e_\Omega$ and $\varphi \approx \omega_0$, we obtain by Eq. (12.3.36) and iterative direct integration of Eq. (12.3.24)

$$\begin{aligned} e(t) &= e_0 + [e_{\omega\Omega}(t)\sin(n_\omega t + \omega_0) + e_\Omega(t)\cos(n_\omega t + \omega_0)] \\ \omega(t) &= \omega_0 + n_\omega t + \tfrac{e_\omega}{e_0}[\cos(n_\omega t + \omega_0) - \cos\omega_0] \\ &\quad + \tfrac{n_{\sin\Omega} + n_{\cos\Omega}}{2(n_\Omega - n_\omega)e_0}[\sin[(n_\Omega - n_\omega)t + \lambda - \omega_0] - \cos(\lambda - \omega_0)] \\ &\quad - \tfrac{n_{\sin\Omega} - n_{\cos\Omega}}{2(n_\Omega + n_\omega)e_0}[\sin[(n_\Omega + n_\omega)t + \lambda + \omega_0] - \cos(\lambda + \omega_0)] \end{aligned} \quad @ \begin{array}{l} e_0 > e_\omega \\ \approx 0.001 \end{array} \tag{12.3.38}$$

We therefore recognize that

Complex Modulation of e_0, ω_0 for a Near-Circular LEO
For near-circular LEO orbits, $0.001 < e_0 < 0.01$, the constant eccentricity, $e = e_0$, and linearly increasing argument of periapsis, $\omega = \omega_0 + n_\omega t$, are complexly modulated with amplitudes of $O(10^{-3})$ chiefly owing to j_3, j_{31}-perturbations.

In the case of a close-circular orbit, $e_0 < e_\omega \approx 0.001$, we have from Eq. (12.3.37) for $e_0 = 0$

$$r = \sqrt{r''^2 \cos^2\lambda + (r'\sin\lambda + e_\omega)^2} = O\left(10^{-3}\right) \quad \begin{matrix} @\ e_0 < e_\omega \\ \approx 0.001 \end{matrix} \tag{12.3.39}$$

We therefore recognize that

Wild and Chaotic Modulation of e_0, ω_0 for a Close-Circular LEO
For initially close-circular LEO orbits, $e_0 < 0.001$, the eccentricity and the argument of periapsis wobble around an average value of $e_{ave}(t) \approx 0.001$ wildly in a very complex way with amplitude $O(10^{-3})$, chiefly owing to j_3, j_{31} perturbations.

In summary we see that no satellite is able to establish zero eccentricity over a finite fraction of time. Mainly j_3- and j_{31}-induced perturbations will at least bring about $e \approx 0.001$. This is why satellites often have a declared $e \approx 0.001$, though they should have $e = 0$. See, e.g., GPS satellites in Sect. 12.4.4.

Observe that as a result of a weak non-vanishing eccentricity, precise orbits, such as those of Earth observation satellites, in the long run need inclination maintenance, because we have from (12.3.20) $\dot{i}_{\text{sec}} = O(j_3 e)$.

Summary
In closing we note that if the argument of periapsis would not rotate by gravitational perturbations but would remain constant, then all orbital elements would grow unlimited. So, by and large it can be stated that the rotation of ω, primarily owing to Earth's oblateness and also to j_3- and j_{31}-perturbations, has a stabilizing influence on orbits.

Numerical simulations with higher multipole moments also reveal that beyond these results no new effects occur and that their contributions are very small. Further analysis of the influence of higher-order perturbations can be found in Chao (2005), Kaula (1966), Beutler (2005b), Vallado (2001), Groves (1960), Campan et al. (1995), Liu (1974), and Fortesque et al. (2003).

12.3.5 Sun-Synchronous Orbits

Is orbit perturbation good or bad for a mission? Well, it depends. To have an orbit shape and orientation devoid of perturbations might be good for some missions. However, remote sensing or communication satellites in LEO require orbits that remain steady relative to Earth's rotating surface or exactly recurr after some days. So, actually an orbit would be useful that is in sync with Earth's rotation. This begs

the question: Can orbit perturbation be utilized to achieve such a sync? The answer in many cases is "yes". In the following we study these cases.

Sun-synchronous orbits, SSOs, are orbits that maintain a constant orientation of the orbit plane toward the Sun in the course of a year. In this case the so-called *beta angle* β, which is the angle at which the sunlight strikes the orbital plane (see Sect. 14.1.1), is constant over the year. This is a useful property since the lighting conditions for the satellite's solar cells then are constant. Because the Earth is revolving around the Sun, sun-synchronicity implies that the orbit plane has to revolve by 360° within a year. Now, a constant beta angle can be achieved by employing the regression of nodes effect such that the nodal rate as given in first order by Eq. (12.3.15) equals that of the Earth's revolution around the Sun, i.e., if

$$\dot{\Omega} = -\sqrt{\frac{\mu_\oplus}{a^3}}\frac{3J_2R_\oplus^2}{2a^2(1-e^2)^2}\cos i = \frac{2\pi}{365.256363}\text{day}^{-1} = 1.7202 \times 10^{-2}\text{day}^{-1}$$

which implies

$$\cos i = -(1-e^2)^2\left(\frac{a}{R_\oplus}\right)^{7/2}\sqrt{\frac{R_\oplus^3}{\mu_\oplus}}\frac{2}{3J_2}1.7202 \times 10^{-2}\text{day}^{-1}$$

or

$$\cos i = -0.098917 \cdot (1-e^2)^2\left(\frac{a}{R_\oplus}\right)^{7/2} \tag{12.3.40}$$

The negative sign implies that SSOs are retrograde, $i > 90°$. In practice, for remote sensing missions circular or near-circular LEOs are chosen frequently with the semi-major axis determined by other mission constraints, such as a repeating ground track (see Sect. 12.4.1). If for such a remote sensing mission the inclination is chosen as given above, this orbit will be sun-synchronous. Sun-synchronous, repeat ground track orbits have typical altitudes of h = 700–900 km and therefore have inclinations $i = 98.2°$–$99.0°$. So-called *magic orbits* are sun-synchronous and type I frozen (see below) at $i = 116.57°$ and with an high eccentricity of $e = 0.345$.

Note that in particular those SSOs will receive continuous solar irradiation that have a beta angle of $\beta = 90°$. In this case the satellite's ground track is just along Earth's terminator. However, this does not provide good lighting conditions for remote sensing, which is why the beta angle is chosen smaller to have good lighting condition in the morning over the areas of interest. It can be shown from geometrical considerations that even these SSOs will never be in eclipse and hence are also permanently irradiated by the Sun if their beta angles obey the relation $\beta > \arcsin(R_\oplus/a)$ see Eq. (14.1.3). It should ne noted that lunisolar perturbations induce an inclination change, which for a typical Sun-synchronous orbit with $h = 850$ km and $i = 98.8°$ amounts to the small value of $\dot{i}_{\text{sec}} \approx 0{-}0.047°$ year^{-1} depending on the beta angle β.

12.3.6 Frozen Orbits

For Earth observation, which is the most important application in LEO, it is of paramount importance to have observational consistency, i.e., to revisit any observation site under nearly identical circumstances. This can be achieved by a spacecraft in a polar, repeating Sun-synchronous orbit (this ensures constant lighting conditions), and with constant orbit geometry keeping the periapsis at the same latitude. We will now explore how such geometrical constancy can be maintained despite orbital perturbations.

There is nothing that can be done to suppress the regression of nodes $\dot{\Omega}$. But this does not impede observation, it only impacts the so-called access area, i.e., the surface area seen at a particular time from orbit. So only $\dot{a},\ \dot{e},\ \dot{i},\ \dot{\omega} \approx 0$ need to be achieved. Orbits that aside from $\dot{a},\ \dot{i} \approx 0$ also exhibit the properties $\dot{e}, \dot{\omega} \approx 0$ are called **frozen orbits** because the rotation of the apse line is stopped. From Eq. (12.3.20) for $\dot{\omega}$ it can be seen that frozen orbits can be obtained in two ways:

Type I Frozen Orbits
If the expression $1 - \frac{5}{4}\sin^2 i = 0$, i.e. if an orbit maintains the critical inclination

$$i_f = \arcsin\sqrt{4/5} = 63.43^\circ \text{ or } 116.57^\circ$$

the orbit is frozen. These are the co-called *Type I frozen orbits*. This frozen condition is utilized by the so-called *Magic, Cobra*, *Molniya,* and *Tundra orbits*. All these are highly elliptic orbits with orbital periods of exactly 3, 8, 12, and 24 h and with perigee/apogee at altitudes 525/7800, 800/27 000, 1000/39 358, and 5370/66 400 km, respectively, which are employed for communication services. The latter are frequently used by Russia. Due to their low pace over Russia at apogee they cover the high latitudes of Russian territory over most of the orbital period. Note that although the eccentricities of all these orbits are very large, $e = 0.3{-}0.7$, and $\dot{i},\ \dot{\Omega} \propto O(j_3 e) \approx 0$ still holds, because $J_3 \approx -2.339 \times 10^{-3} J_2$ (see Table 12.2).

Type II Frozen Orbits
Conditions $\dot{e}, \dot{\omega} \approx 0$ in Eq. (12.3.20) can also be achieved if $\omega_f := \omega = 90^\circ$ or 270° and when $\dot{\omega} = 0$. This implies that

$$0 = 2j_2\left(1 - \frac{5}{4}\sin^2 i\right) + \frac{1}{e}\left[j_{n,odd}\right]\sin\omega + 6j_2^2\left\{\left(1 - \frac{79}{72}\sin^2 i\right)\left(1 - \frac{5}{4}\sin^2 i\right)\right\} - 5j_4\left\{\left(1 - \frac{31}{8}\sin^2 i + \frac{49}{16}\sin^4 i\right)\right\}$$

We first consider only the second order contribution j_3. In this case

$$\left[j_{n,odd}\right] \approx j_3 \sin i\left(1-\frac{5}{4}\sin^2 i\right)$$

and

$$0 = 2j_2 + \frac{\sin i \, \sin\omega}{e} j_3$$

The eccentricity at which for $\omega_f = 90°$ the bracket vanishes is

$$e_{f0} = -\frac{1}{2}\frac{j_3}{j_2}\sin i = -\frac{1}{2}\frac{J_3 R_\oplus}{J_2 a}\sin i = 1.170 \times 10^{-3}\frac{R_\oplus}{a}\sin i \tag{12.3.41}$$

Because of $0 < e_f \ll 1$ it is always possible to achieve, orbits with these conditions, which are called *Type II frozen orbits*.

Taking into account higher-order multipole perturbation as well, we first neglect j_2^2, j_4 contributions. In this case and for $\omega_f = 90°$ we get

$$\begin{aligned} e_f &= \frac{\sin i}{2j_2\left(1-\frac{5}{4}\sin^2 i\right)}\left\{\begin{array}{l} -j_3\left(1-\frac{5}{4}\sin^2 i\right)+\frac{5}{2}j_5\left(1-\frac{7}{2}\sin^2 i+\frac{21}{8}\sin^4 i\right) \\ -\frac{35}{8}j_7\left(1-\frac{27}{4}\sin^2 i+\frac{99}{8}\sin^4 i-\frac{429}{64}\sin^6 i\right)+O(j_{11}) \\ +\frac{105}{16}j_9\left(1-11\sin^2 i+\frac{143}{4}\sin^4 i-\frac{715}{16}\sin^6 i+\frac{2431}{128}\sin^8 i\right) \end{array}\right\} \\ &= e_{f0}[1-O(j_5/j_3,)] = e_{f0}\left[1-O\left(10^{-1}\right)\right] \end{aligned} \tag{12.3.42}$$

Therefore, and as will be shown in the next section, these higher order perturbations j_n, $n \geq 5$, modify the coarse result as given in Eq. (12.3.41) by up to 20%.

To now also account for the j_2^2, j_4 contributions we define

$$e_{f+} = e_f(1+\varepsilon)$$

With this we derive with $\dot{\omega} = 0$ and $\cos\omega_f = \cos 2\omega_f = 0$ from Eq. (12.3.20) iteratively the conditional equation for ε

$$\begin{aligned} 0 = &-2j_2\left(1-\frac{5}{4}\sin^2 i\right)\varepsilon + 6j_2^2\left(1-\frac{79}{72}\sin^2 i\right)\left(1-\frac{5}{4}\sin^2 i\right) \\ &-5j_4\left(1-\frac{31}{8}\sin^2 i+\frac{49}{16}\sin^4 i\right) \end{aligned}$$

hence

$$\varepsilon = 3j_2\left(1-\frac{79}{72}\sin^2 i\right) - \frac{5}{2}\frac{j_4}{j_2}\left(1-\frac{31}{8}\sin^2 i+\frac{49}{16}\sin^4 i\right)/\left(1-\frac{5}{4}\sin^2 i\right)$$

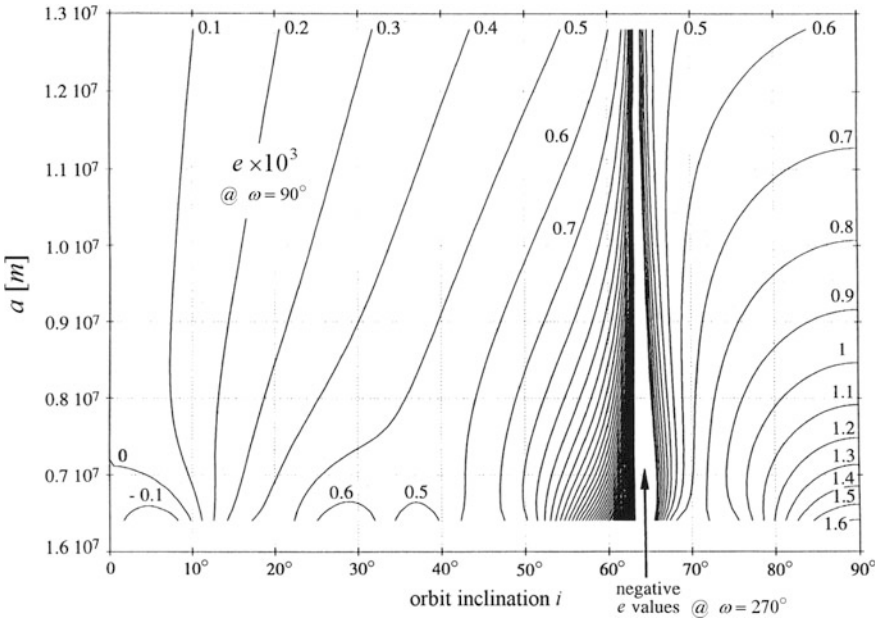

Fig. 12.11 Eccentricity e of type II frozen orbits multiplied by 1000 for prograde orbits, $0 \leq i \leq 90°$, and $R_\oplus \leq a \leq 2R_\oplus$. *Credit* Micheau (1995)

The magnitude of ε therefore is

$$O(\varepsilon) = O(j_2, j_4/j_2) = 10^{-3}$$

Hence, the j_2^2, j_4 contributions can be neglected. We therefore conclude that

> Only odd higher-order multipole perturbations and not even higher-order multipole perturbations or higher-order oblateness perturbations, j_2^2, affect type II frozen orbits significantly.

Since j_n are functions of a, the value of e_f may be parametrized as a function of a and i. Figure 12.11 depicts these dependencies for $0 \leq i \leq 90°$ and $R_\oplus \leq a \leq 2R_\oplus$. There are several things to note. First, for nearly all cases $e_f < 90°$, i.e. type II frozen orbits are all near-circular. Second, at the type I frozen condition $\frac{5}{4}\sin i = 1$, the type II eccentricity becomes ill-defined. Therefore, at the critical inclinations $i_f = \arcsin\sqrt{4/5} = 63.43°$ or $116.57°$, the orbit is naturally frozen (Type I frozen) for the entire range of eccentricity values e. Third, the majority of flown type II frozen orbits have $\omega_f = 90°$.

A good example of a type II frozen orbit is the orbit of the Topex/Poseidon satellite and its follow-ups *Jason 1* and *Jason 2* with $e = 9.5 \times 10^{-5}$, $i = 66.04°$, and $a = 7714.43$ km.

It may be questioned whether under the influence of drag and other perturbations in LEO frozen orbits remain frozen. The answer is affirmative concerning drag. However, solar radiation will gradually destroy the frozen condition. Therefore periodic orbit adjustments are needed to maintain the frozen orbital state.

12.3.7 Frozen Sun-Synchronous Orbits

By applying Eqs. (12.3.40) and (12.3.42) simultaneously it is possible to have a type II frozen Sun-synchronous orbit. From Eq. (12.3.40) follows

$$\sin^2 i = 1 - \cos^2 i = 1 - 0.0097845\left(\frac{a}{R_\oplus}\right)^7 =: 1 - \varepsilon$$

where $\varepsilon \approx 0.01$. Inserting this into Eq. (12.3.42) and expanding ε results for $\omega_f = 90^\circ$ in

$$e_f = -\frac{\sin i}{2j_2}\left\{j_3 + \frac{5}{4}\left[\left(j_5 + \frac{35}{32}j_7 + \frac{147}{128}j_9\right) - \left(9j_5 + \frac{385}{16}j_7 + \frac{5733}{128}j_9\right)\varepsilon\right]\right\}$$

Inserting $\varepsilon = 0.0097845(a/R_\oplus)^7$ and the j-values as given in Eq. (12.3.10) we finally get

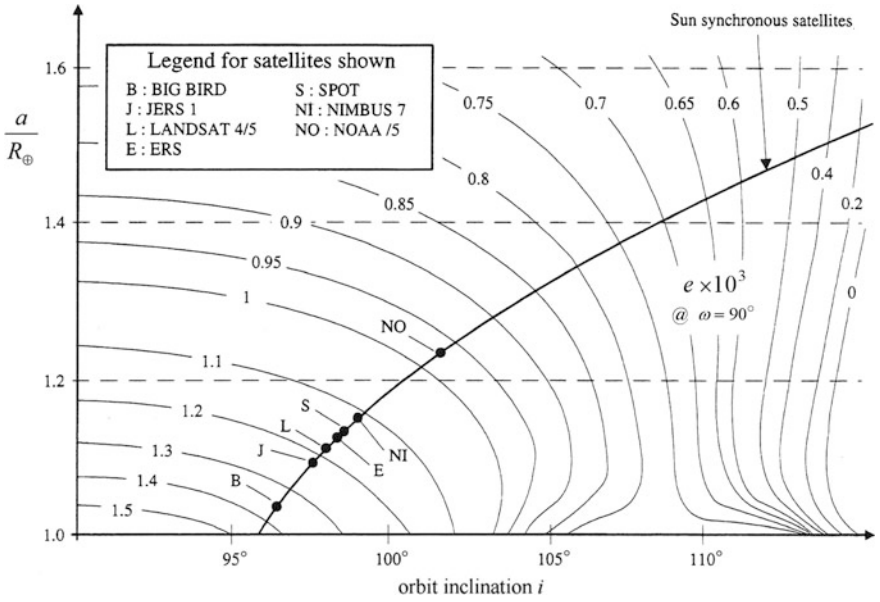

Fig. 12.12 Eccentricity e of Sun-synchronous orbits multiplied by 1000 for retrograde orbits, $90^\circ \le i \le 115^\circ$, and $R_\oplus \le a \le 1.6R_\oplus$. *Credit* Micheau (1995)

$$e_f = 1.170 \times 10^{-3}\gamma\sqrt{1 - 0.0097845\ \gamma^{-7}} \times \left\{1 + \frac{1}{8}\left[\begin{array}{c}\left(0.8975\ \gamma^2 + 1.5217\ \gamma^4 + 0.5470\ \gamma^6\right) \\ -\left(0.0791\ \gamma^{-5} + 0.328\ \gamma^{-3} + 0.208\ \gamma^{-1}\right)\end{array}\right]\right\} \tag{12.3.43}$$

where

$$\gamma = \frac{R_\oplus}{a} < 1$$

The "Sun-synchronous satellites"-line in Fig. 12.12 depicts the above equation in terms of $e_f(a/R_\oplus)$. In addition, the frozen condition can be read off for $90° \leq i \leq 115°$ and $R_\oplus \leq a \leq 1.6R_\oplus$ and thus extends Fig. 12.11 to retrograde orbits.

Nearly all Earth observation satellites, most prominently the US Landsat satellites and the French SPOT satellites, are frozen Sun-synchronous. For instance we have for SPOT 1-5: $e = 1.25 \times 10^{-3}$, $i = 98.7°$, and $a = 7010$ km; for SPOT 6/7: $e = 1.20 \times 10^{-3}$, $i = 98.2°$, and $a = 7072$ km; and for LANDSAT 4/5/7 $e = 1.20 \times 10^{-3}$, $i = 98.2°$, and $a = 7083$ km.

12.4 Resonant Orbits

A resonant orbit is a special type of orbit that spatially "resonates" with the modulations of the gravitational potential. This means that its ground track, i.e., the projection of the orbit vertically onto the surface of the Earth, recurrently passes only over decisive areas. Because this is equivalent to a repeating pattern, resonant orbits are also called *repeat ground track orbits*; and *commensurate orbits* because the recurrence implies that the ground track is in lock-step with Earth's rotation, meaning that its pattern recurs after a certain number of terrestrial revolutions matching a certain number of orbital revolutions.

Resonant orbits exhibit a property that makes them very special. Because their ground tracks recur exactly thus producing a thin line pattern, they do not cover every point of the surface within their repetition period. This is why those tesseral harmonic perturbations J_{nm} with $m \neq 0$ that do not match the ground patterns are insignificant, while those that do match are not averaged out over time. The resonant orbit rather repeatedly picks them up and by this they are amplified leading to significant orbital perturbations, so-called *resonant perturbations.* This type of perturbation due to repeated pattern effects is quite different from the type of perturbation, evaluated in Sect. 12.3, due to single instance effects. For a resonant orbit we rather have to answer the following three questions:

1. What are the key orbital elements of a resonant orbit?
2. For a given resonant orbit which are the relevant spherical harmonics of the gravitational potential?

3. How do these spherical harmonics perturb the resonant orbit?

In the following sections we will give answers to the first two questions for the most important cases of circular and near-circular resonant orbits, $\varepsilon \approx 0$, and we will exemplify for a geostationary orbits and GPS orbits how these are perturbed.

Draconitic Motion

Before we go into the details of resonant orbits first we have to find a measure for recurrence. As the reference point of recurrence one usually chooses the ascending node in the geocentric equatorial reference frame. The orbital period relative to this node is the so-called *draconitic*[1] *period*, T_Ω. To determine it we recall from Sect. 12.3.3—and noting that $\dot{\vartheta} \equiv \langle \dot{\vartheta} \rangle_P$, $\dot{\vartheta} = \dot{a}, \dot{e}, \dot{i}, \dot{\omega}, \dot{\Omega}, \dot{M}$, i.e., orbital elements averaged over one period—that due to the oblateness perturbation the orbit after one revolution suffers the positional shift $(\dot{M} - n)T_\Omega$ in the orbit and the rotation of the orbit's line of apsides $\dot{\omega}\, T_\Omega$. Therefore, the mean draconitic motion, which is the mean motion on the orbit between two passes of the (drifting) ascending node, is

$$\begin{aligned} n_\Omega &= n + \dot{\omega} + (\dot{M} - n) = \dot{\omega} + \dot{M} \qquad \textbf{mean draconitic motion} \\ &= \sqrt{\frac{\mu}{a^3}}\left\{1 + j_2\left[3 - 4\sin^2 i + \left(1 - \frac{3}{2}\sin^2 i\right)\left(\sqrt{1-e^2} - 1\right)\right]\right\} \\ &= \sqrt{\frac{\mu}{a^3}}\left\{1 + j_2\left[3 - 4\sin^2 i + O(e^2)\right]\right\} \quad @\ e \approx 0 \end{aligned} \tag{12.4.1}$$

where the latter relation follows for circular or near-circular orbits from Eq. (12.3.15) as a result of the oblateness perturbation. The n_Ω is nearly unaffected by higher-order perturbations. This follows from our considerations in Sect. 12.3.2 where we have shown that the significant J_3 effect cancels out for the mean draconitic motion. Observe that for $i < \arcsin\sqrt{3/4} = 60^\circ$ a near-circular Earth-orbiting satellite progresses faster between two ascending nodes, or slower otherwise.

The mean draconitic motion deviates from the orbital mean motion n. This can be understood if we interpret the second and third line of Eq. (12.4.1) in terms of a modified standard gravitational parameter $\mu' = \mu\{1 + j_2[\ldots]\}^2$, which is due to the different gravitational pull for on a satellite from Earth's bulge. This pull is positive (negative) for $i < 60^\circ$ ($i > 60^\circ$).

From the mean draconitic motion the draconitic period is easily determined as

$$T_\Omega = \frac{2\pi}{n_\Omega} = 2\pi\sqrt{\frac{a^3}{\mu}}\frac{1}{1 + j_2\left[3 - 4\sin^2 i + O(e^2)\right]} \quad @\ e \approx 0 \quad \textbf{draconitic period} \tag{12.4.2}$$

which is the time between the succeeding passes of the drifting ascending node.

[1]The term *draconitic* (a.k.a. draconic) derives from the ascending node of the Moon's orbit around Earth, which in traditional astrology is called *dragon's head*. The dragon is *draco* in Latin.

12.4.1 Resonance Conditions

In this section we want to figure out the answer to the first question: When does an orbit achieve resonance? We do not want to go into the sophisticated results of resonant perturbations, which are basically laid out originally in Kaula's resonant perturbation theory (Kaula 1966) and summarized in Vallado (2001, Sect. 9.6) but simplify the analysis by restricting ourselves for the rest of Sect. 12.4 to the practically relevant circular or near-circular orbits, $e \approx 0$.

We start our resonance considerations with an arbitrary Earth orbit. The longitude of its ascending node λ_Ω is shifted after one draconitic period T_Ω by the so-called *orbital track interval*

$$\Delta\lambda_\Omega = \left(\omega_\oplus - \dot{\Omega}\right) T_\Omega$$

to westerly longitudes, with $\omega_\oplus = 2\pi/T_{sidereal} = 7.2921150 \times 10^{-5}\ \mathrm{s}^{-1}$. Now, resonance, i.e., repetition of the ground track pattern, is achieved if after k orbital revolutions the total shift $k \cdot \Delta\lambda_\Omega$ equals a multiple l of a terrestrial revolution of 360°, i.e., if

$$k\left(\omega_\oplus - \dot{\Omega}\right) T_\Omega = 2\pi \cdot l$$

where k, l are any non-divisible natural numbers. We call such an orbit a ***k*:*l* commensurate orbit**. With Eqs. (12.4.2) and (12.4.1) we obtain from the above the following resonance condition equation

$$n_\Omega = \frac{k}{l}\left(\omega_\oplus - \dot{\Omega}\right) = \dot{\omega} + \dot{M} \quad \textbf{resonance condition} \tag{12.4.3}$$

Safely neglecting higher perturbational terms j_2^2, j_4 as shown in Sect. 12.3.3 we can insert the expression from Eq. (12.4.1) for n_Ω and from Eq. (12.3.15) for $\langle\dot{\Omega}\rangle$, and obtain the conditional equation for the semi-major axis of a commensurate orbit, a_c,

$$\frac{k}{l}\sqrt{\frac{a_c^3}{\mu}}\,\omega_\oplus = 1 + j_2\left[3 - 4\sin^2 i - \frac{k}{l}\cos i + O\left(e^2\right)\right] \quad @\ e \approx 0$$

with $j_2 = \dfrac{3J_2R_\oplus^2}{2a_c^2} + O\left(e^2\right)$.

Note that only the semi-major axis and not the eccentricity is specified by the resonance condition because the mean motion of an orbit does not depend on its eccentricity. In order to solve for the self-consistent a_c we recall that j_2 is only of order $j_2 \approx 10^{-5}$, which permits us to apply perturbation theory and find the solution by iteration. In zeroth order we set $j_2 = 0$ and with $\sqrt[3]{\mu/\omega_\oplus^2} = 42\,164.17$ km we find

$$a_{c0} = 42\,164.17 \cdot \left(\frac{l}{k}\right)^{2/3} \text{km}$$

Applying this to j_2 we get

$$j_2 = \frac{3}{2}\frac{J_2 R_\oplus^2}{\left(\mu/\omega_\oplus^2\right)^{2/3}}\left(\frac{k}{l}\right)^{4/3} = 3.71595 \times 10^{-5}\left(\frac{k}{l}\right)^{4/3}$$

For a first-order approximation we insert this into the above equation and finally find

$$a_c = a_{c0}(1+\Delta)^{2/3} = 42\,164.17\left[\frac{l}{k}(1+\Delta)\right]^{2/3}\ \text{km} \tag{12.4.4}$$

with

$$\Delta = 3.71595 \times 10^{-5}\left(\frac{k}{l}\right)^{4/3}\left[3 - 4\sin^2 i - \frac{k}{l}\cos i + O\left(e^2\right)\right] \quad @\ e \approx 0$$

This equation provides the semi-major axis of a $k : l$ commensurate orbit subject to gravitational perturbation, which is the key orbital element of a resonant orbit. For low elliptic orbits with altitudes $h \leq 1300$ km we find $\Delta \approx -10^{-2}$, which is considerable. That is to say, the regression of nodes and the progression of the line of apsides due to Earth's oblateness and the orbital inclination have to be taken into account to determine the exact altitude via Eq. (12.4.4).

Repeat Ground Track Orbits in LEO

A good case of commensurate orbits are remote sensing satellites, i.e. Earth observation satellites in low Earth orbits (LEO). Remote sensing mission conditions usually require that the satellite needs to retrace the ground track after a given number of days and hence periodically revisit predetermined areas of interest. Such an orbit is called

> ***Repeat ground track* (RGT) *orbit***, a.k.a. *phased orbit*, denominated as *l*D*k*R. This means that after k integer orbital revolutions and l integer days a RGT satellite will begin to retrace its ground track pattern.

For example a satellite in a 2D14R orbit repeats its identical ground track after 2 days, during which it performs 14 revolutions. *l*D*k*R orbits are therefore $k : l$ commensurate orbits with resonance condition Eq. (12.4.3). In Fig. 12.13 each dot depicts a possible RGT in LEO. So-called

> ***Phased Sun-synchronous orbits*** are RGTs, which in addition are Sun-synchronous and hence are near-polar RGTs.

Today's Earth observation satellites are phased Sun-synchronous having repeat cycles of typically 16 days or more. Good examples are Spot 4 (26D365R) or Landsat 7/8 (16D233R).

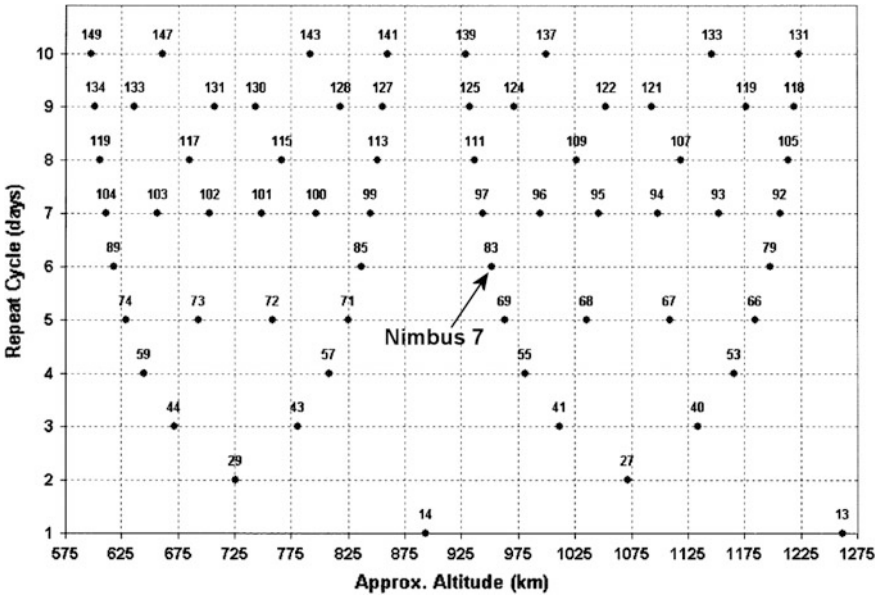

Fig. 12.13 Repeat ground tracks in LEO with altitude given on the horizontal axis. Each dot designates an RGT with repeat cycle l days (vertical axis) after k revolutions (number on top of each RGT dot). Note the degeneracies, e.g. $l{:}k$ = 1:14 (1D14R) = 2:28 (2D28R) = 3:42 (3D42R) = ⋯ *Credit* NASA/Ronald J. Boain

Example

Design a phased Sun-synchronous Earth observation satellite having a circular orbit at altitude of about 700 km.

According to the above we derive from $a_{c0} \approx 7078\ \text{km} = 42\,164.17 \cdot (l/k)^{2/3}$ km a commensurability of $l = 16$, $k = 232.63 \approx 233$. Because Sun-synchronous orbits are at about $i \approx 98°$ we find from Eq. (12.4.4) $a_c \approx 7077.4$ km or $h_c \approx 699.3$ km. To ensure Sun-synchronicity we apply Eq. (12.3.40) and obtain $i = 98.19°$. These are exactly the orbital data of Landsat 7 and 8 satellites having 16D233R.

12.4.2 Resonance Dynamics

Coupling Multipoles

Having found the orbits that revisit certain areas of the Earth's surface regularly we now turn to the next question, namely: Which spherical harmonics are in unison with these specific areas and hence may dynamically affect the resonant orbit? In other words, which are the perturbing multipoles J_{nm} with degree n and order m this commensurate (near-)circular orbit couples to? The answer, again given by Kaula's resonant perturbation theory, turns out to be

$$\frac{k}{l} = \frac{m}{n-2p}, \quad p = 0, 1, 2, 3, \ldots \quad @\ e \approx 0$$

This equation can be fulfilled for all those n, m, p for which holds

$$\begin{array}{l} m = jk \geq 1 \\ n = jl + 2p \geq 2 \end{array} \quad \begin{array}{l} j = 1, 2, 3, 4, \ldots \\ p = 0, 1, 2, 3, \ldots \end{array}, \quad m \leq n \quad @\ e \approx 0 \tag{12.4.5}$$

The equation states that an orbit with $k : l$ resonance will couple to only those multipoles J_{nm} that satisfy Eq. (12.4.5).

Note *Mere zonal multipoles J_{n0} are unable to cause resonant perturbations, because they lack any sectors to cause longitudinal accelerations. Therefore* $1 \leq m \leq n$ holds. Be reminded that $J_{11} = J_{21} = 0$ due to Table 12.2.

Equation (12.4.5) arises from the procedure to match the orbital ground track to the multipole pattern in such a way that the induced acceleration forces add up to a non-vanishing value over one revolution. An example is given in Fig. 12.14 for the ground track for GPS satellites (details see Sect. 12.4.4), which are 2:1 commensurate with Earth's rotation. If the GPS orbit would be circular, only the acceleration forces due to J_{32}, J_{44}, which follow from Eq. (12.4.5), are in lock-step leading to a drift of the resonant orbit. But because GPS satellites exhibit $e = 0.01 - 0.02$ (for details see Sect. 12.4.4) the acceleration forces for the synchronous

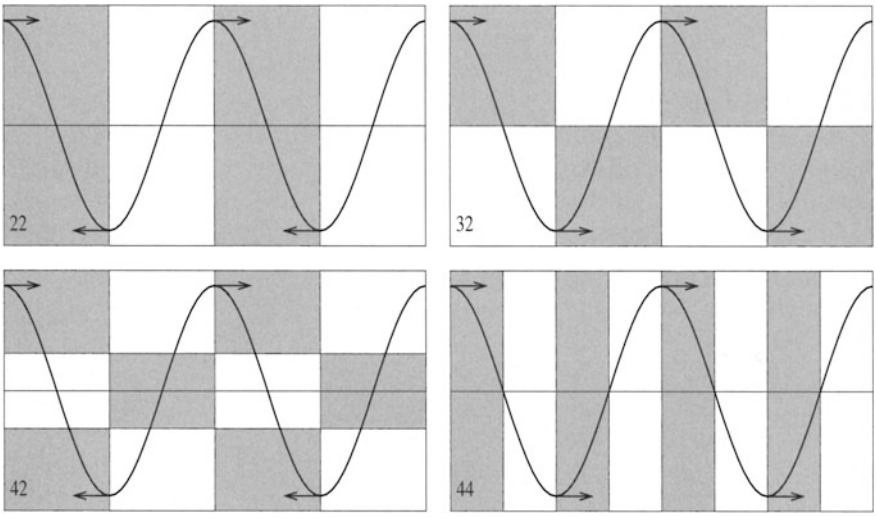

Fig. 12.14 Periodic drift forces indicated as arrows acting on a circular 2:1 commensurate orbit (GPS orbit). The Mercator projection shows gravitational multipole patterns (rectangles) of the Earth with higher (marked gray) and lower (marked white) gravitational attraction. *Credit* Beutler (2005b) and Urs Hugentobler (1998)

apsides J_{22}, J_{42} mutually do not exactly annihilate and hence also have a small impact on the orbit. We will discuss the interaction between a multipole and the resonant orbit in Sect. 12.4.5 for GEO in detail.

Equation of Motion

The resonant gravitational multipoles perturb the commensurate orbit such that tiny forces (see arrows in Fig. 12.14) accelerate or decelerate the body on the orbit along its track. The resulting modified orbital velocity implies an altered centrifugal force, which in turn leads to a variation of the orbital radius equaling the osculating semi-major axis. Assuming near-circular orbits with $e \approx 0$ we get from Eq. (12.2.7) for these variations quite generally

$$\frac{da}{dt} = \frac{2}{an}\frac{\partial R}{\partial M} \quad @\ e \approx 0$$

Owing to $n = \sqrt{\mu/a^3}$ a variation in the semi-major axis translates into variation of mean motion as

$$\dot{n} = -\frac{3}{2}\frac{n}{a}\dot{a} = -\frac{3}{a^2}\frac{\partial R}{\partial M} \quad @\ e \approx 0 \tag{12.4.6}$$

This is quite a telling equation. It states that

Dynamics at Stable and Unstable Positions

At positions where the perturbational acceleration force $\partial R/\partial M > 0$ the body is driven to larger orbital radii, $\dot{a} > 0$. This in turn leads to a slow down, $\dot{n} < 0$, of the orbital velocity and hence, and contrary to first expectations, to a drift of the body (see outer green arrows in Fig. 12.19) opposite to the acceleration forces (minus sign, red arrows in Fig. 12.19) and therefore back to a stable position. At positions with $\partial R/\partial M < 0$ we have the opposite dynamics and hence unstable (metastable) positions.

In effect we have a repulsive force, from which we overall expect an oscillating behavior of the perturbed body on its Keplerian orbit.

According to Eq. (12.4.3) $\dot{n}_\Omega \approx \dot{n}$ translates into a drift rate of the longitude of the ascending node of a commensurate orbit as

$$\ddot{\lambda}_\Omega \approx \frac{l}{k}\dot{n} = -\frac{3}{a^2}\frac{l}{k}\frac{\partial R}{\partial M} \quad @\ e \approx 0 \tag{12.4.7}$$

where according to Eq. (12.2.3)

$$R(a, \beta, \lambda) \ = a^2 n^2 \sum_{n=2}^{\infty} \left(\frac{R_\oplus}{a}\right)^n \sum_{m=1}^{n} J_{nm} P_n^m(\sin\beta) \cos m(\lambda - \lambda_{nm})$$

with $1 \leq m$ (see Note following Eq. (12.4.5)). From this we already can observe that the resonant terms R_{nm} will detune the resonant orbit. The induced motion in phase space (λ_Ω, a) is shown in Fig. 12.15 for a GEO satellite.

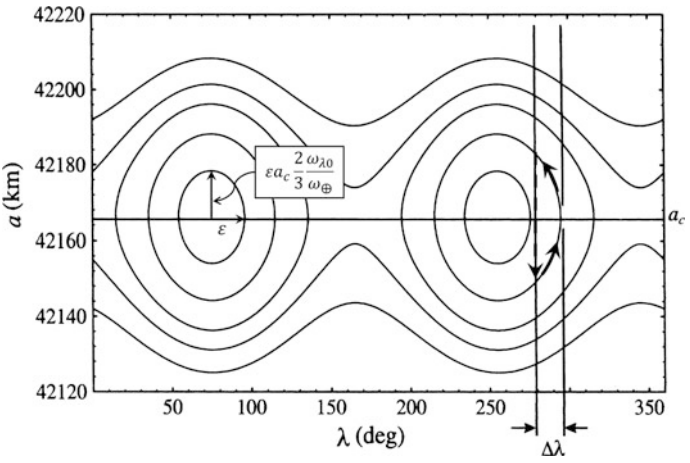

Fig. 12.15 Motion profiles in the (λ_Ω, a) phase space of spacecraft in GEO. The right hand side shows the classical east-west station-keeping strategy in the $\Delta\lambda$ dead-band (cf. Fig. 12.22)

To determine the motional details of resonance dynamics, we have to derive the equation of motion by evaluating $\partial R/\partial M$, which is quite complicated. We therefore again resort to Kaula's resonant perturbation theory where he showed that (see, e.g., Chao (2005)) for near-circular orbits with $e<0.01$

$$\begin{aligned} R &= \frac{\mu}{r}\sum_{n,m}\left(\frac{R_\oplus}{r}\right)^n J_{nm}P_n^m(\sin\beta)\cos m(\lambda-\lambda_{nm}) \\ &= \frac{\mu}{r}\sum_{n,m,p}\left(\frac{R_\oplus}{a}\right)^n J_{nm}F_{nmp}(i)\left\{\begin{array}{ll}\cos m(\lambda_\Omega-\lambda_{nm}) & @\ n-m=even\\ \sin m(\lambda_\Omega-\lambda_{nm}) & @\ n-m=odd\end{array}\right\} \end{aligned} \qquad @\ e<0.01$$

where

$$\lambda_\Omega = \frac{l}{k}(\omega+M)+\Omega-\theta_{GMST},$$

θ_{GMST} is the *Greenwich Mean Sidereal Time*, which in the equatorial plane is the hour angle from the vernal point (First Point of Aries) to the Greenwich Meridian, and $F_{nmp}(i)$ are the so-called *inclination functions* given, e.g., by Chao (2005, Table 4.2).

Remark *For considerably eccentric orbits, i.e., if* $e>0.01$*, an additional index q plus in the right-hand side of the above equation an additional q-sum over eccentricity functions* $G_{npq}(e)$ *shows up in the resonance condition Eq. (12.4.5). For details see e.g., Chao* (2005, *Chapter 4*).

This may hold even for orbits with weak eccentricity if they couple via *the q index to Earth's oblateness which is much more pronounced than any higher-order deformations. However, it can be shown that this applies only to* $k:l=2:1$*, i.e., to commensurate GPS orbits, which is why we treat this problem separately there* (see Sect. 12.4.4).

With $r = a$ we can differentiate the above expression and by defining the symbol

$$\begin{bmatrix} x_{nm} \\ y_{nm} \end{bmatrix} := \begin{Bmatrix} x_{nm}, & n-m = even \\ y_{nm}, & n-m = odd \end{Bmatrix}$$

we finally obtain from Eq. (12.4.7)

$$\ddot{\lambda}_\Omega = 3n^2 \left(\frac{l}{k}\right)^2 \sum_{n/m/p} \left(\frac{R_\oplus}{a_c}\right)^n m J_{nm} F_{nmp} \begin{bmatrix} \sin m(\lambda_\Omega - \lambda_{nm}) \\ -\cos m(\lambda_\Omega - \lambda_{nm}) \end{bmatrix} \quad @\ e < 0.01\ \textbf{EoM} \tag{12.4.8}$$

This is the equation of motion of the longitude of the ascending node of a $k:l$ circular or near-circular commensurate orbit with semi-major axis a_c as given in Eq. (12.4.4), $n \approx n_\Omega = \sqrt{\mu_\oplus / a_c^3}$, $J_{n,m}$, λ_{nm} given by Eq. (12.3.15), and triples $n/m/p$ as obtained from Eq. (12.4.5). It tells us the dynamical behavior of a satellite about a resonant orbit. Note that from Eq. (12.4.3) $n_{\Omega\frac{l}{k}} \approx \omega_\oplus$.

By multiplying the above equation on both sides with $\dot{\lambda}_\Omega$ we can directly integrate it to get the drift velocity

$$\dot{\lambda}_\Omega^2 = 6n^2 \left(\frac{l}{k}\right)^2 \sum_{n/m/p} \left(\frac{R_\oplus}{a_c}\right)^n J_{nm} F_{nmp} \begin{bmatrix} \cos m(\lambda_\Omega - \lambda_{nm}) \\ \sin m(\lambda_\Omega - \lambda_{nm}) \end{bmatrix} + \dot{\lambda}_{\Omega 0}^2$$

Of course the drift velocity becomes maximum or minimum at longitudes, which are the roots of Eq. (12.4.8). This is a differential equation from which $\lambda_\Omega(t)$ might be derived as well.

Dynamics About Stable Positions

According to Eq. (12.4.8) $\ddot{\lambda}_\Omega$ is periodic and thus will have at least $2 \times \min(m)$ roots, half of which have a negative slope (see Fig. 12.16 for GPS and Fig. 12.21 for GEO orbits) dynamics about these longitudes are periodic oscillations. We denote these stable positions as λ_0. To circumstantiate these oscillations we approximate the equation of motion about the stable positions as

$$\ddot{\lambda}_\Omega = \left.\frac{d\ddot{\lambda}_\Omega}{d\lambda_\Omega}\right|_0 (\lambda_\Omega - \lambda_0) =: -\omega_{\lambda 0}^2 (\lambda_\Omega - \lambda_0) \tag{12.4.9}$$

with

$$\omega_{\lambda 0}^2 = -3n^2 \left(\frac{l}{k}\right)^2 \sum_{n/m/p} \left(\frac{R_\oplus}{a_c}\right)^n \mathrm{m}^2 J_{nm} F_{nmp} \begin{bmatrix} \cos m(\lambda_0 - \lambda_{nm}) \\ \sin m(\lambda_0 - \lambda_{nm}) \end{bmatrix}$$

The solution is a harmonic oscillator of general type

$$\lambda_\Omega = \lambda_0 + \varepsilon \sin(\omega_{\lambda 0} t + \varphi)$$

where the amplitude ε and phase φ are given by the initial conditions.

We now consider the drift rate of the semi-major commensurate axis, which according to Eqs. (12.4.6) and (12.4.7) is

$$\dot{a} = -\frac{2}{3}\frac{a_c}{n}\frac{k}{l}\dot{\lambda}_\Omega = -2a_c n\frac{l}{k}\sum_{n/m/p}\left(\frac{R_\oplus}{a_c}\right)^n mJ_{nm}F_{nmp}\begin{bmatrix}\sin m(\lambda_\Omega - \lambda_{nm})\\ -\cos m(\lambda_\Omega - \lambda_{nm})\end{bmatrix}$$

We want to study this drift rate for small oscillations about the stable points. We therefore apply Eq. (12.4.9) and get with $\lambda_\Omega - \lambda_0 = \varepsilon\,\sin(\omega_{\lambda 0}t + \varphi)$ and $n_{\dot{k}}^{l} \approx \omega_\oplus$

$$\dot{a} = \frac{2}{3}\frac{a_c}{n}\frac{k}{l}\omega_{\lambda 0}^2\varepsilon\,\sin(\omega_{\lambda 0}t + \varphi) \approx a_c\varepsilon\frac{2}{3}\frac{\omega_{\lambda 0}^2}{\omega_\oplus}\sin(\omega_{\lambda 0}t + \varphi)$$

We are able to integrate this equation to yield with the initial conditions $\lambda_\Omega(0) = \lambda_0 + \varepsilon$, i.e., $\varphi = \pm 90°$, and $a(0) = a_c$

$$a(t) = a_c\varepsilon\frac{2}{3}\frac{\omega_{\lambda 0}}{\omega_\oplus}\cos(\omega_{\lambda 0}t \pm 90°) + a_c$$

and hence

$$\begin{aligned}\lambda_\Omega(t) &= \lambda_0 + \varepsilon\,\cos\omega_{\lambda 0}t\\ a(t) &= a_c\left(1 \pm \varepsilon\tfrac{2}{3}\tfrac{\omega_{\lambda 0}}{\omega_\oplus}\sin\omega_{\lambda 0}t\right)\end{aligned} \quad @\ e < 0.01,\ \lambda_\Omega(0) = \lambda_0 + \varepsilon \qquad (12.4.10)$$

with $\omega_\oplus = 6.300\ \text{day}^{-1}$ and ε the small amplitude of the longitudinal oscillation. These equations describe an elliptic clock- or anticlockwise harmonic motion in the (λ_Ω, a) plane, the so-called *phase space*, about the center point (λ_0, a_c) with amplitudes $\left(\varepsilon, \varepsilon a_c\frac{2}{3}\omega_{\lambda 0}/\omega_\oplus\right)$ as shown in Fig. 12.15 for GEOs.

Having derived the basic dynamics of resonant orbits we will consider in the following two sections the GPS orbits and geostationary as typical and instructive examples of resonant orbits.

12.4.3 Low Earth Orbits

In LEOs only repeat ground track orbits (see Sect. 12.4.1) with resonances of type $k:1$ (1DkR) suffer considerable resonance dynamics (see dots on bottom line in Fig. 12.14). Higher-order resonances $k:2$, $k:3$, … tend to become less relevant, because then there is an increasing number of sectors "out of resonance sequence", which effectively decreases the overall resonant acceleration, even though the multipole coefficients of the relevant multipoles ($k/2$, m), ($k/3$, m), … are by a factor of about $2^{3/2} = 2.8$, $3^{3/2} = 5.2$, … larger ("Kaula's rule of thumb", Kaula 1966). Therefore the work-horses of remote sensing, Landsat 7/8 with 16D233R = 233:16, are far from suffering any resonance dynamics.

From the rule Eq. (12.4.5) we derive that for these the following multipoles are effective:

$a_{c0} - R_\oplus$ [km]	k:1 resonance	Relevant multipoles (n,m,p)
1248.2	13:1	(13,13,6), (15,13,7), (17,13,8), (19,13,9), …
880.6	14:1	(15,14,7), (17,14,8), (19,14,9), (21,14,10), …
554.2	15:1	(15,15,7), (17,15,8), (19,15,9), (21,15,10), …
262.3	16:1	(17,16,8), (19,16,9), (21,16,10), (23,16,11), …

Note that the 16 : 1 resonance at altitude $h = 262.3$ km is already strongly affected by drag, which continuously lowers the orbit (see Sect. 12.7.3) and so detunes the resonance if no orbit maintenance is performed.

12.4.4 GPS Orbits

The GPS (Global Positioning System) is a US space-based global navigation satellite system where between 24 and 32 (usually 31) active satellites circle Earth equally spaced in six orbital planes (designated A through F) with $\Omega_A = 10^\circ$ and separated by $\Delta\Omega = 60^\circ$. Their specific orbital elements are $i = 55^\circ$, $e = 0.001$, and they exhibit a revolutionary period of exactly half a sidereal day, i.e., they are in a deep $k : l = 2 : 1$ resonance with Earth's rotation. From Eq. (12.4.4) we derive $\Delta = -7.783 \times 10^{-5}$ or a resonant orbital radius of

$$a_{GPS} := a_c = 26\,560.38 \text{ km}$$
$$n_{GPS} = \sqrt{\frac{\mu_\oplus}{a_{GPS}^3}} = 12.602 \text{ day}^{-1}$$
$$\frac{R_\oplus}{a_{GPS}} = 0.24014$$

From Eq. (12.4.5) we infer that for $n \leq 5$ the triples $n/m/p = 321,\ 441,\ 522$ need to be considered. With this resonance condition we obtain from Eqs. (12.4.8) and (12.2.5a), and Table 12.2

$$\ddot{\lambda}_\Omega = \frac{3}{4} n_{GPS}^2 \left[\begin{array}{l} -2\left(\frac{R_\oplus}{a_{GPS}}\right)^3 J_{32} F_{321} \cos 2(\lambda_\Omega - \lambda_{32}) \\ +4\left(\frac{R_\oplus}{a_{GPS}}\right)^4 J_{44} F_{441} \sin 4(\lambda_\Omega - \lambda_{44}) \\ -2\left(\frac{R_\oplus}{a_{GPS}}\right)^5 J_{52} F_{522} \cos 2(\lambda_\Omega - \lambda_{52}) \end{array} \right]$$

with

$$J_{32} = 3.74408 \times 10^{-7}, \quad \lambda_{32} = -17.19^\circ$$
$$J_{44} = 7.64577 \times 10^{-9}, \quad \lambda_{44} = 30.35^\circ$$
$$J_{52} = 1.17815 \times 10^{-7}, \quad \lambda_{52} = -13.18^\circ$$
$$F_{321} = \frac{15}{8}\sin i\left(1 - 2\cos i - 3\cos^2 i\right) = -1.7419$$
$$F_{441} = \frac{105}{4}\sin^2 i(1 + \cos i)^2 = 43.615$$
$$F_{522} = -\frac{105}{16}\sin i\left(1 - 2\cos i - 3\cos^2 i\right) + \frac{315}{32}\sin^3 i\left(1 - 2\cos i - 5\cos^2 i\right) = -3.6000$$

Hence for $e < 0.01$

$$\ddot{\lambda}_\Omega = \frac{1}{2}\omega_\lambda^2[\cos 2(\lambda_\Omega - \lambda_{32}) + 0.2456 \cdot \sin 4(\lambda_\Omega - \lambda_{44}) + 0.0375 \cdot \cos 2(\lambda_\Omega - \lambda_{52})] \tag{12.4.11}$$

with

$$\omega_\lambda = n_{GPS}\sqrt{3J_{32}|F_{321}|\frac{R_\oplus^3}{a_{GPS}^3}} = 0.7577 \text{ year}^{-1}.$$

This drift rate as a function of longitudinal position is depicted in Fig. 12.16. Equation (12.4.11) has four roots at $\lambda_\Omega = 25.9°\text{E}, 118.7°\text{E}, 205.9°\text{E}, 298.7°\text{E}$ with

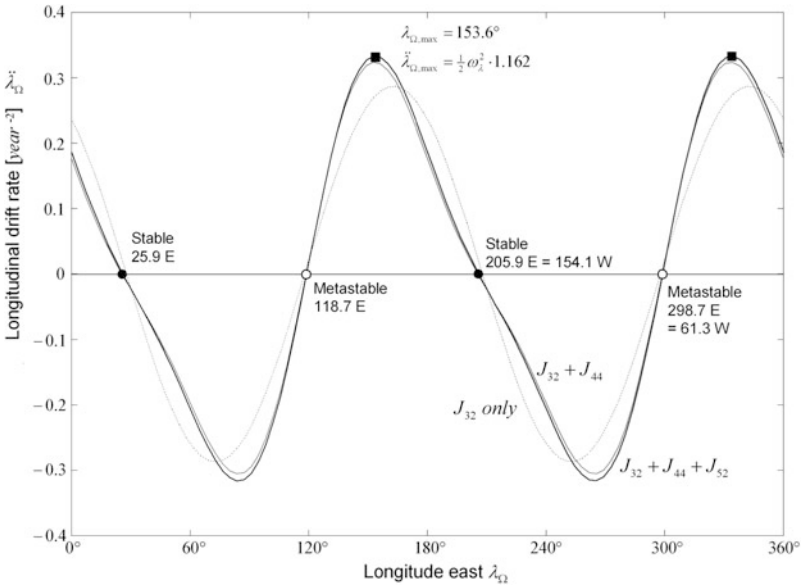

Fig. 12.16 Drift rate of the longitude of the ascending node for GPS satellites

negative slopes (indicating stable positions) at $\lambda_0 = 25.9°\text{E}, 205.9°\text{E}$ and positive slopes (indicating metastable positions) at the other two positions.

The λ_Ω of the GPS satellites are more or less equally distributed over the range 0°–360° and therefore every one of them has an individual drift rate.

Dynamics About Stable Positions

In order to evaluate the dynamic behavior at the stable points we apply Eq. (12.4.9)

$$\begin{aligned}\ddot{\lambda}_\Omega &= \left.\frac{d\ddot{\lambda}_\Omega}{d\lambda_\Omega}\right|_{\lambda_0} (\lambda_\Omega - \lambda_0) \\ &= -\omega_\lambda^2[\sin 2(\lambda_0 - \lambda_{32}) - 2 \cdot 0.2456 \cos 4(\lambda_0 - \lambda_{44}) + 0.0375 \sin 2(\lambda_0 - \lambda_{52})](\lambda_\Omega - \lambda_0) \\ &= -0.5668 \cdot \omega_\lambda^2 \cdot (\lambda_\Omega - \lambda_0) = -\omega_{\lambda 0}^2 \cdot (\lambda_\Omega - \lambda_0)\end{aligned}$$

This is the equation for an oscillating motion with angular frequency

$$\omega_{\lambda 0} = \omega_\lambda \sqrt{0.5668} = 0.5704 \text{ year}^{-1}$$

which equals a period of $T_{\lambda 0} = 2\pi/\omega_{\lambda 0} = 11.0$ years. The negative sign confirms that the longitudes $\lambda_0 = 25.9°\text{E}$, $205.9°\text{E}$ are dynamically stable positions. We determine from Eq. (12.4.10) that the harmonic motion in the phase space (λ_Ω, a) is

$$\begin{aligned}\lambda_\Omega(t) &= \lambda_0 + \varepsilon \cos \omega_{\lambda 0} t \\ a(t) &= a_c\left(1 \pm 1.65 \times 10^{-4} \varepsilon \sin \omega_{\lambda 0} t\right)\end{aligned}$$

The actual anti-clockwise harmonic motion (plus sign) is depicted in Fig. 12.17 for some GPS satellites. Observe that all motions are elliptic, although the longitudinal excursions ε of some satellites exceed the linear range about the stable points. This, however, only implies that the motion is no longer harmonic, i.e., the motion on the ellipse is no longer uniform.

Eccentric GPS Orbits

We note that a more detailed evaluation of the GPS motion would need to consider the fact that due to lunisolar perturbations the long-term eccentricity increases linearly and after 10 years is about e = 0.01–0.02. This implies that according to Eq. (12.4.4) the quantity of the resonant semi-major axis remains practically unaffected by this, but according to the Remark in Sect. 12.4.2 now the J_{22} term has to be taken into account, which contributes the additional two terms

$$\frac{a_{GPS}}{R_\oplus} \frac{J_{22}}{J_{32}|F_{321}|} \{F_{221} G_{211} \sin[2(\lambda_\Omega - \lambda_{22}) - \omega] + F_{220} G_{20-1} \sin[2(\lambda_\Omega - \lambda_{22}) + \omega]\}$$

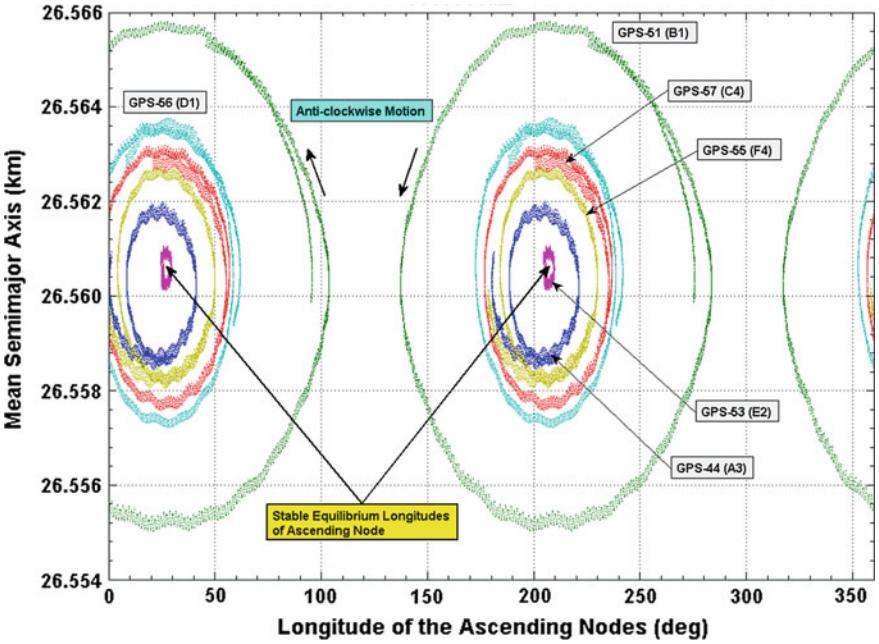

Fig. 12.17 The harmonic motion of selected GPS satellites in the (λ_Ω, a) phase space. *Credit* L. Anselmo and C. Pardini, ISTI/CNR

to the square bracket of Eq. (12.4.11). From Chao (2005, Tables 4.1 and 4.2) we find for the inclination functions $F_{nmp}(i)$ and eccentricity functions $G_{npq}(e)$ with lowest order in e

$$F_{221} = \frac{3}{2}\sin^2 i = 1.0065, \qquad G_{211} = \frac{3}{2}e$$
$$F_{220} = \frac{3}{4}(1+\cos i)^2 = 1.8571, \qquad G_{20-1} = -\frac{1}{2}e$$

With $J_{22} = 1.8155 \times 10^{-6}$ and $\lambda_{22} = -14.93^\circ$ from Eq. (12.2.5a) we then have

$$\ddot{\lambda}_\Omega = \frac{1}{2}\omega_\lambda^2 \left\{ \begin{array}{l} \cos 2(\lambda_\Omega - \lambda_{32}) + 0.2456 \cdot \sin 4(\lambda_\Omega - \lambda_{44}) + 0.0375 \cdot \cos 2(\lambda_\Omega - \lambda_{52}) \\ +e \cdot 17.501 \cdot \sin[2(\lambda_\Omega - \lambda_{22}) - \omega(t)] \\ -e \cdot 10.764 \cdot \sin[2(\lambda_\Omega - \lambda_{22}) + \omega(t)] \end{array} \right\}$$

According to Sect. 12.3.3 $\omega(t) \approx 2n_{GPS}j_2\left(1 - \frac{5}{4}\sin^2 i\right) \cdot t = \dot{\omega}_{GPS}t$ for $e > 0.001$ with $\dot{\omega}_{GPS} = 7.964^\circ \cdot \text{year}^{-1} = 4.405 \times 10^{-9}\ \text{s}^{-1}$. Due to this time dependence the equation of motion then can only be solved numerically.

GLONASS, Compass, and Galileo
The Russian Global Navigation Satellite System, GLONASS, with a target constellation of 24 satellites is in a mild 17 : 8 resonance orbit at $i = 64.8°$, while the 27 MEO satellites of the Chinese satellite navigation system *Compass* is in an insignificant 41 : 22 resonance at $i = 55°$, and the European satellite navigation system *Galileo* with 30 spacecraft (including 3 spares) is chosen to be in a mild 17 : 10 resonance at $i = 56°$. According to Eq. (12.4.4) their semi-major axes hence are $a_{GLONASS} = 25507.60$ km, $a_{Compass} = 27840.96$ km, and $a_{Galileo} = 29600.27$ km. They are thus sufficiently far away from the 2 : 1 resonance and do not suffer from considerable resonance perturbations.

12.4.5 Geostationary Orbit

A geostationary orbit, or GEO for short, with $e = i = 0$ is a prime example of a resonant orbit exhibiting $k = l = 1$, i.e., the orbit is in perfect pace with Earth's rotation. Hence a satellite in GEO seems to be at rest as seen from any position on Earth. This makes GEO a perfect orbit for telecommunication services, in particular broadcasting services, because this ensures a continuous service while the alignment of the satellite dish remains fixed. This is why there are so many communications satellites in GEO, about 450 satellites as of 2018.

From the above properties follows with Eq. (12.4.4) that $\Delta = 2 \times 3.71595 \times 10^{-5} = 7.4319 \times 10^{-5}$. With this we get $a_c = 42\,164.17 \times 1^{2/3}[1 + \Delta]^{2/3}$ km and hence

$$a_{GEO} := a_c = 42\,166.26 \text{ km}$$
$$n_{GEO} = \sqrt{\mu_\oplus / a_{GEO}^3} = \omega_\oplus = 7.2921150 \times 10^{-5} \text{ s}^{-1}$$

for the commensurate GEO radius. We recall from the discussion after Eq. (12.4.1) that rather than having the radius at $a = \sqrt[3]{\mu/\omega_\oplus^2} = 42{,}164.17$ km the somewhat elevated radius is due to an increased gravitational pull of the equatorial bulge to get in pace with Earth's rotational speed $\omega_\oplus$. From Eq. (12.4.5) we derive that J_{22}, J_{31}, J_{32}, and J_{33} are relevant, to name the most significant contributions.

The resonant perturbation of GEO is sometimes called *triaxiality*. "Triaxiality" refers to the triaxiality of the "potato's" potential (see Fig. 12.4, right, and color plates on pages 568 and 569 and Fig. 12.19), which includes zonal, sectorial, and tesseral harmonics (bold multipole coefficients in Table 12.2). The most prominent part of the "potato" is the multipole J_{22}, which looks like a dumbbell as depicted in Fig. 12.18. It stretches along the 15°W–165°E direction.

Because it is this dumbbell that most significantly acts upon GEO we will learn most of GEO's resonant perturbation by explaining how the dumbbell interacts with a satellite's orbit. The masses on both sides of the dumbbell cause a constant lateral gravitational pull on the body in GEO. Its impact on the body depends on its initial

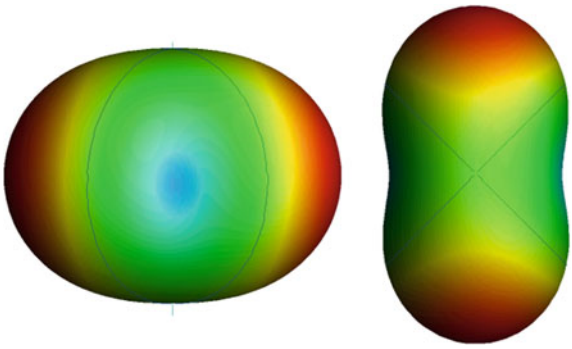

Fig. 12.18 Earth's "dumbbell" multipole J_{22}. (Left) Observed from the terrestrial equatorial plane. (Right) Observed from the terrestrial pole. *Credit* GFZ Potsdam

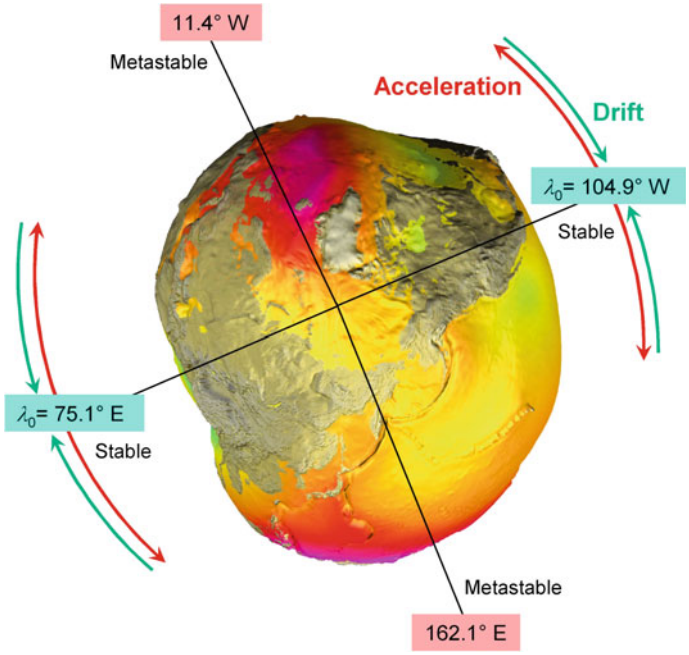

Fig. 12.19 Forces on a body in geostationary orbit at the abeam points of the "triaxial potato". *Credit* GFZ Potsdam

position. If the position is exactly on the dumbbell's lateral axis, i.e., displaced by 90° from the longitudinal 15°W–165°E axis at 75°E or 105°W, then it is subject to the same gravitational pull from both ends of the dumbbell. So the effective gravitational pull is indifferent, and its position would be metastable. If it is displaced by 45° with regard to the longitudinal axis, it is subject to a stronger force from the closer end of the dumbbell. This leads to the motion dynamics as described in sub-section *Dynamics about Stable Positions* in Sect. 12.4.2, depictured in phase space in Fig. 12.16, and plotted in real space in Fig. 12.20.

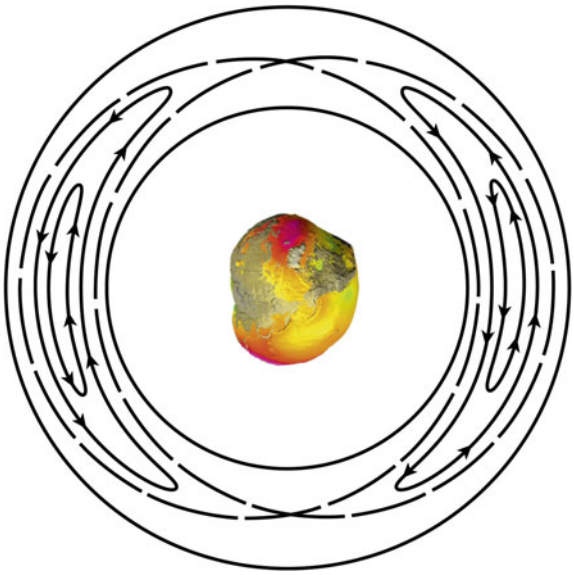

Fig. 12.20 Motion dynamics of a body in an oblate ellipsoidal gravitational potential, which resembles that in a dumbbell potential

So we see that the abeam positions at 75°E and 105°W, though being statically unstable, are actually dynamically stable. This situation is similar to the dynamical stability of a S/C near the statically unstable L_4 and L_5 equilateral libration points (see Sect. 11.5.3). If the body is positioned right above the ends of the dumbbell this would also be an indifferent position. But just a small deviation would cause a tangential acceleration back to the indifferent position, causing a drift even further away from the initial position according to Eq. (12.4.7). The positions above the ends of the longitudinal axis hence turn out to be metastable. The actual values of the stable and metastable positions are slightly different from these, which is due to the J_{31} and J_{33} perturbations (see below).

Equation of Motion

We now want to describe the orbit drifts on mathematical grounds and therefore resort to the results of Sect. 12.4.2. But rather than to use Eq. (12.4.8) (there exists no ascending node for GEOs anyway) we start out with Eq. (12.4.6) and take into account that any variation of the mean motion due to resonance perturbations equals the drift rate of the longitudinal position of the satellite, $\ddot{\lambda} = \dot{n}_{GEO}$. Owing to the circularity of the orbit we also have $dM = d\theta = d\lambda$. This is applied to Eq. (12.4.6), which yields the equation of longitudinal motion

$$\ddot{\lambda} = -\frac{3}{a^2}\frac{\partial R}{\partial \lambda} \tag{12.4.12}$$

with

$$R(a,0,\lambda) = a^2 n^2 \sum_{n=2}^{3} \left(\frac{R_\oplus}{a}\right)^n \sum_{m=1}^{n} J_{nm} P_n^m(0) \cos m(\lambda - \lambda_{nm})$$

where $\beta = 0$ because $i = 0$. From Eq. (12.2.6) with $x = \sin\beta = s = 0$, $c = \cos\beta = 1$ we get

$$P_2^1(0) = 0,\ P_2^2(0) = 3,\ P_3^1(0) = 3/2,\ P_3^2(0) = 0,\ P_3^3(0) = -15$$

which corroborates the finding from Sect. 12.4.2 that only J_{22}, J_{31}, and J_{33} are relevant resonance terms in GEO. It is now easy to evaluate $\partial R/\partial\lambda$ and we obtain for the GEO drift rate

$$\begin{aligned}\ddot{\lambda} &= 3n^2\left\{6\frac{R_\oplus^2}{a^2}J_{22}\sin 2(\lambda-\lambda_{22}) + \frac{R_\oplus^3}{a^3}\left[\frac{3}{2}J_{31}\sin(\lambda-\lambda_{31}) - 45J_{33}\sin 3(\lambda-\lambda_{33})\right]\right\} \\ &= \frac{18R_\oplus^2}{a^2}n^2 J_{22}\left[\sin 2(\lambda-\lambda_{22}) + \frac{1}{4}\frac{R_\oplus}{a}\frac{J_{31}}{J_{22}}\sin(\lambda-\lambda_{31}) - \frac{45}{6}\frac{R_\oplus}{a}\frac{J_{33}}{J_{22}}\sin 3(\lambda-\lambda_{33})\right]\end{aligned}$$

From Eq. (12.2.5a) and Table 12.2 we derive

$$\begin{aligned} J_{22} &= 1.8155\times10^{-6}, \quad \lambda_{22} = -14.93^\circ \\ J_{31} &= 2.2090\times10^{-6}, \quad \lambda_{31} = -173.02^\circ \\ J_{33} &= 0.22137\times10^{-6}, \quad \lambda_{33} = -39.00^\circ \end{aligned}$$

If we insert these values and $a \equiv a_{GEO}$ and $n \equiv n_{GEO}$ for GEO, we finally arrive at the GEO drift rate (cf. Campan 1995)

$$\ddot{\lambda} = \frac{1}{2}\omega_\lambda^2 \cdot [\sin 2(\lambda-\lambda_{22}) + 0.0460\cdot\sin(\lambda-\lambda_{31}) - 0.1383\cdot\sin 3(\lambda-\lambda_{33})] \tag{12.4.13}$$

with angular frequency

$$\omega_\lambda = 6\frac{R_\oplus n_{GEO}}{a_{GEO}}\sqrt{J_{22}} = 2.814\ \text{year}^{-1}$$

This drift rate as a function of longitudinal position is depicted in Fig. 12.21. Equation (12.4.13) has four roots at $\lambda = 75.1^\circ$E, 162.1°E, 255.1°E, 348.6°E with negative slopes (indicating stable positions) at $\lambda_0 = 75.1^\circ$E, 255.1°E and positive slopes (indicating metastable positions) at the other two positions (see Fig. 12.19). Because the perturbation terms J_{31} and J_{33} are an order of magnitude smaller than J_{22}, Eq. (12.4.13) can roughly be approximated just by the J_{22} term

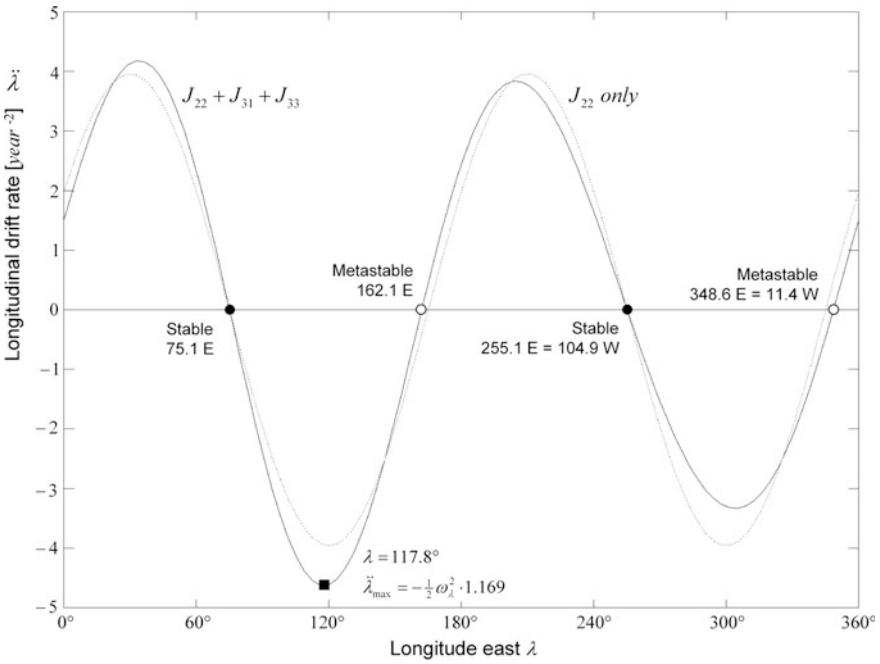

Fig. 12.21 Longitudinal drift rates of a GEO satellite as given by Eq. (12.4.13)

$$\ddot{\lambda} = \frac{1}{2}\omega_\lambda^2 \cdot \sin 2(\lambda - \lambda_{22}) = -\frac{1}{2}\omega_\lambda^2 \cdot \sin 2(\lambda - \lambda_0) \tag{12.4.14}$$

where the latter follows from $\lambda_0 - \lambda_{22} = 90°$.

Dynamics Near Stable Positions

If the body is near a stable position λ_0, in Eq. (12.4.14) the sine for small arguments can be approximated linearly to give

$$\ddot{\lambda} = -\omega_\lambda^2 \cdot (\lambda - \lambda_0)$$

This is a harmonic oscillation around the stable positions with period $T_{\lambda 0} = 2\pi/\omega_\lambda = 2.23$ years. We may improve this calculation by applying Eq. (12.4.9)

$$\begin{aligned}\ddot{\lambda}_\Omega &= \left.\frac{d\ddot{\lambda}_\Omega}{d\lambda_\Omega}\right|_{\lambda_0} (\lambda_\Omega - \lambda_0) \\ &= 0.5 \cdot \omega_\lambda^2 [2\cos 2(\lambda_0 - \lambda_{22}) + 0.0460\cos(\lambda_0 - \lambda_{31}) \\ &\quad + 3 \cdot 0.1383\cos 3(\lambda_0 - \lambda_{33})](\lambda_\Omega - \lambda_0) \\ &= -0.8109 \cdot \omega_\lambda^2 \cdot (\lambda_\Omega - \lambda_0)\end{aligned}$$

This yields a period of $T_{\lambda 0} = 2\pi/\left(\sqrt{0.8109} \cdot \omega_\lambda\right) = 2.48$ years.

Dynamics at Unstable Positions

Let us have a closer look at the time behavior when the body is far away from one of the two equilibrium positions, which usually is the case. For small time periods the instantaneous position λ can be considered almost constant. So the right-hand side of the differential Eq. (12.4.14) is a constant, and the equation can simply be integrated directly

$$\lambda = \lambda_i + \frac{1}{2}\ddot{\lambda} \cdot t^2 \tag{12.4.15}$$

So the body, initially in a resting position, moves away quadratically with time from its initial position λ_i. This is the so-called *east–west drift*.

GEO satellites are required to be kept within a dead-band slot of typical width $\Delta\lambda = 0.1^\circ$ at the center of an allocated standard longitudinal position box of size $\Delta\lambda = 0.1^\circ$ for satellites with inclination limits $i < 1^\circ$ and size $\Delta\lambda = 0.2^\circ$ for satellites with inclination limits $i < 5^\circ$. To counteract the drift, and as depictured in Fig. 12.22 correction burns, so-called *east–west station-keeping maneuers* (E/W drift maneuvers), need to be fired at that side of the box to which the satellite tends to drift freely, which cause the satellite to drift to the other side of the dead-band and back again. The recurrence time and the delta-v demand for one kick-burn can be derived from Eq. (12.4.15) to be

$$\Delta t_{sk} = 2\sqrt{\frac{2 \cdot \Delta\lambda}{|\ddot{\lambda}|}} \geq 20.1 \text{ days}$$

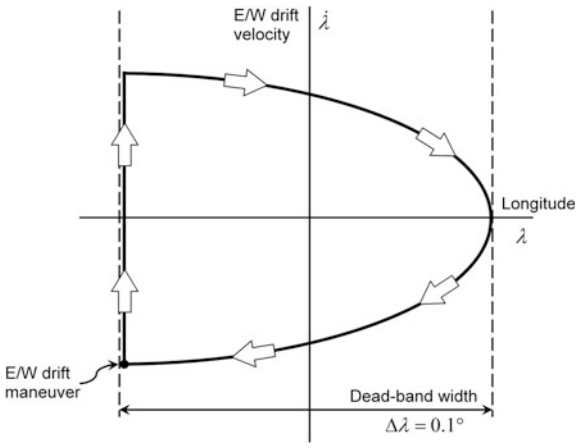

Fig. 12.22 Satellite drift pattern inside its longitude dead-band box

and

$$\Delta v_{sk} = |a_{||}| \cdot \Delta t_{sk} = \frac{2}{3} r \sqrt{2 \cdot \Delta\lambda \cdot |\ddot{\lambda}|} \leq 0.113 \text{ m s}^{-1}$$

The limits are derived from the position $\lambda = 117.8°$ where the longitudinal acceleration has its maximum absolute value with $|\ddot{\lambda}|_{\max} = \frac{1}{2}\omega_{\lambda}^2 \cdot 1.169$ (see Fig. 12.21). In total for east–west station-keeping a yearly delta-v of

$$\boxed{\Delta v = \tfrac{1}{3} r |\ddot{\lambda}| \cdot 1 \text{ year} \leq 2.06 \text{ ms}^{-1}} \text{ per year} \qquad (12.4.16)$$

needs to be taken into account. East–west station-keeping strategies and maneuvers, which also include eccentricity corrections owing to solar radiation pressure (see Sect. 12.5) are discussed at the end of Sect. 12.5.3.

12.5 Solar Radiation Pressure

A S/C orbiting a planet at a distance of r from the Sun will be affected by solar radiation unless it happens to be in the shadow of the planet. A light particle does not possess mass, but according to quantum mechanics it still carries a linear momentum h/λ (h is Planck's constant, λ is the wavelength of the light particle), which, depending on the **surface reflectivity** ρ of the S/C, transfers momentum $\rho h/\lambda$. If the surface is absorbing, then $\rho = 1$; if it is reflecting, $\rho = 2$; and if it is transparent, $\rho = 0$. The solar radiation thus produces a total radiation pressure $p_{S/C}$ on the S/C, which via the mass of the S/C creates the acceleration a_{sun}

$$\frac{m a_{sun}}{A_{\perp}} = p_{S/C} = \rho\, p_{sun}$$

where

$$p_{sun} = \frac{E}{c} = p_0 \left(\frac{r_{\oplus}}{r}\right)^2 \text{N m}^{-2} \quad \textbf{radiation pressure of the Sun} \qquad (12.5.1)$$

with

c	velocity of light
$E = (1372 \pm 45)\left(\frac{r_{\oplus}}{r}\right)^2 \text{W m}^{-2}$	intensity of solar radiation (seasonal)
$p_0 = (4.58 \pm 0.15) \times 10^{-6} \text{ N m}^{-2}$	seasonal
$r_{\oplus} = 1.4962 \times 10^8$ km	mean radius of Earth's orbit
$A_{\perp}$	surface of the S/C projected onto the direction of radiation

This results in the following acceleration of the S/C

$$a_{sun} = p_{sun} \cdot B_r \tag{12.5.2}$$

where we have defined the ballistic radiation coefficient

$$B_r = \rho \frac{A_\perp}{m} \tag{12.5.3}$$

similar to the ballistic drag coefficient in Sect. 6.2.3.

12.5.1 Effects of Solar Radiation

Qualitative Considerations

To derive the effects of solar radiation on the orbital elements, Let us assume a circular or a weakly elliptic orbit of the S/C at any altitude, i.e., $e \approx 0$ in addition to $i \approx 0$. The direction of radiation shall be in the orbital plane and perpendicular to the line of apsides, i.e., the Sun shines "laterally" onto the orbit (see Fig. 12.23). (As we will see in a moment, if we start out with a circular orbit, the solar pressure will cause an eccentricity with the line of apsides perpendicular to the radiation direction. So this assumption always holds.) Due to $e \approx 0$, $i \approx 0$ we can neglect $\dot{\omega}$, $\dot{\Omega}$ effects, and since the radiation force does not have a component vertical to the orbital plane, Table 8.1 tells us that no inclination changes result. So we only have to focus on $\dot{a}$, $\dot{e}$ effects. Table 8.1 also tells us that forces in the orbital plane perpendicular to the path do not change a, yet Eq. (8.1.1) tell us that such forces

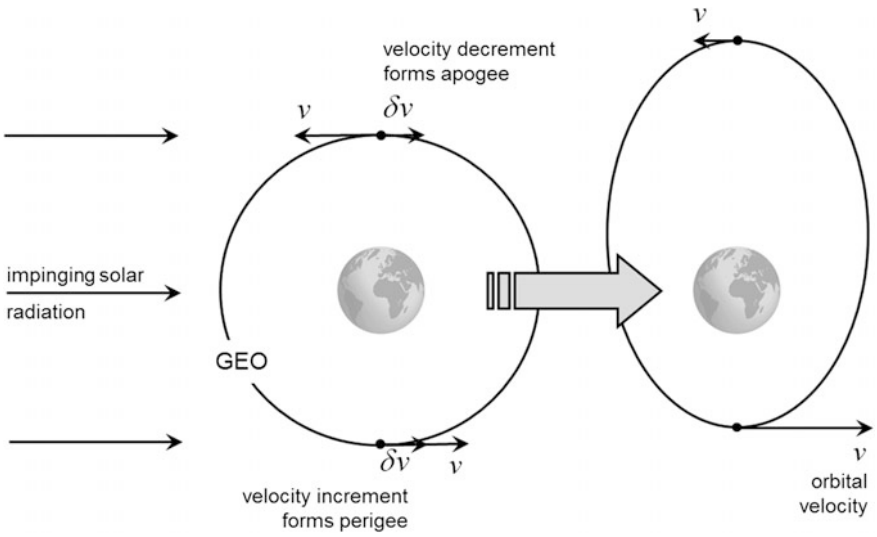

Fig. 12.23 The solar pressure with acceleration effect δv deforms a circular geostationary orbit to an ellipse

change e, but, because the effect of a force with constant direction is opposite on the two sides of the ellipse, they cancel out. So we only have to consider along-track forces at apoapsis and periapsis affecting $\dot{a}$, $\dot{e}$.

Let us assume that the orientation of the orbit is such that the radiation produces a minute push of δv along-track at the periapsis, and the same push in opposite direction at apoapsis. Then the induced change of the semi-major axis and the eccentricity according to Table 8.1 is

$$\frac{\delta a}{a} = \frac{2}{1+e}\frac{(-\delta v)}{v_h} \quad \text{and} \quad \delta e = -2\frac{(-\delta v)}{v_h} \quad @ \text{ apoapsis}$$
$$\frac{\delta a}{a} = \frac{2}{1-e}\frac{(+\delta v)}{v_h} \quad \text{and} \quad \delta e = +2\frac{(+\delta v)}{v_h} \quad @ \text{ periapsis}$$

with

$$v_h = \frac{\mu}{h} = \sqrt{\frac{\mu}{a(1-e^2)}} \approx \sqrt{\frac{\mu}{a}} = v_0$$

where the approximation holds for small eccentricities. So we get

$$\frac{\delta a}{a} \approx 2(e-1)\frac{\delta v}{v_0} \quad \text{and} \quad \delta e = 2\frac{\delta v}{v_0} \quad @ \text{ apoapsis}$$
$$\frac{\delta a}{a} \approx 2(e+1)\frac{\delta v}{v_0} \quad \text{and} \quad \delta e = 2\frac{\delta v}{v_0} \quad @ \text{ periapsis}$$

If we add up both impacts, we get the following changes

$$\frac{\delta a}{a} = 4e\frac{\delta v}{v_0} \quad \text{per revolution} \tag{12.5.4a}$$

$$\delta e = 4\frac{\delta v}{v_0} \quad \text{per revolution} \tag{12.5.4b}$$

The result $\delta e > 0$ positively feeds back our assumption that the solar radiation is parallel to the orbital velocity vector at periapsis. So starting out with a circular orbit, solar radiation will increase the orbital speed on one lateral side of the orbit and decrease is on the opposite side, thus inducing an eccentricity with a lateral line of apsides. With this constellation, the eccentricity will constantly increase with each revolution. So, we can say the following:

Impact of Solar Radiation on a Circular Orbit
For solar radiation impinging a circular or near-circular orbit the semi-major axis and hence the orbital period remains unaffected. However, an eccentricity laterally to the radiation direction develops, which constantly increases.

Quantitative Perturbation Calculation

We start out to determine the variation of the eccentricity quantitatively by refining the above considerations. Because the change of eccentricity comes from the along-track accelerations around the periapsis and apoapsis we have to estimate the integral of their impact over one revolution around these points. To estimate this, we apply Eq. (12.5.4a) with $\delta v = a_{sun} \cdot \delta t$, where δt is the effective impact time per revolution, which we estimate to be $\delta t \approx T/2$. As $T = 2\pi\sqrt{a^3/\mu}$ holds for an elliptic and a circular orbit, with $v_0 = \sqrt{\mu/a}$ we get

$$\delta e = 4\pi \cdot p_{sun} B_r \frac{a^2}{\mu} \quad \text{per revolution}$$

This is a first rough estimate. In order to derive the orbit changes exactly, we need to determine the components of the solar force in radial direction and vertically to it and then integrate their effects over one orbit according to the Gaussian variational equations (12.1.4). Because the line of apsides is lateral to the radiation, we find from Fig. 12.24 for the acceleration components due to the solar pressure

$$\boldsymbol{a}_{sun} = (a_r, a_\theta, a_h) = a_{sun}(\sin\theta, \cos\theta, 0)$$

and with Eq. (12.1.4) for the variations of the semi-major axis and eccentricity per revolution

$$\delta a = \frac{2a^2}{h} a_{sun} \int_0^T \left(e \sin^2\theta + \cos\theta + e \cos^2\theta\right) dt$$

$$\delta e = \frac{a}{h} a_{sun} \int_0^T \left(\sin^2\theta + e \cos\theta + \cos^2\theta - e \cos^3\theta + \cos^2\theta\right) dt$$

where we have linearized all terms because $e \ll 1$. From Eq. (7.3.8) we find

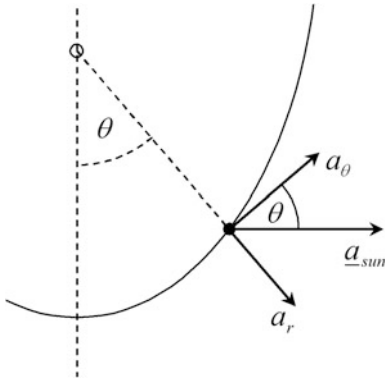

Fig. 12.24 Solar radiation acceleration components

$$dt = \frac{h^3/\mu^2}{(1+e\,\cos\theta)^2}d\theta \approx \frac{h^3}{\mu^2}(1-2e\,\cos\theta)d\theta$$

from which with $h^2 = \mu a(1-e^2) \approx \mu a$ we obtain

$$\delta a = \frac{2a^3}{\mu}a_{sun}\int_0^{2\pi}\left(e+\cos\theta+e\,\cos^2\theta\right)d\theta$$

$$\delta e = \frac{a^2}{\mu}a_{sun}\int_0^{2\pi}\left(1+e\,\cos\theta+\cos^2\theta-e\,\cos^3\theta-2e\,\cos\theta-2e\,\cos^3\theta\right)d\theta$$

$$= \frac{a^2}{\mu}a_{sun}\int_0^{2\pi}\left(1-e\,\cos\theta+\cos^2\theta-3e\,\cos^3\theta\right)d\theta$$

Because from symmetry considerations $\langle\cos\theta\rangle_\theta = \langle\cos^3\theta\rangle_\theta = 0$ and because

$$\int_0^{2\pi}\left(1+\cos^2\theta\right)d\theta = \left(\theta+\frac{1}{2}\sin\theta\,\cos\theta+\frac{\theta}{2}\right)\Big|_0^{2\pi} = 3\pi$$

we finally derive with Eq. (12.5.2)

$$\begin{aligned}\delta a &= 6\pi\,p_{sun}B_r\frac{a^3}{\mu}e+O(e^2)\approx 0\\ \delta e &= 3\pi\,p_{sun}B_r\frac{a^2}{\mu}+O(e^2)\end{aligned}\quad\text{per revolution, @ } e\ll 1 \tag{12.5.5}$$

This nicely agrees with our qualitative and rough quantitative considerations above. Because δe increases quadratically with the semi-major axis, this effect is 50 times bigger in GEO than in LEO.

We shall now concern ourselves with the other orbital elements. Applying $(a_r, a_\theta, a_h) = p_{sun}B_r(\sin\theta, \cos\theta, 0)$ for $e \approx 0$ to Eq. (12.1.2) we find

$$\begin{aligned}\delta i &= \delta\Omega = 0\\ \delta\omega &= -\delta(M-nT) = \frac{hp_{sun}B_r}{2e\mu}\sin 2\theta\end{aligned}$$

Note that from this follows that in a geocentric-equatorial reference frame the mean position on the orbit, i.e., the mean longitude (see Sect. 7.3.5),

$$l = \Omega + \omega + M = \Omega_0 + \delta\Omega + \omega_0 + \delta\omega + M_0 + \delta(M - nT)$$
$$= \Omega_0 + \omega_0 + M_0$$

remains unaffected by solarization. This implies that the mean position of a GEO satellite relative to an observer on Earth remains unchanged, but will only begin to oscillate sideways about its mean position (details see Sect. 12.5.3) with increasing eccentricity. This is good news from an east-west station-keeping point of view.

In summary, for $e \approx 0$ solar radiation essentially increases the eccentricity and the line of apsides rotates. So, effectively only the eccentricity vector $\boldsymbol{e}$ changes.

12.5.2 Orbital Evolution

We want to determine the temporal evolution of the eccentricity vector $\boldsymbol{e}$. To do so we need an equation of motion for it. We first introduce an appropriate reference frame with x-axis along the line of apsides and the y-axis vertical to it. The above considerations dealt with e_x, for which we get the equation of motion

$$\frac{de_x}{dt} = \frac{\delta e}{T} = \frac{3\pi}{2\pi} \cdot p_{sun} B_r \sqrt{\frac{\mu}{a^3}} \frac{a^2}{\mu} = \frac{3}{2} \cdot p_{sun} B_r \sqrt{\frac{a}{\mu}} = \frac{3 p_{sun} B_r}{2na} =: \kappa B_r$$

with

$$\kappa = \frac{3 p_{sun}}{2na} = (2.23 \pm 0.07) \times 10^{-9}\,\mathrm{kg\,m^{-2}} s^{-1} \quad @\ \mathrm{GEO}$$

if the Sun's rays are vertically to the line of apsides of a GEO. In case they are not vertical, the angle between the solar radiation direction and the line of apsides is defined as the mean longitude of the Sun: $\lambda_* = n_* t + \lambda_0$ with

$$n_* = 0.9856^\circ\,\mathrm{day}^{-1} = 0.01720\,\mathrm{rad\,day}^{-1}$$

the mean motion of the Sun. With this we obtain for the Sun-angle-dependent variation of the eccentricity component along the line of apsides

$$\frac{de_x}{dt} = -\kappa B_r \sin(n_* t + \lambda_0) \tag{12.5.6}$$

It can be shown (see Campan et al. (1995)) that the line of apsides follows the motion of the Sun angle. We therefore obtain for the e_y component

$$\frac{de_y}{dt} = \kappa B_r \cos(n_* t + \lambda_0) \tag{12.5.7}$$

The solutions to the above equations of motion are easy to find:

$$\begin{aligned} e_x(t) &= e_{x0} + \frac{\kappa B_r}{n_*} \cos(n_* t + \lambda_0) \\ e_y(t) &= e_{y0} + \frac{\kappa B_r}{n_*} \sin(n_* t + \lambda_0) \end{aligned} \tag{12.5.8}$$

The tip of the eccentricity vector with initial value $\boldsymbol{e}_0 = \big(e_x(t_0),\ e_y(t_0)\big)$ therefore describes a circle with radius (see Fig. 12.25).

$$\frac{\kappa B_r}{n_*} = (0.0112 \pm 0.0004)\,\mathrm{kg\,m^{-2}} \cdot B_r \quad @\ \mathrm{GEO}$$

This description is based on the assumption that the Sun moves on a circle in the equatorial plane of the Earth, which is not quite true. Its inclination (angle between equatorial plane and ecliptic) causes the circle to be actually a weak ellipse. In addition other perturbations (J_{20} term of the geoid, lunisolar perturbation) lead to rosette-type deviations from the circle including the effect that the initial and final points no longer coincide (see Fig. 12.26).

Eccentricity Evolution

We first want to know the eccentricity evolution of an initially circular GEO, i.e., $\boldsymbol{e}(t = 0) = \mathbf{0}$ and $\lambda_0 = 90°$ (see Fig. 12.23). Applying this to Eq. (12.5.8) yields

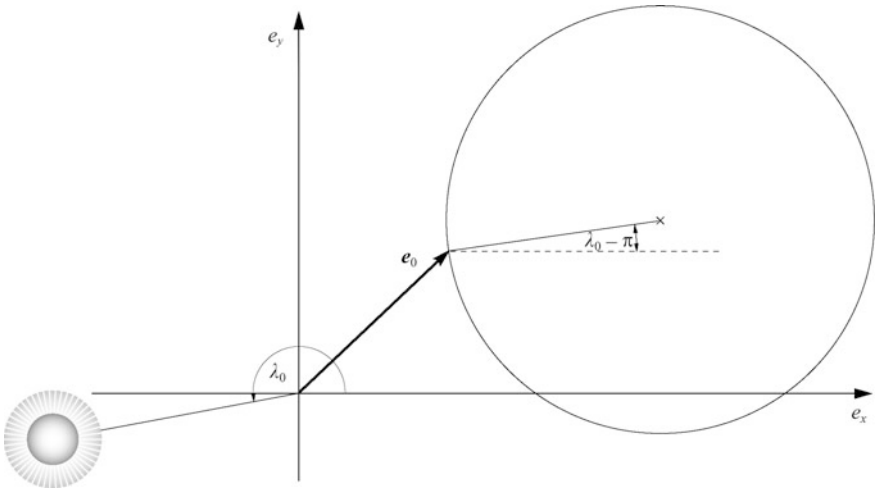

Fig. 12.25 The circular motion of the tip of the GEO eccentricity vector with initial value e_0 within a year. *Credit* Campan (1995), © CNES/CÉPADUÈS

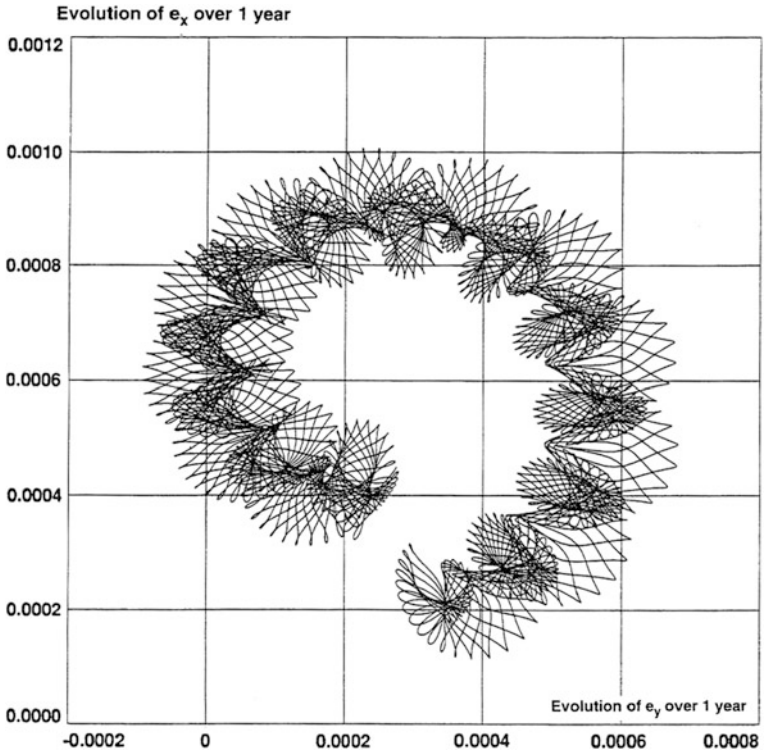

Fig. 12.26 The yearly motion of the GEO eccentricity vector under the action of all orbital perturbations. *Credit* Campan (1995), © CNES/CÉPADUÈS

$$\begin{aligned} e_x(t) &= -\frac{\kappa B_r}{n_*}\sin n_* t \\ e_y(t) &= -\frac{\kappa B_r}{n_*}(1-\cos n_* t) \end{aligned} \tag{12.5.9}$$

For the absolute value of the eccentricity we therefore obtain

$$e(t) = 2\frac{\kappa B_r}{n_*}\sin\frac{n_* t}{2} = \kappa B_r t\left[1-\frac{1}{24}(n_* t)^2 + O\left((n_* t)^4\right)\right] \quad @\ e_0 = 0 \tag{12.5.10}$$

and

$$\frac{de}{dt} = \kappa B_r \cos\frac{n_* t}{2} = \kappa B_r\left[1-\frac{1}{8}(n_* t)^2 + O\left((n_* t)^4\right)\right] \tag{12.5.11}$$

A communication relay satellite in GEO typically has $B_r \approx 0.05\ \mathrm{m}^2/\mathrm{kg}$ implying an initial

$$\delta e \approx 1 \times 10^{-5} \quad \text{per revolution} \tag{12.5.12}$$

Alternatively we could choose the initial condition such that the center point of the circle described by the eccentricity vector is at $\boldsymbol{e} = 0$. In this case

$$\begin{aligned} e_x(t) &= \frac{\kappa B_r}{n_*}\cos(n_* t + \lambda_0) \\ e_y(t) &= \frac{\kappa B_r}{n_*}\sin(n_* t + \lambda_0) \end{aligned} \tag{12.5.13}$$

implying that the absolute value of the eccentricity equaling the radius of the circle is constant

$$e = e_0 = \frac{\kappa B_r}{n_*} = const \tag{12.5.14}$$

This strategy is adopted for the European communications relay satellite ARTEMIS, which exhibits $B_r = 0.0369\ \mathrm{m}^2/\mathrm{kg}$ and therefore has a constant eccentricity of $e = 4.13 \times 10^{-4}$.

12.5.3 Correction Maneuvers

The yearly drag-induced motion of the eccentricity vector $\boldsymbol{e}$ however is of no relevance, because in GEO the absolute amount of eccentricity has to be regularly erased by correction maneuvers. To understand why, we have to know what the implications of a non-vanishing eccentricity are. Let us examine the periodic deviations of the orbital radius and the true anomaly caused by a body in an orbit with small eccentricity relative to a body in a circular orbit (so-called *guiding center*) with the same semi-major axis. This deviation is the apparent periodic horizontal motion of the position of the body in GEO as observed from the rotating Earth. To do this, we recall Eq. (7.3.9)

$$\frac{\mu^2}{h^3}(t - t_p) = \int_0^\theta \frac{d\theta'}{(1 + e \cdot \cos\theta')^2}$$

Because $e \ll 1$, $h^2 = \mu a(1 - e^2) \approx \mu a$ and $n = \sqrt{\mu/a^3}$, and by choosing $t_p = 0$, we get

$$nt \approx \int_0^\theta (1 - 2e \cdot \cos\theta')d\theta' = \theta - 2e\ \sin\theta$$

So, in zero-order approximation we get for $\theta(t)$ a circular orbit with $\theta = nt$ and in first-order approximation we have

$$\theta \approx nt + 2e\,\sin(nt) =: nt + \Delta\theta$$

i.e., compared with a circular orbit with $r = a$ the deviations are

$$\begin{aligned} \Delta\theta(t) &= 2e\,\sin(nt) \\ \Delta r(t) &= -e\,a\,\cos(nt) \end{aligned} \tag{12.5.15}$$

The latter is obtained from the orbit Eq. (7.4.14a) with $E \approx M = nt$ (see Eq. (7.4.15)). Because for small lateral deviations Δs the relation $\Delta s = a \cdot \Delta\theta$ holds, Eq. (12.5.15) describes an elliptic motion in the orbit plane (see Fig. 12.27) around the guiding center. Its semi-minor axis is ea in the radial direction and its semi-major axis is $2ea$ in the lateral direction, both of which increase with growing eccentricity. For the lateral oscillation range we find $\delta\theta = \Delta\theta_{\max} - \Delta\theta_{\min} = 4e$. As geostationary satellites are kept in an assigned dead-band slot of typical width $\Delta\theta = 0.1^\circ = 1.745 \times 10^{-3}$ rad , we get the following limit for the slowly increasing eccentricity

$$e_{\max} \leq \frac{1.745 \times 10^{-3}}{4} = 4.36 \times 10^{-4} \tag{12.5.16}$$

In the case when the orbit strategy is to always reset the eccentricity to zero when it reaches this limiting value, a correction maneuver has to be carried out at that point, which occurs after about 45 days for a typical $B_r \approx 0.05\ \mathrm{m^2\,kg^{-1}}$. Since the correction maneuver should not change the semi-major axis and with it the orbiting time, this has to be done according to Eq. (8.1.8) by two eccentricity correction maneuvers at both the peri- and apoapsis.

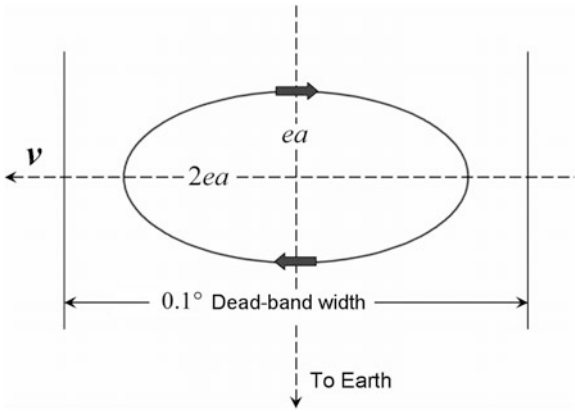

Fig. 12.27 Apparent motion of a geostationary satellite with eccentricity e in the guiding center system, i.e., the motion as seen in an Earth-fixed reference frame

$$2 \times \left|\Delta v_{||}\right| = \frac{1.745 \times 10^{-3}}{16} \sqrt{\frac{\mu}{a}} = 0.67 \text{ m/s} \tag{12.5.17}$$

Note that in this case Δv adds up to about $5\,\mathrm{m\,s^{-1}}$ within a year and hence makes up a significant share of the station-keeping effort.

In the other strategy case when the eccentricity vector rotates with a constant absolute value, the need for a correction maneuver depends on the amount of this value. For ARTEMIS $e = 4.13 \times 10^{-4} < e_{\max}$ and therefore in principle no correction maneuver would be needed to be performed.

East–West Station-Keeping Strategies

In practice triaxiality plus solar radiation together make up the two most effectual sources (and lunisolar perturbations a minor source) of east–west excursions. Depending on which of the sources is dominating (B_r and hence eccentricity versus longitudinal position and hence drift (see Fig. 12.19)) there are two basic strategies for east–west station-keeping (a.k.a. *longitude station-keeping*; see Soop (1994) or Chao (2005)):

1. *The drift due to triaxiality is dominating*.
   In this case *longitude control* is performed with correction strategy as laid out in Fig. 12.22. By doing so one gets the eccentricity control as a free by-product. The behavior of such a satellite is shown in Fig. 12.28. East-west

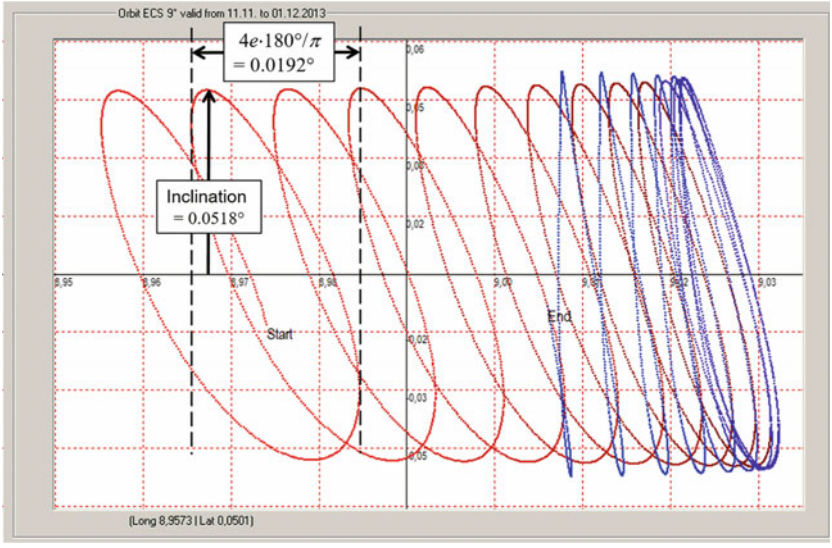

Fig. 12.28 Inclination and longitude (mean longitude 9°) of Eutelsat's ECS-9 GEO satellite under longitude control during 11-Nov-2013 to 01-Dec-2013 measured in the guiding center system. Every loop corresponds to one day. While drifting from West to East (red path) and back (blue path) its inclination of initially 0.052° increases slowly to 0.056° while its eccentricity decreases. (© Chr. Gleich/TUM)

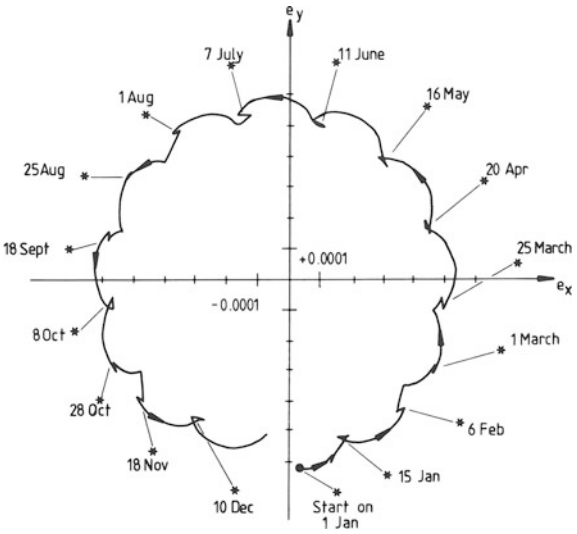

Fig. 12.29 The eccentricity vector under a SPPS-strategy over one year of a GEO satellite with B = 0.058 m^2/kg. *Credit* Soop (1994), © ESA

station-keeping maneuvers of this type are performed for broadcasting satellites (typically about once a week).

2. *The eccentricity-induced excursions due to solar radiation are dominating*. In this case eccentricity needs to be counteracted by the so-called *Sun-pointing perigee strategy SPPS*. This method minimizes the eccentricity variation around a small induced value by keeping the orbit's perigee pointing to the Sun as closely as possible. This is achieved by performing the longitude station-keeping maneuvers at some location away from perigee or apogee. Thereby the longitudinal drift compensation is provided as a free by-product. The path of the eccentricity vector of a SPPS-controlled satellite is shown in Fig. 12.29.

Most telecommunication satellites with their large solar panels usually belong to the second category. But ARTEMIS positioned at $\lambda = 21.40°$E and hence exhibiting a strong triaxiality drift but moderate B_r belongs to the first one.

12.6 Celestial Perturbations

12.6.1 Lunisolar Perturbations

We recall from Table 12.2 that apart from perturbations by the Earth's asymmetrical gravitational potential, also the Sun and the Moon perturb Earth orbits. Their effects are noticeable in particular in GEO because they are no more concealed by the gravitational perturbations as in LEO. The analytical description of these lunisolar perturbations is very complicated and complex (see Campan et al. (1995) or Noton (1998, p.70, and Appendix A.1)). This is why we will treat them only qualitatively.

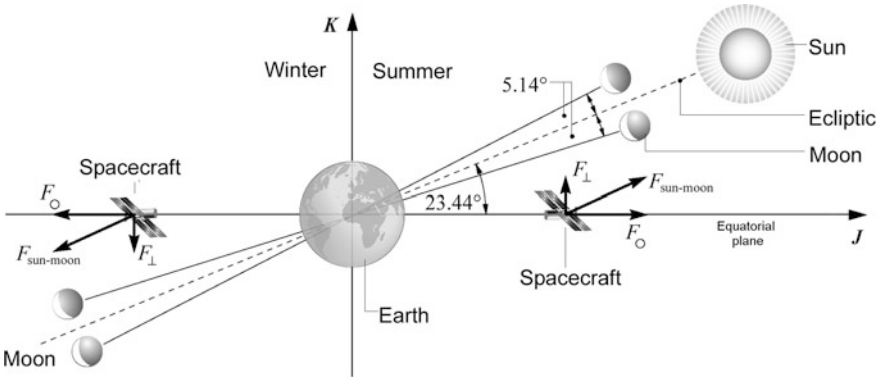

Fig. 12.30 Lunisolar perturbation force $F_{sun-moon}$ acting on a S/C in an equatorial orbit decomposed into a force component F_O in the orbital plane and $F_\perp$ perpendicular to the orbital plane

Because the terrestrial equatorial plane makes an inclination of 23.44° against the ecliptic and of 23.5 ± 5.1° against the lunar plane, the gravitational force of the Sun and the Moon can be decomposed into a component acting in the equatorial plane, i.e., in the GEO orbital plane, F_O, and one perpendicular to the equatorial plane $F_\perp$ (see Fig. 12.30).

In-Plane Force Effects

Let us consider first the effect of a revolving constant in-plane force F_O of a perturbing celestial body with standard gravitational parameter μ_P and position $\boldsymbol{R}$ from the center of the S/C orbit. The perturbation acceleration $\boldsymbol{a}_O$ on the S/C with position vector $\boldsymbol{r}$ is

$$\boldsymbol{a} = \mu_p \frac{\boldsymbol{R} - \boldsymbol{r}}{|\boldsymbol{R} - \boldsymbol{r}|^3} \tag{12.6.1}$$

Because in the orbital plane $\hat{\boldsymbol{R}} = \hat{\boldsymbol{r}}\cos\theta - \boldsymbol{e}_\theta \sin\theta = \boldsymbol{e}_r \cos\theta - \boldsymbol{e}_\theta \sin\theta$, where and $\cos\theta = \hat{\boldsymbol{r}}\hat{\boldsymbol{R}}$, we have for the in-plane acceleration $\boldsymbol{a}_O = a_r \boldsymbol{e}_r + a_\theta \boldsymbol{e}_\theta$ with

$$a_r = \mu_p \frac{R\cos\theta - r}{|\boldsymbol{R} - \boldsymbol{r}|^3}, \quad a_\theta = -\mu_p \frac{R\sin\theta}{|\boldsymbol{R} - \boldsymbol{r}|^3}$$

$$|\boldsymbol{R} - \boldsymbol{r}|^{-3} = \left(R^2 + r^2 - 2rR\cos\theta\right)^{-3/2}$$

$$\approx \frac{1}{R^3}\left(1 - 2\frac{r}{R}\cos\theta\right)^{-3/2} \approx \frac{1}{R^3}\left(1 + 3\frac{r}{R}\cos\theta\right)$$

We hence have the symmetry properties

$$a_r(-\theta) = a_r(\theta), \quad a_\theta(-\theta) = -a_\theta(\theta)$$

Applying these properties to the Gaussian variational equations (12.1.4) we see that $\dot{i} = \dot{\Omega} = 0$, and $\dot{a}(-\theta) = -\dot{a}(\theta)$, $\dot{e}(-\theta) = -\dot{e}(\theta)$. Because $\dot{\omega}$ is not relevant for a circular orbit, we arrive at the result that a revolving constant in-plane force F_{O} does not have a secular effect on the orbital elements of a body that circles Earth. Because the symmetry properties do not change if the Moon or Sun are in opposite locations around the Earth, the variation of orbital elements over one revolution of the Moon or Sun around the Earth also averages out. So there are no secular effects whatsoever.

Out-of-Plane Force Effects

The component $F_{\perp}$ perpendicular to the orbital plane, on the other hand, does have secular effects. To see which, we recognize that $F_{\perp}$ causes an perturbational acceleration a_h normal to the orbit plane. From Eq. (12.1.4) we see that such an a_h affects only the orbital elements i, ω and Ω. Due to $\dot{e} = 0$ and therefore a steady $e = 0$ for a GEO, ω and hence $\dot{\omega}$ are not relevant.

We therefore only have to evaluate $i(t)$, $\Omega(t)$. We do so by employing the concept of the three-dimensional inclination vector. According to Eq. (7.3.25) it is given by

$$\boldsymbol{I} \equiv \hat{\boldsymbol{h}} = \begin{pmatrix} \sin\Omega \sin i \\ -\cos\Omega \sin i \\ \cos i \end{pmatrix}_{IJK}$$

According to the above, the motion of this vector fully describes the effect of lunisolar perturbations. Figure 12.31 shows a typical example of the track of the inclination vector of a S/C in a GEO on the celestial sphere under the influence of the Sun and the Moon.

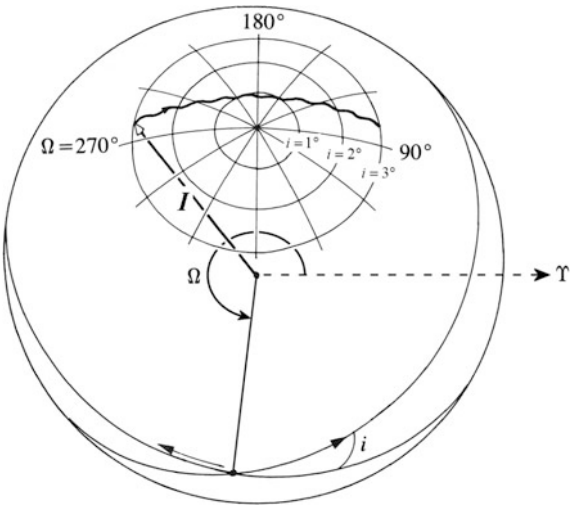

Fig. 12.31 Trace of the tip of the inclination vector of a GEO on the celestial sphere. *Credit* Berlin (1988)

To understand how this motion comes about, we assume that the S/C initially is in a circular orbit with $i = 0$. According to Eq. (8.1.14), a_h, which is locally equivalent to the acceleration due to a $\delta v_{\perp\perp}$ kick-burn, initiates an inclination with an argument of latitude of the S/C

$$u = \begin{cases} 0^\circ & @\ a_h > 0 \\ 180^\circ & @\ a_h < 0 \end{cases}$$

Because the nodal line of the ecliptic plane and equatorial plane points to the First point of Aries Υ, Moon and Sun cause no vertical perturbation when they cross the equatorial plane, i.e. when they are in the direction of Υ or on the opposite side. We therefore expect the initial inclination δi when $a_h > 0$ is maximum abeam from the nodal line and hence at $\Omega = u + 90^\circ = 90^\circ$. As the S/C revolves once in its orbit for a steady position of the Sun and Moon, i.e., $a_h \approx const \rightarrow \delta v_{\perp\perp} \approx const$, the S/C experiences a $-\delta i$ at the opposite location, i.e. at $u = 180^\circ$, which cancels the first one. Thus the average over one S/C orbit produces no secular inclination.

However, the situation is different at other positions on the orbit as the Moon and Sun move around the Earth. According to the Gaussian variational equations (12.1.4), when they are at -90° from the nodal line with $a_h > 0$ they cause an $\delta i > 0$ and when they are at 90° from the nodal line with $a_h < 0$ they cause the same $\delta i > 0$. Therefore the revolution of the Moon and the Sun about the Earth constantly increase the inclination at $\Omega = 90^\circ$. The inclination vector hence initially displays the following motion $\boldsymbol{I}(t) \approx (i(t),\ 0,\ 0)_{IJK}$, that is, it tilts towards the First point of Aries Υ. When the Sun or Moon are just off the abeam positions they also tilt the inclination vector minimally to the side. However, because this is not a secular effect, the evolution of the inclination as shown in Fig. 12.32 just displays small wiggles with twice the frequency of the revolution of the corresponding celestial body about the Earth. Therefore the Sun causes two wiggles while the Moon causes 25 wiggles per year.

The actual motion of the inclination vector over the years depends on the initial RAAN and is depicted for a GEO in Fig. 12.33.

The inclination vector is also subject to the oblateness perturbation of Earth's gravitational field (see Sect. 12.3.3), which gives rise to a regression of nodes $\dot{\Omega} < 0$

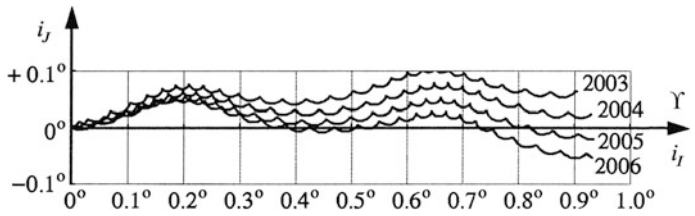

Fig. 12.32 Evolution of the inclination vector components for a GEO over a year for 2003–2006 with inclination set to zero at the beginning of each year. *Credit* Soop (1994), © ESA

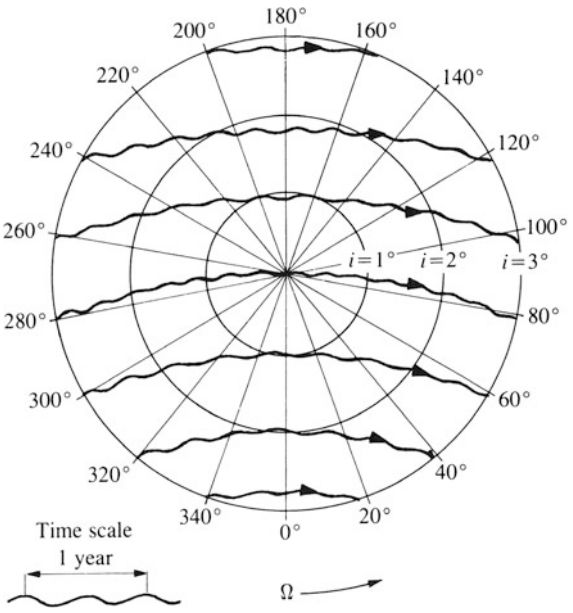

Fig. 12.33 Evolution of the inclination vector of a GEO in the i-Ω diagram depending on the initial RAAN. *Credit* Berlin (1988)

(see Eq. (12.3.15)), which effectively curves the trace of the inclination vector in the i-Ω diagram as seen in Fig. 12.33 (for more details see Berlin (1988, p. 60ff) and Soop (1994, p. 86)).

For the determination of the quantitative secular variation of inclination we refer to Campan (1995), who shows that in first-order perturbation calculations the mean secular inclination change is

$$n \cdot \dot{i}_{\text{sec}} = \frac{3}{8} n_b^2 \mu_b \sin 2\langle i_b \rangle = \begin{cases} 0.533^{\circ 2}\text{day}^{-2} & @\ b = Moon \\ 0.268^{\circ 2}\text{day}^{-2} & @\ b = Sun \end{cases} \tag{12.6.2}$$

with $\langle i_b \rangle$, its inclination with regard to the equatorial plane; $n_b = 360^\circ / T_b$, its mean motion; n the mean motion of the perturbed satellite; and

$$\mu_b = \frac{m_b}{m_b + m_\oplus} = \left\{ \begin{matrix} 1 & @\ b = Sun \\ 1/82.3 & @\ b = Moon \end{matrix} \right\}$$

If the inclination is not controlled, as for dead satellites in the graveyard orbit, the lunisolar perturbations act upon the inclination while Earth's oblateness causes a precessional motion of the orbital plane. As shown in Fig. 12.34 both together over long time spans cause an oscillation of inclination in the range $0 \le i \le 15^\circ$ jointly with a precessional motion of the orbital plane inclination within the limits $0 \le \Omega \le 100^\circ$ or $260^\circ \le \Omega \le 360^\circ$.

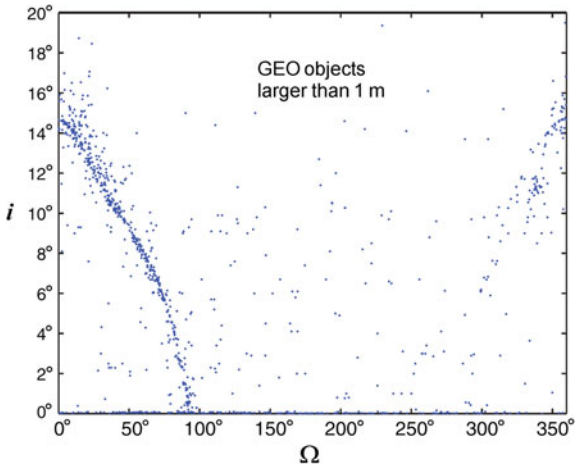

Fig. 12.34 Distribution of space objects at GEO in i-Ω space. *Credit* A. Rossi, IFAC-CNR, 2010

Low Earth Orbits

From this we find for equatorial LEOs at $h = 600$ km, equaling $n = 5362^\circ\ \text{day}^{-1}$, the yearly inclination change rate of

$$\dot{i}_{\text{sec}} = \begin{cases} 0.036^\circ\ \text{yr}^{-1} & @\ \textit{Moon} \\ 0.018^\circ\ \text{yr}^{-1} & @\ \textit{Sun} \end{cases} \quad @\ \text{equatorial LEO}$$

and hence for both perturbations $\dot{i}_{\text{sec}} \approx 0.054^\circ\ \text{yr}^{-1}$. Taking all planetary perturbations into account we have

$$\dot{i}_{\text{sec}} \approx 0.062^\circ\ \text{yr}^{-1} \quad @\ \text{equatorial LEO} \tag{12.6.3}$$

which is a typical value for LEOs in general. This is very small but nevertheless bigger than that caused by gravitational perturbations for near-circular orbits (see Sect. 12.3.4).

Geostationary Orbits

GEOs are more prone to lunisolar perturbations because bodies on such orbits move slower and hence the time-averaging effect is lower. With $n = 360.99^\circ\ \text{day}^{-1}$

$$\dot{i}_{\text{sec}} = \begin{cases} 0.539^\circ\ \text{yr}^{-1} & @\ \textit{Moon} \\ 0.271^\circ\ \text{yr}^{-1} & @\ \textit{Sun} \end{cases} \quad @\ \text{GEO}$$

If one allows also higher orders of perturbation $k \cdot n_b$, then one obtains for the yearly rate of the inclination variation $\dot{i}_{\text{sec}} = 0.478^\circ\ \text{yr}^{-1}$ by lunar and $\dot{i}_{\text{sec}} \approx 0.319^\circ\ \text{yr}^{-1}$ by solar perturbations, whereby the latter varies from year to year somewhat. So, for both perturbations together we find $\dot{i}_{\text{sec}} = 0.797^\circ\ \text{yr}^{-1}$. Again, taking all planetary perturbations into account we have

$$\dot{i}_{\text{sec}} = 0.854^\circ \pm 12\%\ \text{yr}^{-1} \quad @\ \text{GEO} \tag{12.6.4}$$

The 12% variation is due to the periodic variation of the Moon's orbit inclination relative to the ecliptic with a period of 18.6 years. Because from Earth the movement of a body in an inclined geostationary orbit looks like a vertical oscillation, it is called *North–South drift*. The **North–South station-keeping** (a.k.a. *inclination station-keeping*) effort depends on the station-keeping maneuvers applied. A straightforward maneuver is to remove the inclination by a direct maneuver performed at one of the nodes (see Fig. 8.4). The mean delta-v effort can be calculated from Eq. (8.1.23) to be

$$\Delta v = 2v_{GEO} \sin\frac{\Delta i}{2}$$

With $\Delta i = \dot{i}_{\text{sec}} \cdot 1\ \text{yr} = 0.854^\circ$ and $v_{GEO} = 3.066\ \text{km s}^{-1}$ and therefore obtain

$$\Delta v = 45.7 \pm 12\%\ \ \text{m s}^{-1}\,\text{yr}^{-1} \quad @\ \text{inclination removal maneuver}$$

Rather than just eliminate the induced inclination it is obvious that it is better (see Fig. 12.33) to overact and place the inclination vector at a small $i < 1^\circ$ with $\Omega = 270^\circ$ and let it drift through $i = 0^\circ$ to the same i with $\Omega = 90^\circ$. At this point a RAAN adjustment maneuver is performed, which places the S/C again at i with $\Omega = 270^\circ$, where the cycle starts anew. The delta-v effort for such a maneuver is given by Eq. (8.1.21) with $v_1 = v_2 = v_{GEO}$ as

$$\Delta v = 2v_{GEO} \sin i \cdot \sin 90^\circ$$

and hence

$$\Delta v = 6.132 \cdot \sin i\ \ \text{km s}^{-1} \quad @\ \text{cyclic RAAN adjustment}, i < 1^\circ \tag{12.6.5}$$

With an mean annual secular perturbation of $\dot{i}_{\text{sec}} = 0.854^\circ \pm 12\%\ \text{yr}^{-1}$ and adjustments for $i \leq 0.917^\circ$ and accounting for the phase of Moon's orbit inclination relative to the ecliptic we have

$$\boxed{\Delta v = 45.7 - 5.2 \sin\left(2\pi \frac{yy - 1992}{18.6}\right)\ \text{m s}^{-1}\,\text{yr}^{-1}} \quad @\ \text{cyclic RAAN adjustment}, i < 1^\circ \tag{12.6.6}$$

where *yy* is the Gregorian year in question. This result of course is identical to the inclination removal maneuver because turning the inclination vector by 180° is the same as applying the inclination removal twice.

However, the cyclic RAAN adjustment maneuver becomes slightly more efficient if there are no drift constraints in North–South direction, because such drifts do not interfere with adjacent satellites. In this case the yearly adjustment effort drops because the trace of the inclination vector is curved. For instance and as

shown in Fig. 12.33, the inclination vector takes 7.5 years to drift from $i = 3°$, $\Omega = 280°$ $\rightarrow$ $i = 0$ $\rightarrow$ $i = 3°$, $\Omega = 80°$ from where it is placed with a cyclic RAAN maneuver back at $i = 3°$, $\Omega = 280°$. According to Eq. (8.1.21) the delta-v effort for this maneuver is

$$\Delta v = 2v_{GEO} \sin 3° \cdot \sin[360° - (280° - 80°)]/2 = 0.316 \text{ km s}^{-1}$$

and we have a yearly delta-v effort of only

$$\Delta v = 42.1 \pm 12\% \text{ m s}^{-1} \text{ yr}^{-1} \text{ @ cyclic RAAN adjustment}, i = 3°$$

Yet, this is still more than one order of magnitude bigger than the east–west station–keeping in the worst case (see Eq. (12.4.16)) and hence more decisive for the propulsion demand for orbit control. This result confirms the rule of thumb that inclination changes in astronautics always imply high propulsion efforts.

North-South station-keeping maneuvers are performed about once or twice every two weeks, often alternating with an East-West station-keeping maneuver (see end of Sect. 12.5.3).

12.6.2 Relativistic Perturbations

In Sect. 12.6.1 we have seen that lunisolar perturbations cause a constant shift of the true anomaly of an elliptic Earth orbit and hence a progression of line of apsides. This effect of course holds also for planetary elliptic orbits that are affected by gravitational fields of the Sun and all other planets in the solar system leading to a perihel motion for all solar planets. For Mercury, where this effect is most pronounced, this can be calculated to amount to 1.28 arcsec per revolution, equaling 532 arcsec per century.

It was a puzzle for astronomers at the beginning of the twentieth century that the observed perihel motion of Mercury was actually found to be 575 arcsec per century. So, 43 arcsec were missing. It was one of the great triumphs of Albert Einstein to show that his theory of general relativity is able to fully account for the missing gap and hence to prove that General Relativity Theory is true. Let us see how general relativity adds perihel motion to planetary orbits.

In General Relativity Theory the equation of motion for an orbit is modified in terms of Sect. 7.6.1, subsection "3-dim Universe", to be (see, e.g., Beutler 2005a, p. 148)

$$\rho'' + \rho = \frac{\mu}{h^2} + \frac{3\mu}{c^2}\rho^2 \tag{12.6.7}$$

We recall from Sect. 7.6.1 that $\rho = 1/r$ and $\rho' = d\rho/d\theta$, and c is the speed of light. Since for a near-circular orbit $v \approx \sqrt{\mu/r}$ is its orbital speed, the ratio of the two terms on the right-hand side of the equation is

$$\frac{3\mu\rho^2/c^2}{\mu/h^2} \approx \frac{3\mu a}{c^2 r^2} \approx \frac{3\mu}{c^2 r} \approx 3\frac{v^2}{c^2} \ll 1$$

Therefore the contribution due to relativity is very small. This is why we can perform a calculation of perturbation in that we first neglect the relativistic perturbation. We thus find according to Eq. 7.3.5 the solution of the Keplerian orbit

$$\rho = \frac{\mu}{h^2}(1 + e\,\cos\theta)$$

We insert this solution into Eq. (12.6.7) and neglecting $O(e^2)$ we find the equation of motion

$$\rho'' + \rho = \frac{1}{p}[1 + \varepsilon(1 + 2e\,\cos\theta)] \tag{12.6.8}$$

with semi-latus rectum $p = h^2/\mu = a(1 - e^2)$ and $\varepsilon := 3\mu/(c^2 p)$. Because we expect the perturbed solution close to the unperturbed we make the ansatz

$$\rho = \frac{1}{p}[1 + e\,\cos\theta + f(\theta)]$$

Inserting this into Eq. (12.6.8) leads to equation of motion for the residual $f(\theta)$

$$f'' + f = \varepsilon(1 + 2e\,\cos\theta)$$

A particular solution to this equation is

$$f = \varepsilon(1 + e\theta\,\sin\theta)$$

as can be easily verified by insertion. The general solution therefore is

$$p\rho = (1 + \varepsilon) + e(\cos\theta + \varepsilon\theta\,\sin\theta) \approx (1 + \varepsilon) + e\,\cos(\theta - \varepsilon\theta)$$

The last step holds if we neglect terms of ε^2. Hence we finally find the orbit equation

$$\frac{p}{1 + \varepsilon}\rho = 1 + \frac{e}{1 + \varepsilon}\cos(\theta - \varepsilon\theta) \tag{12.6.9}$$

If we compare this result with the unperturbed orbit $p\rho = 1 + e\,\cos\theta$ we recognize that the relativistic orbit suffers a tiny shrinkage $a \to a/(1 + \varepsilon)$, a marginally reduced eccentricity $e \to e/(1 + \varepsilon)$, and a small prograde perihel motion per revolution of

$$\Delta\omega = 2\pi\varepsilon = \frac{6\pi\mu}{c^2 p} = \frac{6\pi\mu}{a(1-e^2)c^2} \text{ per revolution} \tag{12.6.10}$$

Since the orbital period is $T = 2\pi\sqrt{a^3/\mu}$ we have for the perihel motion per century (100 *y*)

$$\Delta\omega_{100y} = \Delta\omega\frac{100\ y}{T} = \frac{3}{a(1-e^2)c^2}\left(\frac{\mu}{a}\right)^{3/2} 100\ y$$

From Table A.1 in Appendix A we insert the orbital elements of Mercury, which due to its closest solar orbit is expected to suffer mostly from relativistic gravitational effects, and find

$$\Delta\omega_{100y} = 42.98 \text{ arcsec} \quad @ \text{ Mercury}$$

This is the celebrated relativistic contribution, which perfectly explains the missing gap of 43 arcsec.

Remark *In the 1960s there has been a considerable controversy over whether the solar oblateness J_2, which must also contribute to Mercury's perihel motion and was not considered to that date, might prove general relativity wrong. From* Eq. (12.3.15) *we can derive the oblateness' contribution to be* $\Delta\omega_{100y} = 2.54 \times 10^5 \cdot J_2$ arcsec. *With today's observational value of* $J_2 = (1.9 \pm 0.3) \times 10^{-7}$ *we arrive at* $\Delta\omega_{100y} = 0.05$ arcsec, *which is negligible compared to the inaccuracies of the planet's contributions. The missing gap therefore is solely due to general relativity.*

It should be mentioned that in general an orbit about a central body is perturbed by other relativistic effects. In particular, if the central body rotates its mass currents produce a so-called gravitomagnetic dipole field, which via relativistic space frame dragging (so-called Lense-Thirring effect) in general causes a retrograde motion of the periapsis plus a precession of the orbital plane. These two effects, however, are so weak that they could be observed to date only in the very strong gravitational fields of binary pulsars.

12.7 Drag

In low Earth orbits the atmospheric density cannot be neglected and therefore may exert a marked resistance on a circulating spacecraft. In this chapter we want to determine how the orbit—specifically, how the orbital elements—will be affected by atmospheric drag.

12.7.1 Drag Perturbations

According to Sect. 6.2.3 the atmospheric deceleration can be described in dependence on the drag D as

$$a_D = \frac{D}{m} = \frac{C_D}{2}\frac{A_\perp}{m}\rho v_a^2 = \frac{B}{2}\rho v_a^2 \quad @\ h > 150\ \text{km} \tag{12.7.1}$$

We now want to determine the impact of atmospheric drag on the orbital elements. We identify the drag force as an orbital perturbation, which we split into radial, cross-radial, and vertical components and derive from Fig. 12.35 with the above result

$$\boldsymbol{a}_D = (a_r, a_\theta, a_h) = -\frac{B}{2}\rho(r) \cdot v_a^2(\sin\gamma, \cos\gamma, 0) \tag{12.7.2}$$

The negative sign denotes that the S/C is decelerated by the drag. According to Eq. (7.3.16) the flight path angle γ is related to the true anomaly by

$$\sin\gamma = \frac{e\ \sin\theta}{\sqrt{1 + 2e\ \cos\theta + e^2}}$$
$$\cos\gamma = \frac{1 + e\ \cos\theta}{\sqrt{1 + 2e\ \cos\theta + e^2}}$$

We insert this perturbation into the Gaussian variational equations (12.1.4) and find for the wanted variations of orbital elements

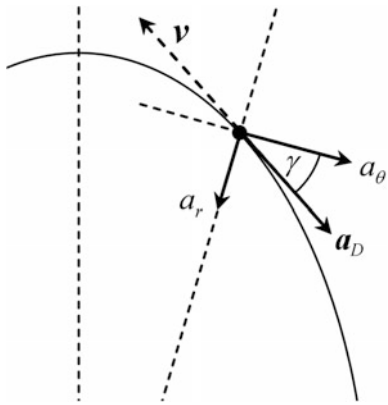

Fig. 12.35 Decomposition of the atmospheric drag into radial and lateral components

$$\begin{aligned}
\dot{a} &= -\frac{B\rho v_a^2}{n}\frac{1}{\xi(e,\theta)} \\
\dot{e} &= -\frac{B\rho v_a^2}{na}\xi(e,\theta)(e+\cos\theta) \\
\dot{\omega} &= -\frac{B\rho v_a^2}{nae}\xi(e,\theta)\sin\theta \\
\dot{M}-n &= \frac{B\rho v_a^2}{nae}\xi(e,\theta)\frac{\sin\theta\cdot(1+e\cos\theta+e^2)}{(1+e\cos\theta)}\sqrt{1-e^2} \\
\dot{i} &= \dot{\Omega} = 0
\end{aligned} \tag{12.7.3}$$

with

$$\xi(e,\theta) = \frac{\sqrt{1-e^2}}{\sqrt{1+2e\cos\theta+e^2}} = \sqrt{\frac{\mu}{a}}\frac{\sqrt{1-e^2}}{v}$$

In the following we are only interested in the mean variations of the orbital elements over one orbital period. So, in the absence of slow variables we only have to integrate over one orbit. From the above equations we establish $\dot{\omega}(-\theta) = -\dot{\omega}(\theta)$ and $\dot{M}(-\theta) = -\dot{M}(\theta)$, implying that each periodic variation is compensated by an equally negative variation on the other side of the orbit. We therefore find

$$\dot{\omega}_{\text{sec}} = \frac{1}{2\pi}\int_{-\pi}^{\pi}\dot{\omega}(r,\theta)\cdot dM = 0$$

$$\dot{M}_{\text{sec}} - n = \frac{1}{2\pi}\int_{-\pi}^{\pi}\left[\dot{M}(r,\theta)-n\right]\cdot dM = 0$$

We therefore arrive at the following important result:

Impact of Drag on Orbital Elements
Drag secularly affects only the eccentricity and the size of the semi-major axis.

12.7.2 Orbit Circularization

We now want to figure out how large the mean variations of a and e are. The mean variation is the integral over the total atmospheric drag of one orbit. Due to the exponential dependence of the atmospheric density, drag is by far the strongest around the periapsis, $\theta \approx 0$, for an elliptic orbit. In order to be able to carry out the integration, we need to know the θ dependences of all factors in Eq. (12.7.3). This is particularly true for the atmospheric density $\rho(\theta)$. To find it out we expand the orbit equation $r = a(1-e^2)/(1+e\cos\theta)$ for small angles at the periapsis

$$r \approx r_{per}\left[1+\frac{e}{2(1+e)}\theta^2\right] = r_{per} + a\frac{1-e}{1+e}\frac{e}{2}\theta^2$$

With this expression $\rho(\theta)$ can be written as

$$\rho(\theta) = \rho_{per}\exp\left(-\frac{r-r_{per}}{H_{per}}\right) \approx \rho_{per}\exp\left(-\frac{ae}{2H_{per}}\frac{1-e}{1+e}\theta^2\right)$$

hence

$$\rho(\theta) = \rho_{per}\exp\left(-\frac{\theta^2}{2\sigma^2}\right) \tag{12.7.4}$$

with

$$\sigma = \sqrt{\frac{H_{per}}{ea}\frac{1+e}{1-e}}$$

where $\rho_{per} = \rho\left(r_{per}\right)$ is the atmospheric density at periapsis. By the same token we expand the other terms in Eq. (12.7.3) and find with Eq. (7.4.11)

$$v_a^2 = \frac{\mu(1+2e\,\cos\theta+e^2)}{a(1-e^2)} \approx \frac{\mu}{a}\frac{1+e}{1-e}\left[1-\frac{e}{(1+e)^2}\theta^2\right]$$

and

$$\xi(e,\theta) \approx \sqrt{\frac{1-e}{1+e}}\left[1+\frac{e}{2(1+e)^2}\theta^2\right]$$

We insert these expressions into Eq. (12.7.3) and obtain

$$\dot{a} \approx -B\rho_{per}\sqrt{\mu a}\left(\frac{1+e}{1-e}\right)^{3/2}\exp\left(-\frac{\theta^2}{2\sigma^2}\right)\left[1-\frac{3e}{2(1+e)^2}\theta^2\right]$$

$$\dot{e} \approx -B\rho_{per}\sqrt{\frac{\mu}{a}}\frac{(1+e)^{3/2}}{(1-e)^{1/2}}\exp\left(-\frac{\theta^2}{2\sigma^2}\right)\left[1-\frac{1+2e}{2(1+e)^2}\theta^2\right]$$

We now carry out the integration over one orbital period by assuming that $\sigma<\theta \ll 1$, i.e., $e \gg H_{per}/a$. This condition ensures that the density decays within the θ-range where our expansion is valid. Note that for the Earth $0.001 \le H_{per}/a < 0.01$, where the lower limit holds for $h<120$ km and the upper limit for $h > 300$ km. We then get with

$$\frac{1}{2\pi}\int_{-\pi}^{\pi}\exp\left(-\frac{\theta^2}{2\sigma^2}\right)\cdot\,d\theta \approx \frac{\sigma}{\sqrt{2\pi}}$$

$$\frac{1}{2\pi}\int_{-\pi}^{\pi}\exp\left(-\frac{\theta^2}{2\sigma^2}\right)\theta^2\cdot\,d\theta \approx \frac{\sigma^3}{\sqrt{2\pi}}$$

finally the wanted equations of mean variation:

$$\begin{aligned}
\langle \dot{a} \rangle &= -B\rho_{per}\left(\tfrac{1+e}{1-e}\right)^2 \sqrt{\tfrac{\mu H_{per}}{2\pi e}}\left[1 - \tfrac{3H_{per}}{2a(1-e^2)}\right] \\
&\approx -B\rho_{per}\left(\tfrac{1+e}{1-e}\right)^2 \sqrt{\tfrac{\mu H_{per}}{2\pi e}} = \langle \dot{a}_{circle} \rangle \tfrac{\sigma}{\sqrt{2\pi}} \ll \langle \dot{a}_{circle} \rangle \qquad @\ e \gg \frac{H_{per}}{a} \\
\langle \dot{e} \rangle &= -B\rho_{per} \tfrac{(1+e)^2}{1-e} \tfrac{1}{a} \sqrt{\tfrac{\mu H_{per}}{2\pi e}}\left[1 - \tfrac{H_{per}}{2ea} \tfrac{1+2e}{1-e^2}\right] \\
&\approx -B\rho_{per} \tfrac{(1+e)^2}{1-e} \tfrac{1}{a} \sqrt{\tfrac{\mu H_{per}}{2\pi e}} = (1-e)\tfrac{\langle \dot{a} \rangle}{a}
\end{aligned} \tag{12.7.5}$$

where $\langle \dot{a}_{circle} \rangle$ is the mean variation of a circle with $a_{circle} = r_{per}$. So, the impact of drag on the semi-major axis and the eccentricity of an elliptic orbit is about the same. However, because for an elliptic orbit the drag impacts the body only around the periapsis, and is much less than that for a circular orbit, which is continuously exposed to the drag, the elliptic semi-major axis does not decrease as fast as the radius of a comparable circular orbit.

Decoupling the Differential Equations

These coupled differential equations can be solved by separating the variables in the second equation (because we will deal only with mean variations of orbital elements in the following, we drop the average sign $\langle . \rangle$ for convenience)

$$\frac{de}{1-e} = \frac{da}{a}$$

with the solution (see Eq. (7.4.6))

$$r_{per} = a(1-e) = const \tag{12.7.6}$$

The periapsis hence remains unaffected, while the apoapsis

$$\dot{r}_{apo} = \dot{a}(1+e) + a\dot{e} = \dot{a}(1+e) + \dot{a}(1-e) = 2\dot{a} < 0$$

decreases. This behavior can be seized quite easily if we consider the temporary drag at the periapsis as a deceleration kick-burn. According to Eq. (8.1.11) such a kick-burn lowers the apsis on the opposite side of the orbit. With that we arrive at the important result:

How Drag Removes Eccentricity
Drag circularizes elliptic orbits by lowering the apoapsis, but maintaining the periapsis.

This aerobraking property as displayed in Figs. 12.36 and 12.37 is often used after planetary or aerocapture at Mars or Venus to turn the highly elliptic initial orbit down to a circular target orbit without any propulsion effort.

By making use of Eq. (12.7.6) one finally obtains from Eq. (12.7.5) the decoupled differential equations for the mean orbital elements

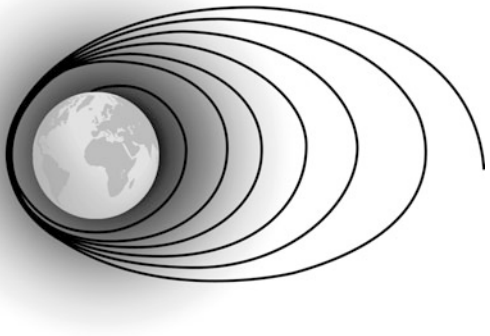

Fig. 12.36 Circularization and decay of an elliptic orbit due to drag

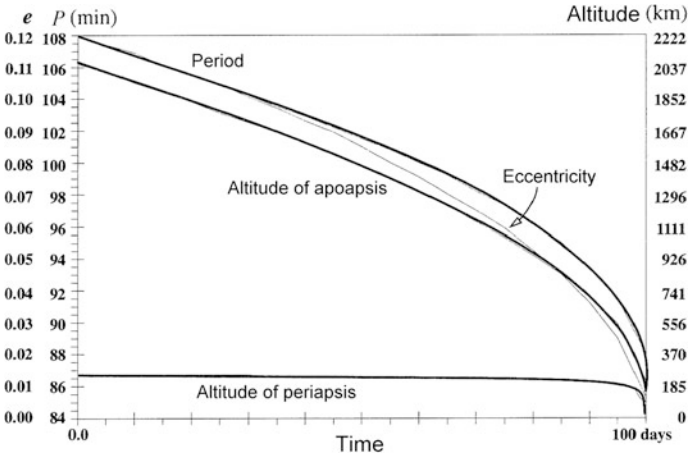

Fig. 12.37 Drag-induced decay of orbit parameters with $e_0 = 0.12$ and $h_{per} = 200$ km. P is the orbital period. *Credit* Vallado (2007)

$$\begin{aligned} \dot{a} &= -B\rho_{per}\sqrt{\frac{\mu H_{per}}{2\pi}}\left(\frac{2a}{r_{per}}-1\right)^2\sqrt{\frac{1}{1-r_{per}/a}} \\ \dot{e} &= -\frac{B\rho_{per}}{r_{per}}\sqrt{\frac{\mu H_{per}}{2\pi}}\frac{(1+e)^2}{\sqrt{e}} \end{aligned} \quad @\ e \gg \frac{H_{per}}{a} \tag{12.7.7}$$

Circularization Time

We are now seeking for solutions of the decoupled differential equations with the initial conditions $a_0 = a(t_0),\ e_0 = e(t_0)$. In the second equation we separate the variables

$$\frac{\sqrt{e}}{(1+e)^2}de = -\frac{B\rho_{per}}{r_{per}}\sqrt{\frac{\mu H_{per}}{2\pi}}dt$$

and find from relevant mathematical tables of integrals the following time-dependence of the eccentricity

$$\arctan\sqrt{e} - \frac{\sqrt{e}}{1+e} = \arctan\sqrt{e_0} - \frac{\sqrt{e_0}}{1+e_0} - \frac{B\rho_{per}}{r_{per}}\sqrt{\frac{\mu H_{per}}{2\pi}}(t-t_0) \qquad (12.7.8)$$

Since

$$\arctan\sqrt{e} - \frac{\sqrt{e}}{1+e} = e^{3/2}\left(\frac{2}{3} - \frac{4}{5}e + \frac{6}{7}e^2 - \cdots\right)$$

we can approximate

$$e^{3/2}(t) = e_0^{3/2} - \frac{3B\rho_{per}}{2r_{per}}\sqrt{\frac{\mu H_{per}}{2\pi}}(t-t_0) \quad @ \quad \frac{H_{per}}{a} \ll e < 0.02$$

Because we have $a(1-e) = r_{per} = const$, and with Eq. (7.4.9) it follows

$$e(t) = 1 - \frac{r_{per}}{a(t)} = \frac{r_{apo}(t) - r_{per}}{r_{apo}(t) + r_{per}}$$

from which we obtain by insertion the analytical orbit equation also for $a(t)$ and $r_{apo}(t)$.

How long would it take to circularize an elliptic orbit? This can be determined quite easily. The circularization time t_{cir} is the time to $e = 0$, i.e., $t_{cir} = t(e = 0)$. Inserting this condition into the above equations we find with $t_0 = 0$

$$t_{cir} = \frac{r_{per}}{B\rho_{per}}\sqrt{\frac{2\pi}{\mu H_{per}}}\left(\arctan\sqrt{e_0} - \frac{\sqrt{e_0}}{1+e_0}\right) \quad \textbf{circularization time} \qquad (12.7.9)$$

or

$$t_{cir} = \frac{2r_{per}e_0^{3/2}}{3B\rho_{per}}\sqrt{\frac{2\pi}{\mu H_{per}}} \quad @ \quad \frac{H_{per}}{a} \ll e < 0.02 \qquad (12.7.10)$$

with e_0 the initial eccentricity, and ρ_{per} the atmospheric density and H_{per} the scale height at periapsis. When tracing back the cause for the $e_0^{3/2}$ dependence we find its origin in the fact that, for increasing eccentricities, the stretch s within which the S/C dives into the dense portion of the atmosphere decreases with $s \approx 2\sigma \propto 1/\sqrt{e}$ (see Eq. (12.7.4)). The integral of this dependence then leads to the $e_0^{3/2}$ dependence.

12.7.3 Circular Orbits

When the ellipse is circularized down to $e < H(a)/a$, the body encounters a constant drag upon circling the planet with radius a. To determine the element changes of a circular orbit, we have to re-examine the second expression of Eq. (12.7.3). To derive the mean changes of e we have to average it with $e = 0$ and hence $\xi(e, \theta) = 1$ over one orbit. Because of $\langle \cos\theta \rangle_\theta = 0$ and as in a circular orbit $v^2 = \mu/a$ (Eq. 7.4.3) and $n^2 = \mu/a^3$(Eq. 7.3.10), we get $v_a^2 = n^2 a^2$ and thus

$$\begin{aligned} \dot{a} &= -\frac{B\rho\, v_a^2}{n} = -B\rho(a)\sqrt{\mu a} \\ \dot{e}_{\text{sec}} &= 0 \end{aligned} \qquad @\ e < \frac{H(a)}{a} \tag{12.7.11}$$

So we can make the following statement:

Impact of Drag on Semi-Major-Axis
Drag constantly decreases the radius of a circular orbit, without changing its eccentricity.

Ballistic Coefficient B from NORAD TLE
Quite generally, it is hard to come by the ballistic coefficient B of a S/C. From Eq. (12.7.11) one could presume that if the momentary orbit radius a of a S/C and atmospheric density $\rho(a)$ is known one would be able to determine it from its orbital decay $\dot{a}$ as

$$B\rho(a) = -\frac{\dot{a}}{\sqrt{\mu a}}$$

As a matter of fact, the NORADS TLE (two-line elements (see e.g. www.space-track.org) provide the figures $n\ \left[\text{rev}\cdot\text{day}^{-1}\right]$ and $\dot{n}/2\ \left[\text{rev}\cdot\text{day}^{-2}\right]$ in the said units. The orbital decay rate $\dot{a}$ can be derived via $a^3 = \mu_\oplus/n^2$ and hence $3\dot{a}/a = -2\dot{n}/n$ from this. With this and with $\sqrt{\mu a} = (\mu^2/n)^{1/3}$ we find

$$B\rho(a)\ \left[\text{km}^{-1}\right] = 5.024 \times 10^{-6} \frac{\dot{n}/2\ \left[\text{rev}\cdot\text{day}^{-2}\right]}{\left(n\ \left[\text{rev}\cdot\text{day}^{-1}\right]\right)^{4/3}} \qquad @\ \text{Earth}, e < \frac{H(a)}{a} \tag{12.7.12}$$

To determine from this the ballistic coefficient B, the atmospheric density averaged over one elliptic orbit at the altitude $h = a - R_\oplus$, where the S/C suffered the decay, needs to be known. This can, for instance, be derived from Fig. 6.3 in Sect. 6.1.2 by applying current solar flux figures $F_{10.7}$ from https://spawx.nwra.com/spawx/f10.html.

Example

What is the ballistic coefficient of the International Space Station in its torque equilibrium attitude (TEA)?

TEA is an "airplane like" attitude maintained relative to the Local Vertical Local Horizontal (LVLH, see Sect. 15.1.3). The pitch angle is $-10° \pm 5°$ depending on the altitude and hence on the residual atmosphere. For this attitude the residual drag torque counterbalances the gravity–gradient torque (see Sect. 15.4.1). The TLE of the ISS on April 6, 2018, 05:45:34 UTC was given as

1 25544*U* 98067*A* 18096.20365559 .00002236 00000−0 40882−4 0 9998
2 25544 51.6441 17.5650 0001462 307.6006 167.7216 15.54202230107329

From this we find $n = 15.5420\,\text{rev} \cdot \text{day}^{-1}$ and $\dot{n}/2 = 2.24 \times 10^{-5}\,\text{rev} \cdot \text{day}^{-2}$. This yields an altitude of

$$h[\text{km}] = a - a_{\oplus} = 4.224 \times 10^4 \left(n\left[\text{rev} \cdot \text{day}^{-1}\right]\right)^{-2/3} - 6378\,\text{km} = 404\,\text{km}$$

and with Eq. (12.7.12) $B_{ISS}\rho(404\,\text{km}) = 2.90 \times 10^{-12}\text{km}^{-1}$. At that time the atmospheric density was given as $\rho(404\,\text{km}) = 4.76 \times 10^{-13}\text{kg m}^{-3}$ (low solar activity, $F_{10.7} = 67$). With this we derive the ISS ballistic coefficient in the TEA attitude mode to be B = 0.0061 $\text{m}^2\ \text{kg}^{-1}$.

Remark (NORAD's Bstar) *This procedure in fact is done by the North American Aerospace Defense Command, NORAD. It publishes the orbital elements as the so-called two-line elements derived from their observations as two line elements, TLEs, at celestrak.com/NORAD/elements. The third last entry in the first line of a TLE, the so-called* B^* *(Bstar, dimensionless), reflects the decay and is related to B* via $B^* = R_{\oplus}\rho_{120}B/2$, *where* $R_{\oplus} = 6378.13$ *km and* $\rho_{120} = \rho(h = 120\ km)$. *NORAD in its so-called Simplified General Perturbation Model SGP, in which* B^* *is derived from the observed orbital decay data, employs a simplified static atmospheric model (Lane's model), which assumes a standard value* $\rho_{120} \equiv \rho_0 = 2.461 \times 10^{-8}\ kg\ m^{-3}$. *Because* ρ_{120} *actually may vary by more than an order of magnitude depending on the solar and geomagnetic activities it is useless to determine B from* B^* with $\rho_{120} = 2.461 \times 10^{-8}\ kg\ m^{-3}$ *as sometimes recommended. For instance, at 400 km altitude (about ISS orbit) the ballistic coefficients* B_{TLE} *derived from* B^* *related to the true ones are* $B_{TLE}/B_{true} = 1.83,\ 7.08,\ 0.080$ *for mean, extremely high, and low solar activities, respectively. Therefore* B^* *should be considered only as a fudge parameter to adequately describe the momentary orbit decay with the SGP propagator algorithm and its derivatives.*

Orbit Decay

To describe the orbit decay quantitatively we need to solve the differential Eq. (12.7.11). Separating the variables in the first equation results in

$$dt = -\frac{1}{B\sqrt{\mu}}\frac{da}{\sqrt{a}\rho(a)}$$

from which by integration follows:

$$t - t_0 = -\frac{1}{B\sqrt{\mu}}\int_{a_0}^{a}\frac{da}{\sqrt{a}\rho(a)} = \frac{1}{B\sqrt{\mu}}\int_{a}^{a_0}\frac{da}{\sqrt{a}\rho(a)} \tag{12.7.13}$$

where a_0, t_0 are the initial values of the orbit. To further evaluate the integral analytically, $\rho(a)$ has to be expressed, according to Eq. (6.1.8), in a piecewise exponential form

$$\rho(a) = \rho_i \exp\left(-\frac{h-h_i}{H_i}\right) = \rho_{i+1}\exp\left(-\frac{h-h_{i+1}}{H_i}\right) \quad @\ h_i < h < h_{i+1} \tag{12.7.14}$$

where $h = a - R_\oplus$, h_i is the base altitude, and H_i the scale height for the ith altitude interval as given in Table 6.2. Correspondingly we also achieve only a piecewise description of the orbit trajectory. For the initial part of the decaying orbit we therefore make the ansatz

$$\rho(a) = \rho_0 \exp\left(-\frac{h-h_0}{H_0}\right) \quad @\ h < h_0$$

where ρ_0 is the atmospheric mass density at the initial altitude h_0 and H_0 the mean scale height over the integration interval just below the initial altitude. If integration is performed over the interval $h_i < h < h_{i+1} = h_0$ as given by Table 6.2 in Sect. 6.1.4 then the values of $\rho_0 = \rho_{i+1}$ and $H_0 = H_i$ (cf. Eq. (12.7.14)) can be taken from Table 6.2. With this and with the substitution $a = h + R_\oplus =: x + R_\oplus$ we get from Eq. (12.7.13)

$$t - t_0 = \frac{1}{B\rho_0\sqrt{\mu}}\int_{h}^{h_0}\frac{e^{(x-h_0)/H_0}}{\sqrt{x+R_\oplus}}dx \tag{12.7.15}$$

Because by far the biggest contributions to the integral come from the initial altitude, we can safely approximate

$$\begin{aligned}\int_h^{h_0} \frac{e^{(x-h_0)/H_0}}{\sqrt{x+R_\oplus}}dx &= \frac{1}{\sqrt{a_0}}\int_h^{h_0} \frac{e^{(x-h_0)/H_0}}{\sqrt{1+(x-h_0)/a_0}}dx \\ &\approx \frac{1}{\sqrt{a_0}}\int_h^{h_0} e^{(x-h_0)/H_0}\left(1-\frac{x-h_0}{2a_0}\right)dx \\ &= \frac{H_0}{\sqrt{a_0}}e^{(x-h_0)/H_0}\left(1-\frac{x-h_0+H_0}{2a_0}\right)\Bigg|_h^{h_0} \\ &= \frac{H_0}{\sqrt{a_0}}\left[\left(1+\frac{H_0}{2a_0}\right)-e^{(h-h_0)/H_0}\left(1-\frac{h-h_0}{2a_0}+\frac{H_0}{2a_0}\right)\right] \\ &\approx \frac{H_0}{\sqrt{a_0}}\left[1-e^{(h-h_0)/H_0}\left(1-\frac{h-h_0}{2a_0}\right)\right]\end{aligned} \tag{12.7.16}$$

The last term arises when $H_0/2a_0 < 0.0001$.

Orbit Trajectory
For LEOs with $h_0 \leq 1000$ km we have $h_0/2a_0 < 0.07$. Therefore

$$t - t_0 \approx \frac{H_0}{B\rho_0\sqrt{\mu a_0}}\left[1-e^{(h-h_0)/H_0}\right]$$

With this and with $h - h_0 = a - a_0$ we derive for the initial trajectory of a circular orbit

$$a(t) = a_0 + H_0 \ln\left[1-\frac{B\rho_0\sqrt{\mu a_0}}{H_0}(t-t_0)\right] \quad @ \quad e < \frac{H(a)}{a} \tag{12.7.17}$$

As an example, Fig. 12.38 depicts $a(t)$ of the International Space Station, from which the decay and the reboosts are clearly visible.

12.7.4 Orbit Lifetime

When does a S/C in a circular or near-circular low Earth orbit without orbit maintenance burn up in the Earth's atmosphere? In the following, we want to determine this so-called orbit life t_L of a circular orbit from a given initial altitude. As we only want to estimate the orbit lifetime we apply Eq. (12.7.16) and use it with the initial values right down to $h = 0$, whereby we only slightly overestimate the orbit lifetime. With this approximation and setting $t_0 = 0$ we get

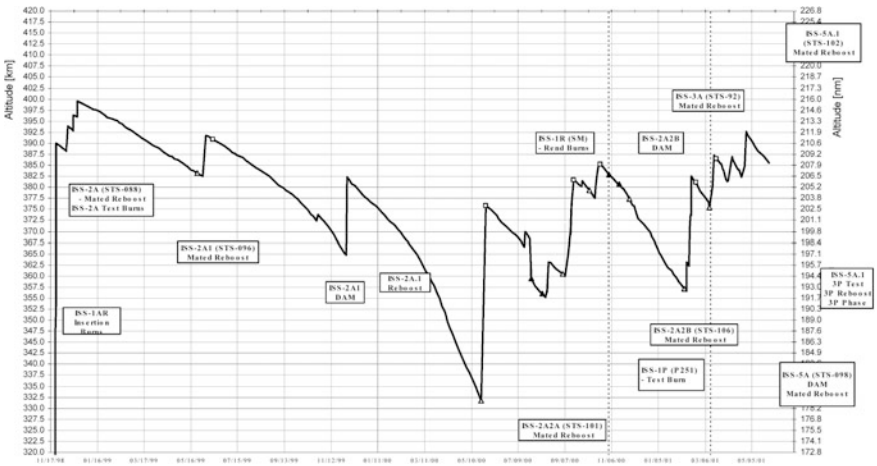

Fig. 12.38 The as-flown altitude profile of the International Space Station between its first assembly flight in November 1998 and May 2001. *Credit* NASA

$$t_L = \frac{H_0}{B\rho_0\sqrt{\mu a_0}}\left[1 - e^{-h_0/H_0}\left(1 + \frac{h_0}{2a_0}\right)\right]$$

Because $h_0/H_0 > 10$ we get with Eq. (12.7.11) in excellent approximation

$$\boxed{t_L = \frac{H_0}{B\rho_0\sqrt{\mu a_0}} = \frac{H_0}{|\dot{a}_0|}} \quad @ \quad e < H_0/a_0 \tag{12.7.18}$$

with

$a_0 = h_0 + R_\oplus$ initial radius of the circular orbit

$\rho_0 = \rho(h_0)$ atmospheric density at the initial altitude h_0

$H_0 = H(h_0)$ atmospheric scale height just below the initial altitude h_0

If the initial altitude coincides with a base altitude $h_0 = h_i$ as given in Table 6.2 in Sect. 6.1.4 then $\rho_0 = \rho_i$ and $H_0 = H_{i-1}$ as given in Table 6.2. Note that according to the end of Sect. 6.2.4 the ballistic coefficient B can vary by as much as 80% over a wide range of altitudes and solar activity phases. Therefore, the mean ballistic coefficient at the initial altitude is decisive.

Example

What is the mean orbit lifetime of the International Space Station in TEA attitude mode at its common altitude of 350 km and at a mean solar activity of $F_{10.7} = 140$?

From the Example in Sect. 12.7.3 we have for the ISS $B_{ISS} = 0.0061\ m^2\ kg^{-1}$. From the MSISE-90 model follows for a mean solar activity at altitude 350 km that $\rho(350\ km) = 9.80 \times 10^{-12}\ kg\ m^{-3}$ and $H_0 = 53.1$ km. With $\mu = 3.986 \cdot 10^5\ km^3 s^{-2}$ Eq. (12.7.18) furnishes $t_L \approx 200$ days.

Alternatively, we find from Fig. 12.38 for the time frame May 27, 2000 to July 15, 2000 a decay rate of $\dot{a}_0 = -0.18$ km day^{-1} at an altitude of $h = 370$ km. From $H_0 = 53.3$ km we find with Eq. (12.7.18) $t_L \approx 300$ days. Note that only six months later, in the time frame December 6, 2000 to Janunary 5, 2001, the ISS at the same altitude decayed at a rate $\dot{a}_0 = -0.28$ km day^{-1} implying an expected orbit lifetime of only $t_L \approx 190$ days. This big difference reflects the variation of the mean daily atmospheric density at such altitudes (see also Remark NORAD's Bstar in Sect. 12.7.3).

Remark *To maintain the space station at an altitude of 350–400 km, routine reboosts of currently about once a month are performed. The required propellant for this is about* 7500 kg year^{-1}.

If one evaluates the integral in Eq. (12.7.13) numerically with the atmospheric density as given by Eq. (6.1.8) one obtains the mean orbit lifetime as displayed in Fig. 12.39 for a spacecraft with various ballistic coefficients. $B = 0.005$ m^2/kg is a good average value.

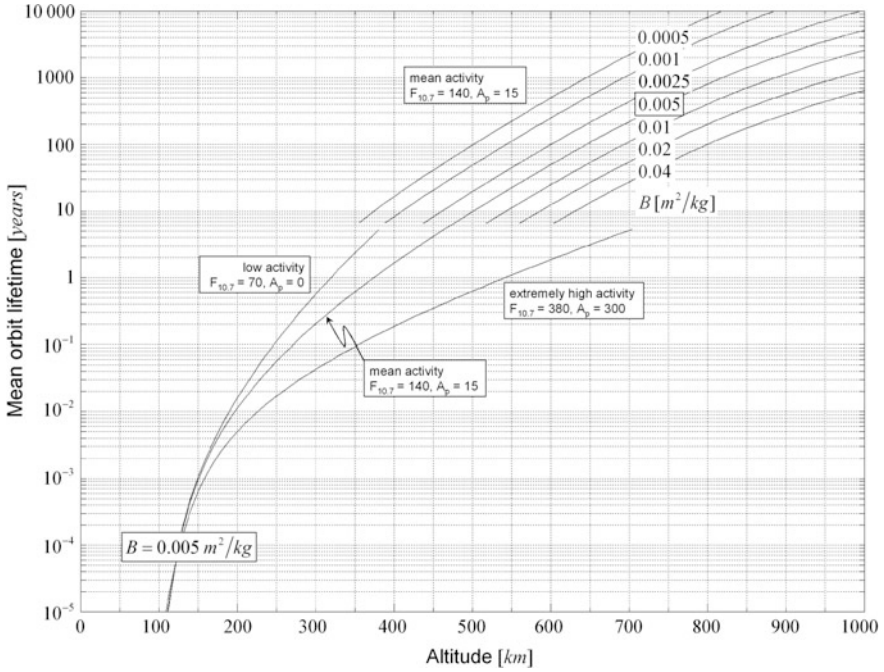

Fig. 12.39 In the upper part the mean orbit lifetime of a circular orbit as a function of altitude for various ballistic coefficients B is given. If the orbit life time of a S/C is less than 6 years it varies drastically by more than one order of magnitude due to the actual solar activity. In the lower part these variances are given for a mean $B = 0.005$ m^2 kg^{-1}

Rule of Thumb

From Table 6.2 we observe that above an altitude of 200 km roughly $H \approx 0.14 \cdot h$ holds. Because the atmospheric density about an altitude h_0 varies exponentially as given by Eq. (12.7.14) and therefore $t_L \approx t_{L0}\, e^{(h-h_0)/H_0}$ an increase of the orbital radius by $\Delta h = H_0 \ln 2 \approx 0.1 \cdot h_0$, i.e., an about 10% altitude increase, doubles the orbit life time in LEO. This in turn gives rise to the assumption that the orbit life time $t_L(h)$ is subject to a power law. We therefore make the ansatz $t_L = t_{L0}(h/h_0)^x$, fit this ansatz to the numerical data, and arrive at the approximate equation

$$t_L \approx 1.7 \frac{0.005}{B} \left(\frac{h}{400} \right)^{8.4} \quad @\ 300\ \text{km} < h < 900\ \text{km},\ e < H_0/a_0 \tag{12.7.19}$$

Here the ballistic coefficient B is to be provided in units $m^2 kg^{-1}$, h in km, and t_L then is given in *years*. Compared to Fig. 12.39, Eq. (12.7.19) has an error of only up to 10% in the range 350–650 km increasing to 30% at the altitudes 300 and 900 km.

If we set $h = h_0(1+\varepsilon)$ and solve Eq. (12.7.19) for $t_L = 2t_{L0}$ we find $\varepsilon = 2^{1/8.4} - 1 = 0.086$. This yields the key rule of thumb:

Rule of Thumb for Orbit Life Time
An increase of a circular orbital altitude in LEO by 10% roughly doubles the orbit life time.

Orbit Lifetime from NORAD TLE

The initial orbital decay rate $\dot{a}_0$ in Earth's atmosphere can be derived via $a^3 = \mu_\oplus / n^2$ and hence $3\dot{a}/a = -2\dot{n}/n$ as

$$\dot{a}_0 \left[\text{km day}^{-1}\right] = -1.769 \times 10^5 \frac{\dot{n}_0/2 \left[\text{rev day}^{-2}\right]}{\left(n_0 \left[\text{rev} \cdot \text{day}^{-1}\right]\right)^{5/3}} \quad @\ \text{Earth}$$

Since n_0 and $\dot{n}_0/2$ are given by NORAD TLE in the said units the orbit lifetime of a NORAD catalog object can immediately be derived from Eq. (12.7.18) as

$$t_L[\text{days}] = \frac{H_0}{|\dot{a}_0|} = 5.652 \times 10^{-6} \frac{\left(n_0 \left[\text{rev day}^{-1}\right]\right)^{5/3}}{\dot{n}_0/2 \left[\text{rev day}^{-2}\right]} H_0[\text{km}] \quad @\ \text{Earth} \tag{12.7.20}$$

Example

What would be the mean orbit lifetime of the International Space Station in TEA attitude mode on April 6, 2018, 05:45:34 UTC?

According to the Example in Sect. 12.7.3 we have for the ISS at that point in time $n_0 = 15.5420\,\text{rev} \cdot \text{day}^{-1}$ and $\dot{n}_0/2 = 2.24 \times 10^{-5}\,\text{rev} \cdot \text{day}^{-2}$, and for low activity from the MSISE-90 model H_0 = 41.95 km. With Eq. (12.7.20) we therefore derive t_L = 1024 days = 2.8 years. This very high value is due to the low activity of the Sun in 2018, i.e., a low atmospheric density, plus the high altitude of the ISS of h = 404.47 km.

Total Orbit Lifetime of Elliptic Orbits

If the initial orbit is elliptic, the total orbit lifetime is the circularization time plus circular orbit lifetime. Which of the two is prevailing? Since, at the transition between the two phases, $r_0 = r_{per}$, we derive from Eqs. (12.7.10) and (12.7.18) the following ratio of the two contributions:

$$\frac{t_{cir}}{t_L} = \sqrt{2\pi}\left(\frac{r_{per}}{H_{per}}\right)^{3/2}\left(\arctan\sqrt{e_0} - \frac{\sqrt{e_0}}{1+e_0}\right) \approx \sqrt{2\pi}\left(\frac{r_{per}}{H_{per}}\right)^{3/2}\frac{2}{3}e_0^{3/2}$$

From $e_0 \gg \frac{H_{per}}{a} \approx \frac{H_{per}}{r_{per}}$ we get

$$\frac{t_{cir}}{t_L} \gg \frac{2}{3}\sqrt{2\pi} = 1.7 \tag{12.7.21}$$

So, circularization time is much bigger than the circular orbit lifetime. This has the following practical consequence that for a planetary capture and a subsequent circularization to a circular target orbit, the periapsis has to be chosen lower than the target radius to more rapidly turn down the elliptic orbit. When the apoapsis attains the target orbit radius, a kick-burn at the apoapsis (see Eq. (8.1.11)) will increase the periapsis to the target radius. Though this maneuver requires some propulsion effort, it is much less demanding than to circularize the ellipse by propulsion only without making use of the atmospheric drag.

Example

On October 28, 2010, the European satellite operator Eutelsat lost its communications satellite W3B due to a sizeable leak in its fuel tank just after it was placed with Ariane 5 into the highly elliptic transfer orbit with a perigee of 249.2 km and an apogee of 35,907 km. After considering moving W3B to a graveyard orbit or guiding the satellite to destruction over the Pacific Ocean, managers ultimately concluded their only option was to leave the satellite where it was. Under the given ballistic coefficient of $B = 0.015\ \mathrm{m^2\,kg^{-1}}$ when will W3B been circularized and burn up in the atmosphere?

With the given perigee and apogee of the transfer orbit we find from Eq. (7.4.9) that the orbit's initial eccentricity is $e_0 = 0.729$. At the perigee altitude of 250 km we have from Table 6.2 $H \approx 40$ km and $\rho = 7.25 \times 10^{-11}\ \mathrm{kg\,m^{-3}}$. From Eq. (12.7.9) we therefore derive a circularization time of $t_{cir} = 25.8$ yrs. Compared to this and according to Fig. 12.39 the orbital life time is $t_L < 0.01$ yr. As a result, W3B will burn up in about 26 years.

12.8 Problems

Problem 12.1 *Gaussian Variational Equations*
To prove the Gaussian Variational Equations (12.1.4) proceed as follows: First prove Eq. (8.1.1) and then apply the reverse transformation as given before in Eq. (8.1.1).

1. Prove Eq. (8.1.1)

Do this by first considering kick-burns only within the orbital plane and then out of the plane:

(a) To derive the change of orbital elements for in-plane kick-burns first introduce the angle changes:

$$d\gamma := \frac{dv_{\perp \mathrm{O}}}{v}, \quad d\phi := \frac{dv_{\perp\perp}}{v} \quad \text{and} \quad d\eta := \frac{dv_{\parallel}}{v} = \frac{dv}{v}$$

To simplify calculations we define

$$s := \frac{rv^2}{\mu}$$

With this rewrite the vis-viva Eq. (7.2.15) to

$$r = (2 - s)a \tag{a}$$

From Eqs. (13.1.8) and (13.1.9) follows

$$\boldsymbol{v} = \left(\frac{e\mu}{h}\sin\theta, \frac{h}{r}\right) = v(\sin\gamma, \cos\gamma)$$

Therefore $h = rv\cos\gamma$. Show that from $h^2 = \mu a(1 - e^2)$, Eq. (7.3.7), follows

$$e^2 = 1 - s(2 - s)\cos^2\gamma \tag{b}$$

and

$$\sin\theta = \frac{s}{2e}\sin 2\gamma \tag{c}$$

Convince yourself by a drawing that if a kick-burn takes place at a certain position $\boldsymbol{r}$ in space, which remains constant during the kick-burn maneuver, then any change in θ corresponds to a negative change in ω, i.e., $d\omega = -d\theta$. With this and from Eqs. (a) to (c) prove with the relations $s\cos^2\gamma = 1 + e\cos\theta$, $s\cos 2\gamma = 1 + 2e\cos\theta - e\cos E$, and $s\sin 2\gamma = 2e\sin\theta$ the differential equations

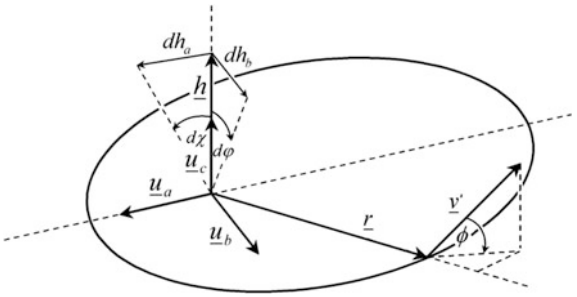

Fig. 12.40 Definition of angles for out-of-the-plane kick-burns

$$da = \frac{a}{2-s}ds = \frac{2as}{2-s}d\eta$$
$$de = 2(e + \cos\theta) \cdot d\eta + \frac{r}{a}\sin\theta \cdot d\gamma$$
$$e \cdot d\omega = 2\sin\theta \cdot d\eta - (e + \cos E)d\gamma$$

(b) To derive the changes of orbital elements for out-of-plane kick-burns consider the definitions made in Fig. 12.40

Show that from

$$d\boldsymbol{v} = \frac{\partial \boldsymbol{v}}{\partial \gamma}d\gamma + \frac{\partial \boldsymbol{v}}{\partial \phi}d\phi + \frac{\partial \boldsymbol{v}}{\partial \eta}d\eta$$

follows

$$d\boldsymbol{v} = v \cdot [\cos(\theta-\gamma) \cdot d\gamma,\ \sin(\theta-\gamma) \cdot d\gamma,\ d\phi] + v \cdot [-\sin(\theta-\gamma),\ \cos(\theta-\gamma),\ 0]d\eta$$

and therefore

$$d\boldsymbol{h} = d(\boldsymbol{r} \times \boldsymbol{v}) = \boldsymbol{r} \times d\boldsymbol{v}$$
$$= rv[\sin\theta \cdot d\phi, -\cos\theta \cdot d\phi, -\sin\gamma \cdot d\gamma + \cos\gamma \cdot d\eta]$$

Because on the other hand $d\boldsymbol{h} = (dh_a,\ dh_b,\ dh_c) = (h \cdot d\chi,\ h \cdot d\varphi,\ dh)$ follows

$$d\chi = \frac{\sin\theta}{\cos\gamma}d\phi, \quad d\varphi = -\frac{\cos\theta}{\cos\gamma}d\phi, \quad \frac{dh}{h} = -\tan\gamma \cdot d\gamma + d\eta$$

Let $d\sigma_a, d\sigma_b, d\sigma_c$ be the positive deflections around the coordinate axes $(\boldsymbol{u}_a, \boldsymbol{u}_b, \boldsymbol{u}_c)$ for which holds (see, e.g., Kaplan 1976, Eq. (1.28))

$$\begin{pmatrix} d\Omega \\ di \\ d\omega \end{pmatrix} = \frac{1}{\sin i} \begin{bmatrix} \sin\omega & \cos\omega & 0 \\ \cos\omega \sin i & -\sin\omega \sin i & 0 \\ -\sin\omega \cos i & -\cos\omega \cos i & \sin i \end{bmatrix} \begin{pmatrix} d\sigma_a \\ d\sigma_b \\ d\sigma_c \end{pmatrix}$$

Show that

$$\begin{pmatrix} d\sigma_a \\ d\sigma_b \\ d\sigma_c \end{pmatrix} = \begin{pmatrix} -d\varphi \\ d\chi \\ -d\theta \end{pmatrix}$$

from which the desired change of orbital elements are derived.

2. Apply the reverse transformation of (see equations before Eq. (8.1.1))

$$a_r = \cos\gamma \cdot \delta v_{\perp O} + \sin\gamma \cdot \delta v_{||}$$
$$a_\theta = -\sin\gamma \cdot \delta v_{\perp O} + \cos\gamma \cdot \delta v_{||}$$

to finally derive the Gaussian Variational Eq. (12.1.2).

Problem 12.2 *Earth's Oblateness and J*
Prove by the use of $P_2^0 = P_2 = \frac{1}{2}(3\sin^2\beta - 1)$ the relation

$$J \approx f - \frac{\omega^2 R_\oplus^3}{2\mu_\oplus}$$

between the harmonic coefficient

$$J := \frac{3}{2} J_2 := -\frac{3}{2} C_2^0 = 0.001623945$$

and Earth's oblateness

$$f := \frac{R_\oplus - R_{polar}}{R_\oplus} \approx \frac{1}{298.2564}$$

Hint: The shape of the Earth's surface forms under the physical *principle of least action*. Due to this principle the so-called *Lagrangian* $L = U_\omega - U_{pot}$ must be minimal and constant over the entire Earth surface. Use Eq. (7.2.16) to determine U_ω at different latitudes and Earth's gravitational potential $U = U_{pot}$ up to order P_2^0.
Note: When also taking P_4^0 into account one derives the refined solution (see Kaula (1966))

$$J = f\left(1 - \frac{1}{2}f\right) - \frac{\omega^2 R_\oplus^3}{2\mu_\oplus}\left(1 - \frac{3\omega^2 R_\oplus^3}{2\mu_\oplus} - \frac{2}{7}f\right).$$

Problem 12.3 *Triaxial Motion*
Show that the equation of motion (12.4.14) for a satellite at an unstable GEO position

$$\ddot{\lambda} = -\frac{1}{2}\omega_\lambda^2 \cdot \sin 2(\lambda - \lambda_0)$$

with initial condition $\lambda = \lambda_i \neq \lambda_0$ has the approximate solution

$$\lambda = \lambda_i - \frac{1}{4}\omega_\lambda^2 \sin[2(\lambda_i - \lambda_0)] \cdot t^2 + \frac{1}{96}\omega_\lambda^4 \sin[4(\lambda_i - \lambda_0)] \cdot t^4 - O(t^6)$$

Problem 12.4 *Orbit Changes by Atmospheric Maneuvers*

(1) After the Columbia accident on February 1, 2003, NASA administrator O'Keefe canceled any Hubble repair mission, because from the Hubble telescope the Space Shuttle was not supposed to be able to reach the ISS as a safe haven. Given the orbit elements of ISS (*altitude* = 400 km, $i = 51.63°$, $e \approx 0$) and the Hubble telescope (*altitude* = 590 km, $i = 28.5°$, $e \approx 0$) and the fact that the OMS engines of a shuttle can only provide a delta-v of about $\Delta v = 200$ m/s, show that O'Keefe was right.

(2) We have seen in Sect. 12.7.2 that it is possible to change the semi-major axis of an orbit by dragging through the atmosphere at the periapsis of an elliptic orbit. Suppose the vehicle has also lift. The vehicle then receives the delta-v changes $\delta v_{||}$, $\delta v_{\perp O}$ or $\delta v_{||}$, $\delta v_{\perp\perp}$ depending on the orientation of the lift vector. Show by a similar procedure as in Sect. 12.7.2 that the delta-v change due to one fly-through the periapsis of an ellipse is given by

$$|\delta v_{||}| \approx \frac{C_D}{2}\frac{\rho_{per} A_\perp}{m}(1+e)\sqrt{\frac{2\pi\mu H_{per}}{e}}$$

$$|\delta v_{\perp O}| = |\delta v_{\perp\perp}| \approx \frac{C_L}{2}\frac{\rho_{per} A_\perp}{m}(1+e)\sqrt{\frac{2\pi\mu H_{per}}{e}}$$

(3) Now consider a life threatening situation onboard the Space Shuttle during Hubble repair. Show that, though an inclination turn is in principle possible with an atmospheric maneuver, the following orbit maneuver would not be feasible: lower one side of the shuttle orbit by a small deorbit burn such that the now slightly elliptic orbit would touch the atmosphere at its periapsis. The shuttle would not only receive a delta-v of $\delta v_{||}$, $\delta v_{\perp\perp}$ thereby decelerating but also change the inclination $28.5° \rightarrow 51.63°$ due to its lift, $C_L/C_D = L/D \approx 1.3$. Finally the elliptic orbit would be raised to a circular ISS LEO and the shuttle maneuvered to the ISS by some negligible rendezvous maneuvers.

Hint: Consult Table 8.1.

Problem 12.5 *King-Hele's Orbit Lifetime*
In his reputed book King-Hele (1987, p. 60ff) provides the following expression for the orbit life time of a satellite in a LEO

$$t_L \approx -\frac{3e_0T_0}{4\dot{T}_0}\frac{I_0(z_0)}{I_1(z_0)}\left(1+2e_0\frac{I_1(z_0)}{I_0(z_0)}-\frac{9e_0z_0}{40}+\frac{H}{2a_0}\right) \quad @ \quad z_0=\frac{a_0e_0}{H_0}<3$$

with

$$I_0(z)=1+\frac{z^2}{4}+\frac{z^4}{64}+\frac{z^6}{2304}+\cdots \quad \text{Bessel function of the first kind and order 0}$$

$$I_1(z)=\frac{z}{2}\left(1-\frac{z^2}{8}+\frac{z^4}{192}-\frac{z^6}{9216}+\cdots\right) \quad \text{Bessel function of the first kind and order 1}$$

and $T_0=2\pi\sqrt{a_0^3/\mu}$.

Show that for an elliptic orbit from the above follows

$$t_L \approx \frac{H_0}{B\rho_0\sqrt{\mu a_0}}\left(1+\frac{H_0}{2a_0}\right) \approx \frac{H_0}{B\rho_0\sqrt{\mu a_0}}\left(1+\frac{H_0}{2R_\oplus}\right)$$

and therefore concurs with Eq. (12.7.18).